Chapter 3. Creating a Spatially Heterogeneous Full Stress Tensor

The previous chapter discussed how one would filter a scalar quantity in three dimensions. The ultimate goal is to filter both full and deviatoric stress tensors, which are comprised of six and five independent quantities respectively.

Rotational equilibrium requires that a 3D stress tensor is symmetric. This symmetry means that six degrees of freedom are required to specify stress. The other equilibrium condition, $\sum_{j=1}^{3} \frac{\partial \sigma_{ij}}{\partial x_j} = f_i$, which specifies no internal accelerations if there are no internal sources, provides an additional three constraints; however, the introduction of this equilibrium condition would force us to introduce random sources (dislocations) within the medium to produce our heterogeneous slip. Otherwise, by St. Venant's principle, the inside of a medium far away from the external boundaries and with no internal sources would have an approximately uniform stress distribution by definition if $\sum_{j=1}^{3} \frac{\partial \sigma_{ij}}{\partial x_j} = f_i$ is satisfied. Since the introduction of random sources requires additional assumptions about the statistics of fault distributions, fault sizes, slip on faults, etc., in this study we opt for not satisfying $\sum_{j=1}^{3} \frac{\partial \sigma_{ij}}{\partial x_j} = f_i$ so that we can produce stress heterogeneity without the introduction of internal sources. Again in this study we are primarily interested in producing a first-cut statistical description of the Earth's crust, parameterized by two numbers, *Heterogeneity Ratio* and α, without having to model the individual sources that create the heterogeneity.

For deviatoric stress tensors, the pressure is subtracted out such that the trace (summation of the diagonal elements) equals zero. This additional constraint reduces the degrees of freedom from six to five. The formula for pressure is

$$p = (1/3)(\sigma_{11} + \sigma_{22} + \sigma_{33}) \tag{3.1}$$

and when we subtract the pressure from our stress tensor, we have the following deviatoric stress tensor,

$$\begin{pmatrix} \sigma_{11} - p & \sigma_{12} & \sigma_{13} \\ \sigma_{12} & \sigma_{22} - p & \sigma_{23} \\ \sigma_{13} & \sigma_{23} & \sigma_{33} - p \end{pmatrix} = \begin{pmatrix} \sigma'_{11} & \sigma'_{12} & \sigma'_{13} \\ \sigma'_{12} & \sigma'_{22} & \sigma'_{23} \\ \sigma'_{13} & \sigma'_{23} & \sigma'_{33} \end{pmatrix}, \tag{3.2}$$

where

$$\sigma'_{11} + \sigma'_{22} + \sigma'_{33} = 0. \tag{3.3}$$

The constraint can also be written as

$$\sigma'_{22} = -(\sigma'_{11} + \sigma'_{33}), \tag{3.4}$$

and our deviatoric stress tensor can be rewritten as

$$\begin{pmatrix} \sigma'_{11} & \sigma'_{12} & \sigma'_{13} \\ \sigma'_{12} & -(\sigma'_{11} + \sigma'_{33}) & \sigma'_{23} \\ \sigma'_{13} & \sigma'_{23} & \sigma'_{33} \end{pmatrix}. \quad [\text{5 D.O.F. for a symmetric, deviatoric stress tensor}] \tag{3.5}$$

Recognizing that a symmetric, full stress tensor has six degrees of freedom and a symmetric, deviatoric stress tensor has five degrees of freedom, the question arises, "How does one filter a tensor with five or six degrees of freedom?" At first glance we might wish to simply filter σ_{11}, σ_{22}, σ_{33} σ_{12}, σ_{23}, and σ_{13} as six independent scalar quantities for the full stress tensor or filter σ'_{11}, σ'_{33}, σ'_{12}, σ'_{23}, and σ'_{13} as five independent scalar quantities for the deviatoric stress tensor, using the strategy outlined

in Chapter 2. Unfortunately, σ_{ij} and σ'_{ij} are always defined for a particular coordinate system. If we filter in this way, then we find that the general characteristics of the filtered stress are changed when we rotate from one coordinate frame to another. To resolve this problem, we need to rethink how to write our stress tensors.

An alternative way would be to represent the five degrees of freedom of the deviatoric stress tensor in terms of two scalar invariants of the stress tensor, and three orientation angles. Likewise, we can represent the full stress tensor with three scalar invariants and three orientation angles.

Invariant Filtering

It is fairly staightforward to filter invariants, quantities that remain unchanged upon rotation of the stress tensor or coordinate system. We have many choices of invariants to choose from. For simplicity, we choose to filter the principal stresses (σ_1, σ_2, and σ_3). For the full stress tensor, we use all three of these principal stresses and for the deviatoric stress tensor we will filter σ_1, σ_2, and σ_3 then subtract out the pressure, p, so that

$$\begin{aligned} \sigma'_1 &= \sigma_1 - p \\ \sigma'_2 &= \sigma_2 - p \\ \sigma'_3 &= \sigma_3 - p. \end{aligned} \tag{3.6}$$

This reduces the independent invariant quantities from three to two because $\sigma'_1 + \sigma'_2 + \sigma'_3 = 0$.

When generating and filtering each scalar principal stress (σ_1, σ_2, or σ_3), we begin with Gaussian random noise, clip it at the three standard deviation level, and then

apply the 3D filtering described in Chapter 2 to produce 3D filtered heterogeneity with 1D spectral falloffs of some specified α. The Gaussian white noise that we start with is clipped at the three standard deviation level to remove extreme outliers because in the real Earth there is probably a limit on the amplitude of deviatoric stress, perhaps 200 MPa, beyond which the rock will begin to fail. Each scalar is given a zero mean; then the composite set of principal stresses (σ_1, σ_2, and σ_3) are given an overall size defined by $\bar{I}_2' = 1.0$, where

$$I_2' = {\sigma_{11}'}^2 + {\sigma_{22}'}^2 + {\sigma_{33}'}^2 + 2{\sigma_{12}'}^2 + 2{\sigma_{23}'}^2 + 2{\sigma_{13}'}^2 \tag{3.7}$$

or

$$I_2' = {\sigma_1'}^2 + {\sigma_2'}^2 + {\sigma_3'}^2. \tag{3.8}$$

We choose $\bar{\sigma}_1 = 0.0$, $\bar{\sigma}_2 = 0.0$, and $\bar{\sigma}_3 = 0.0$ when generating our heterogeneous stress tensor, $\boldsymbol{\sigma}_H'(\mathbf{x}_i)$, so that any mean values will be subsumed into the spatially homogeneous background stress tensor, $\boldsymbol{\sigma}_B'$. This means that there are times when $\sigma_3 > \sigma_2 > \sigma_1$ does not hold for the heterogeneous principal stresses. The problem can be solved by sorting the principal stresses and their associated orientations to produce degenerate principal stress orientations. However, we will visualize the principal stresses in Figures 3.1–3.2 without sorting.

Figure 3.1 shows σ_1 and σ_1' for 10,000 Gaussian random points along a 1D length, filtered with $\alpha = 0.0$, $\alpha = 0.5$, $\alpha = 1.0$, and $\alpha = 1.5$. The left-hand plots display the filtered principal stresses, and the right-hand plots display the Fourier transform of the principal stresses as a function of spatial frequency. Additionally, on the right-hand plots, a straight, thick black line shows the expected α spectral falloff. Since σ_1, σ_2,

and σ_3 are generated using the identical process, it is only necessary to plot one of the principal stresses to show the filtered properties. The main point of the plots in Figure 3.1 is to show that indeed our principal stresses, σ_1, σ_2, and σ_3, and deviatoric principal stresses, σ_1', σ_2', and σ_3', have the correct spectral falloff. They should because it is a simple application of the principle already demonstrated in Chapter 2. It is not unexpected that our deviatoric principal stresses also have the correct spectral falloff. Deviatoric stresses are the principal stresses with the pressure subtracted, where the pressure is described by equation (3.1). We know that for filtered random processes, the linear sum of filtered random processes have the same spectral properties as the two individual processes if the same filter is used. Specifically, if $R_1(x)$ and $R_2(x)$ are two Gaussian processes, then if

$$R(x) = R_1(x) + R_2(x) \tag{3.9}$$

and if $F(x)$ is a spatial filter,

$$\begin{aligned} F(x) * R(x) &= F(x) * \left[R_1(x) + R_2(x) \right] \\ &= F(x) * R_1(x) + F(x) * R_2(x). \end{aligned} \tag{3.10}$$

Figure 3.2 shows plots of 2D cross sections through 3D grids of 201x201x201 points. The principal stress, σ_1, the deviatoric principal stress, σ_1', and the pressure, p, are shown for $\alpha = 0.0$, $\alpha = 0.5$, $\alpha = 1.0$, and $\alpha = 1.5$. For each α, the 2D cross section of stress is visualized two different ways: 1) On the left, are surface plots where the vertical amplitude and color corresponds to the amplitude of the scalar principal stress. 2) On the right, are map view plots, where only the color corresponds to the amplitude of the scalar principal stress. The 2D cross sections are taken from the same location in each 3D grid, about halfway along the $\hat{z}$ axis.

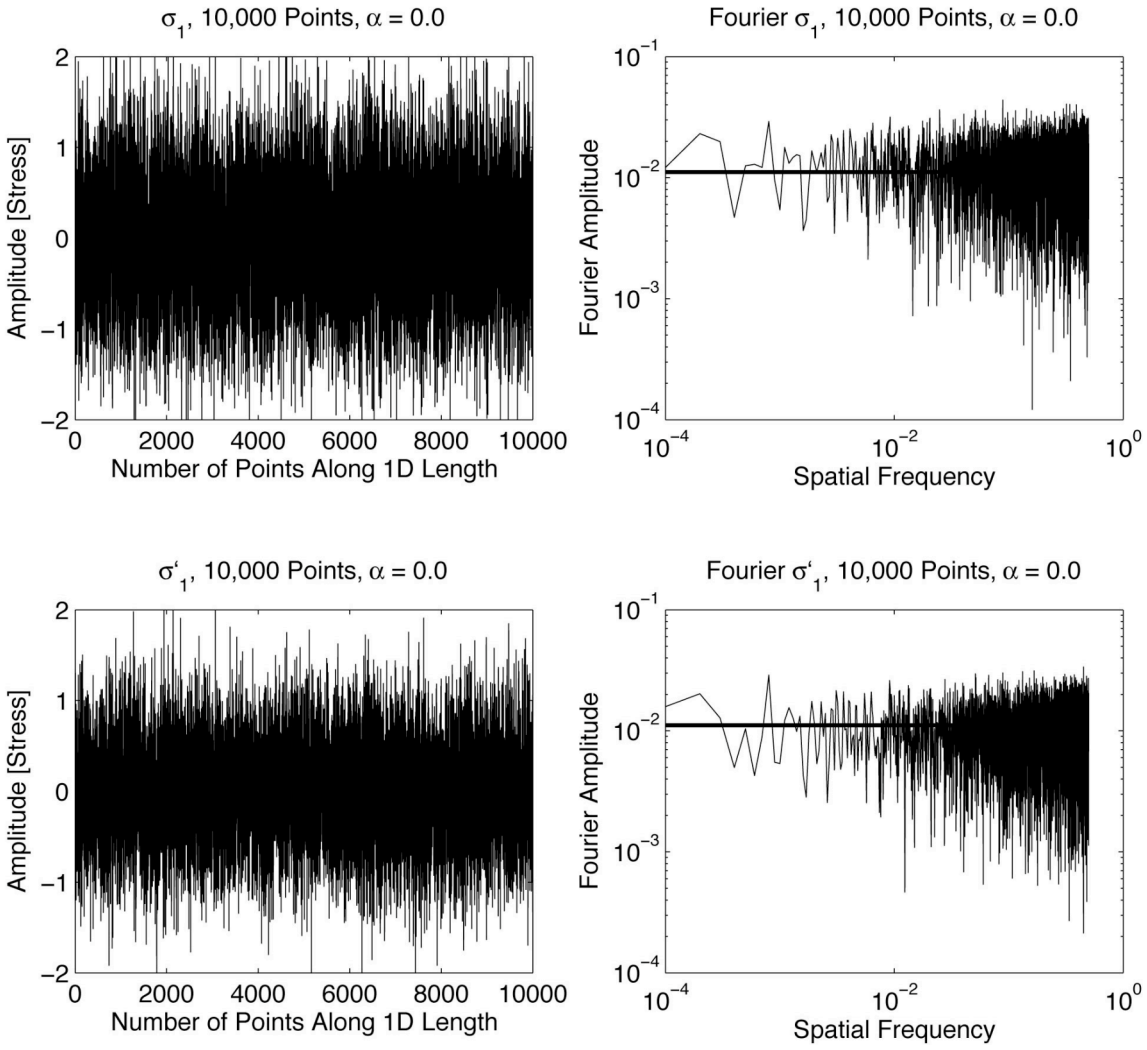
σ1, 10,000 Points, α = 0.0
Amplitude [Stress]
Number of Points Along 1D Length
Fourier σ1, 10,000 Points, α = 0.0
Fourier Amplitude
Spatial Frequency
σ'1, 10,000 Points, α = 0.0
Amplitude [Stress]
Number of Points Along 1D Length
Fourier σ'1, 10,000 Points, α = 0.0
Fourier Amplitude
Spatial Frequency

Figure 3.1 a)

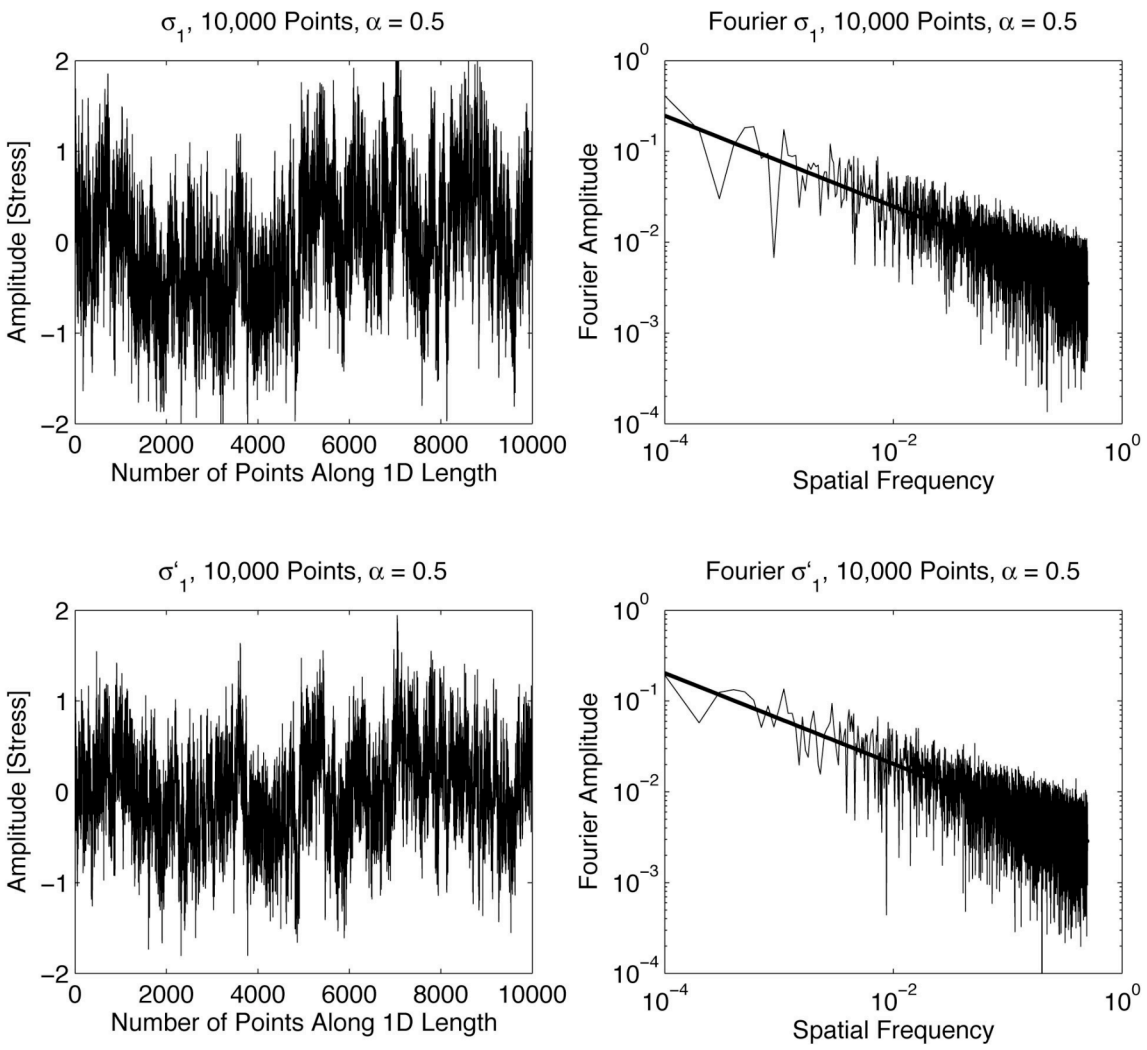
σ1, 10,000 Points, α = 0.5
Amplitude [Stress]
Number of Points Along 1D Length
Fourier σ1, 10,000 Points, α = 0.5
Fourier Amplitude
Spatial Frequency
σ'1, 10,000 Points, α = 0.5
Amplitude [Stress]
Number of Points Along 1D Length
Fourier σ'1, 10,000 Points, α = 0.5
Fourier Amplitude
Spatial Frequency

Figure 3.1 b)

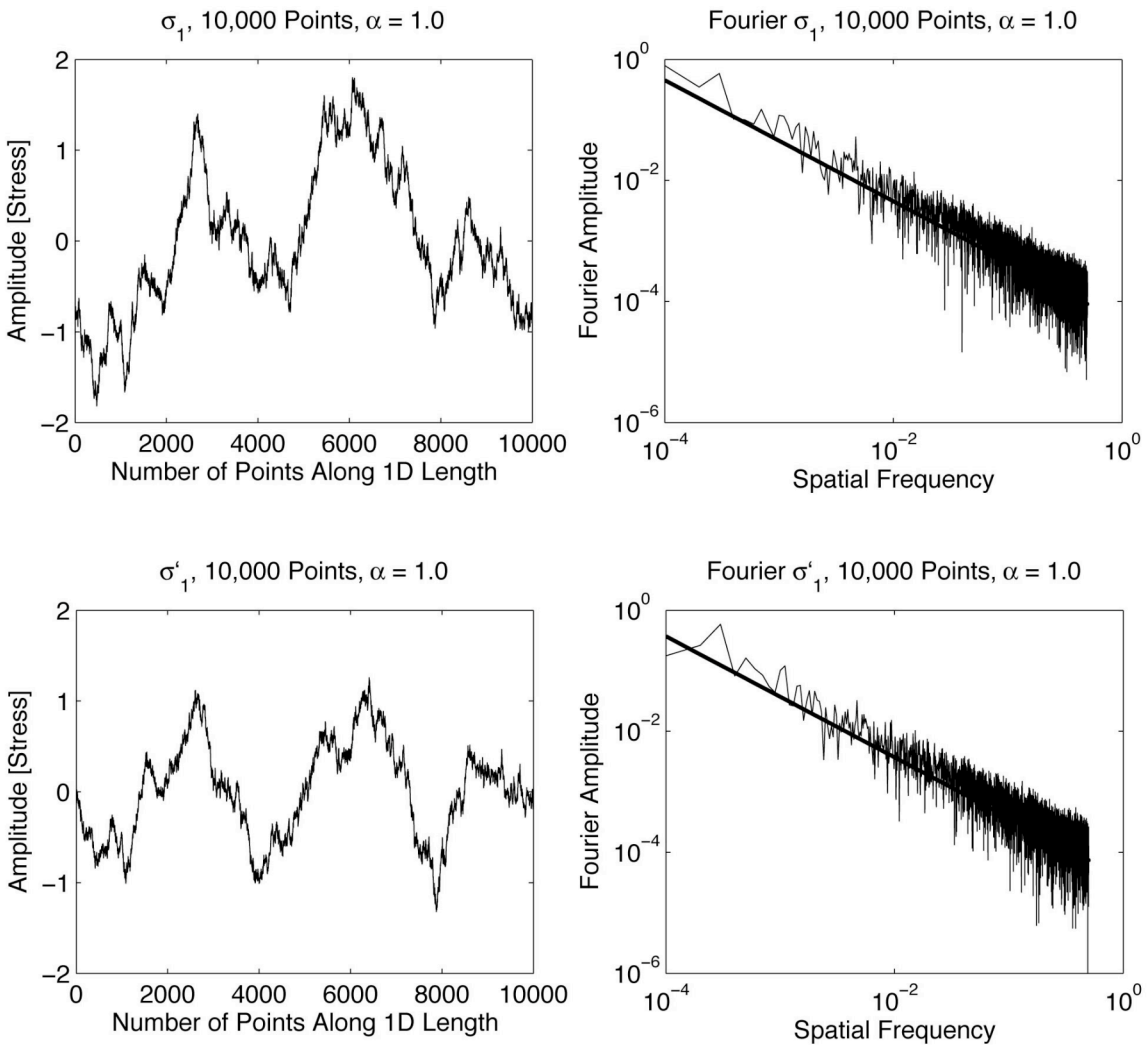
σ1, 10,000 Points, α = 1.0
Amplitude [Stress]
Number of Points Along 1D Length
Fourier σ1, 10,000 Points, α = 1.0
Fourier Amplitude
Spatial Frequency
σ'1, 10,000 Points, α = 1.0
Amplitude [Stress]
Number of Points Along 1D Length
Fourier σ'1, 10,000 Points, α = 1.0
Fourier Amplitude
Spatial Frequency

Figure 3.1 c)

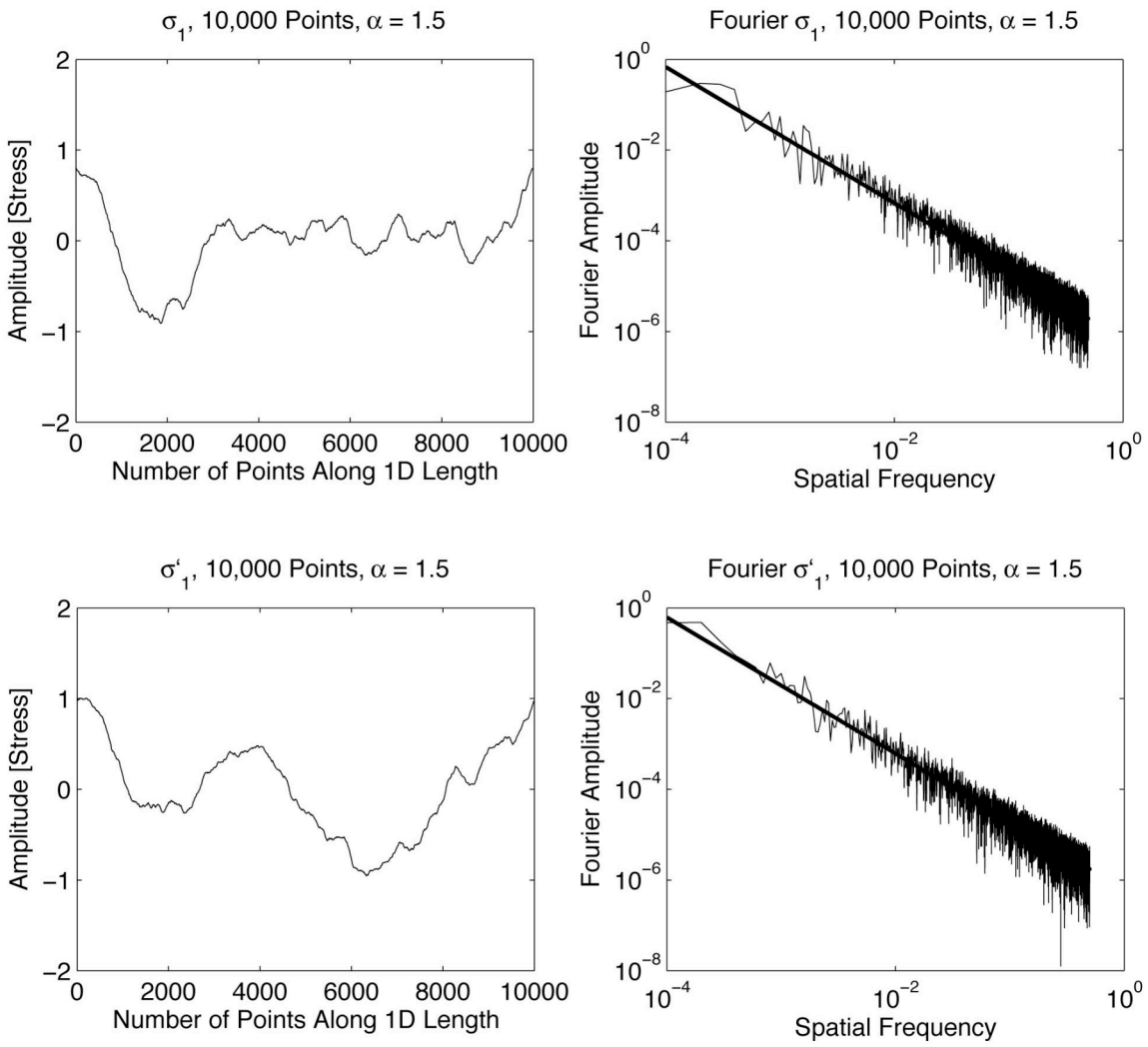
σ1, 10,000 Points, α = 1.5
Amplitude [Stress]
Number of Points Along 1D Length
Fourier σ1, 10,000 Points, α = 1.5
Fourier Amplitude
Spatial Frequency
σ'1, 10,000 Points, α = 1.5
Amplitude [Stress]
Number of Points Along 1D Length
Fourier σ'1, 10,000 Points, α = 1.5
Fourier Amplitude
Spatial Frequency

Figure 3.1 d)

Figure 3.1. *Filtered scalar invariants,* σ_1 *and* σ_1'*, for 10,000 points in 1D. We start with Gaussian white noise and apply the filtering strategy from Chapter 2 to produce* σ_1 *with spectral 1D falloffs of* α*. In* ***a)*** $\alpha = 0.0$ *is applied, which means no filtering of the Gaussian white noise,* ***b)*** $\alpha = 0.5$ *is applied,* ***c)*** $\alpha = 1.0$ *is applied, and* ***d)*** $\alpha = 1.5$ *is applied. Then we subtract out the pressure,* $p = (1/3)(\sigma_1 + \sigma_2 + \sigma_3)$ *to produce* σ_1' *with the same spectral 1D falloff as* σ_1*. On the left are plots of the filtered stresses as a function of 1D length, and on the right are the Fourier transforms of the stresses plotted as a function of spectral frequency. The desired* α *spectral falloff is represented by a thick black line, and we find that indeed the spectral falloff of the filtered principal stresses closely follows the desired falloff represented by the thick line.*

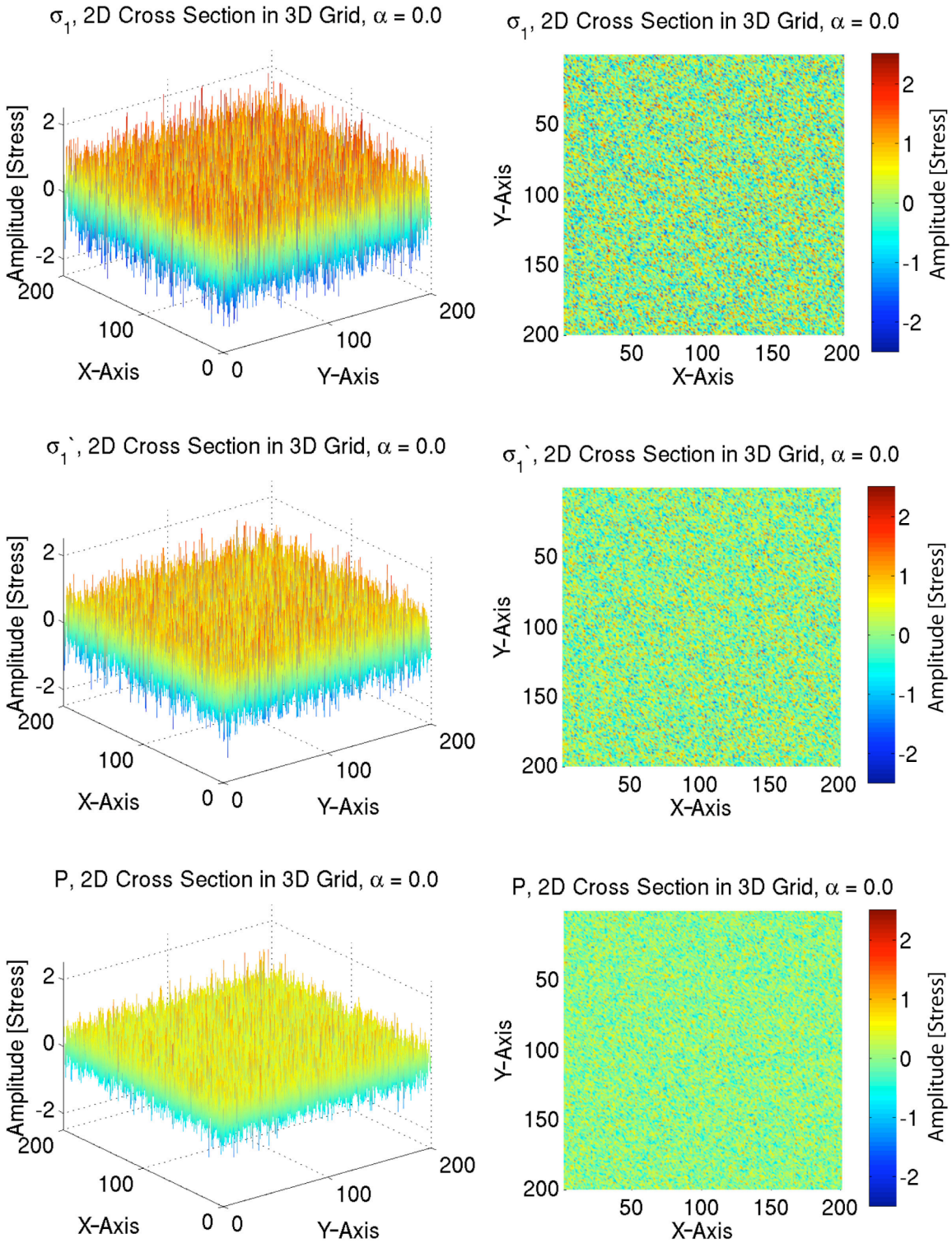
σ1, 2D Cross Section in 3D Grid, α = 0.0
Amplitude [Stress]
X-Axis
Y-Axis
σ1, 2D Cross Section in 3D Grid, α = 0.0
Y-Axis
X-Axis
Amplitude [Stress]
σ1`, 2D Cross Section in 3D Grid, α = 0.0
Amplitude [Stress]
X-Axis
Y-Axis
σ1`, 2D Cross Section in 3D Grid, α = 0.0
Y-Axis
X-Axis
Amplitude [Stress]
P, 2D Cross Section in 3D Grid, α = 0.0
Amplitude [Stress]
X-Axis
Y-Axis
P, 2D Cross Section in 3D Grid, α = 0.0
Y-Axis
X-Axis
Amplitude [Stress]

Figure 3.2 a)

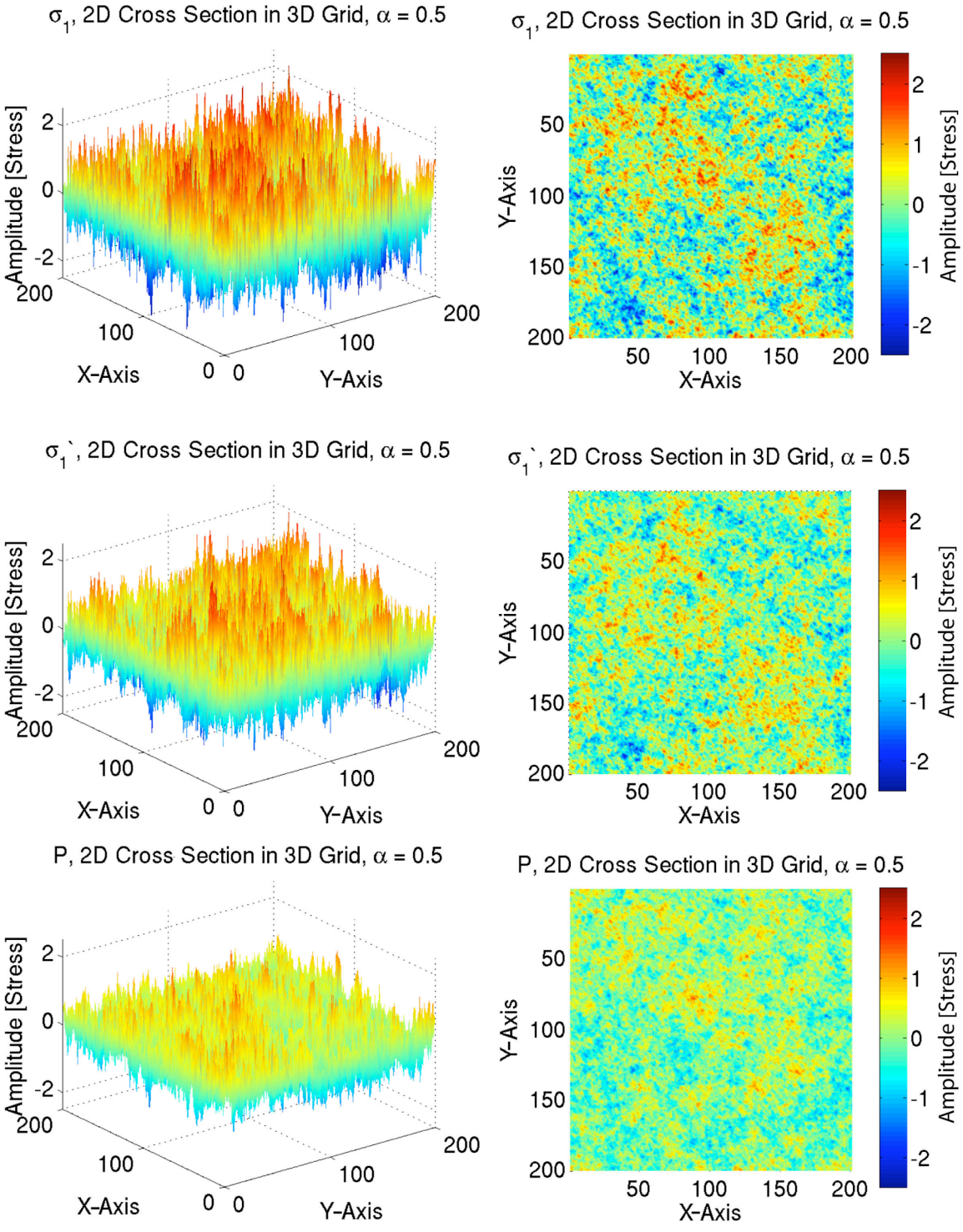
σ1, 2D Cross Section in 3D Grid, α = 0.5
Amplitude [Stress]
X-Axis
Y-Axis
σ1, 2D Cross Section in 3D Grid, α = 0.5
Y-Axis
X-Axis
Amplitude [Stress]
σ1`, 2D Cross Section in 3D Grid, α = 0.5
Amplitude [Stress]
X-Axis
Y-Axis
σ1`, 2D Cross Section in 3D Grid, α = 0.5
Y-Axis
X-Axis
Amplitude [Stress]
P, 2D Cross Section in 3D Grid, α = 0.5
Amplitude [Stress]
X-Axis
Y-Axis
P, 2D Cross Section in 3D Grid, α = 0.5
Y-Axis
X-Axis
Amplitude [Stress]

Figure 3.2 b)

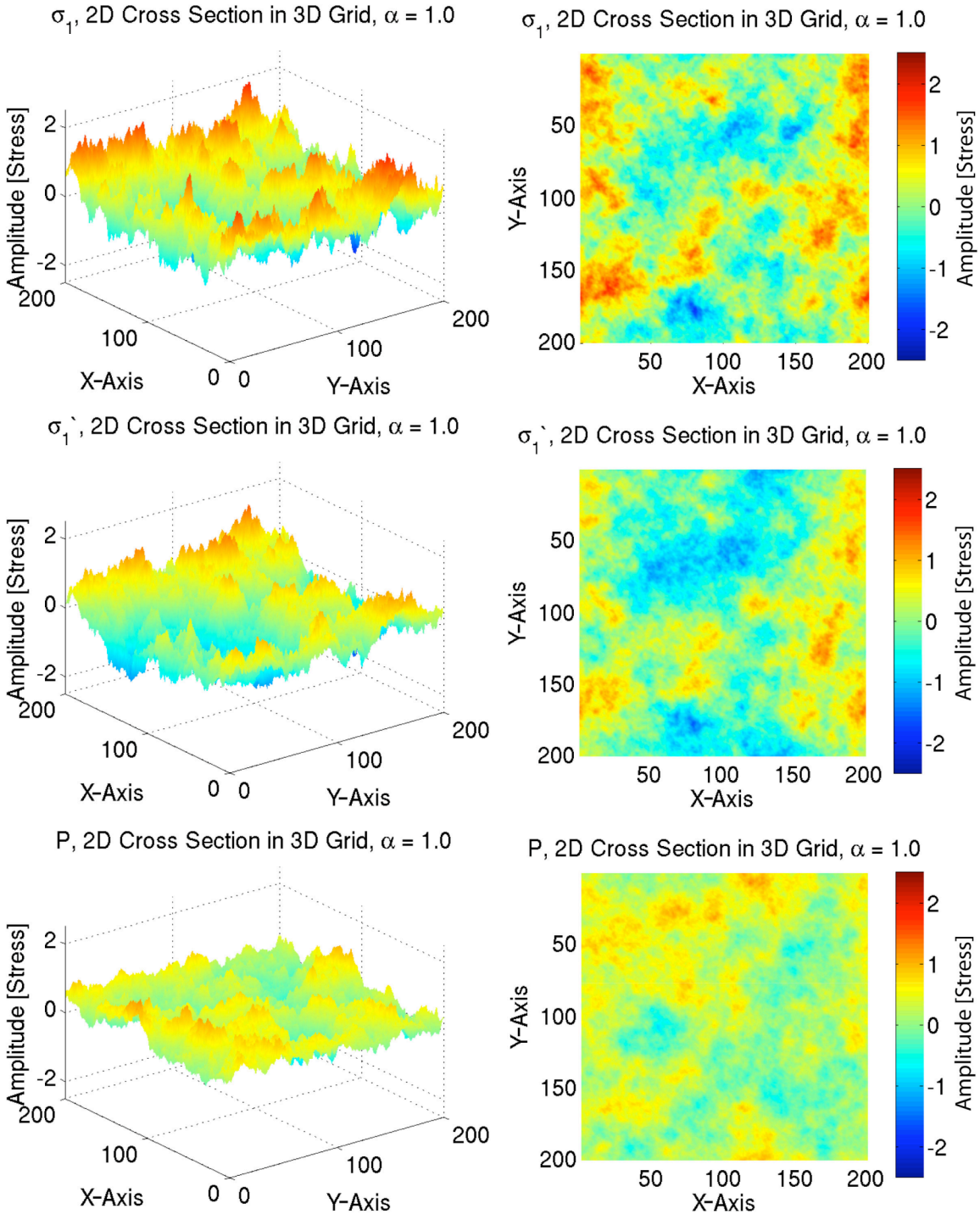
σ1, 2D Cross Section in 3D Grid, α = 1.0
Amplitude [Stress]
X-Axis
Y-Axis
σ1, 2D Cross Section in 3D Grid, α = 1.0
Y-Axis
X-Axis
Amplitude [Stress]
σ1`, 2D Cross Section in 3D Grid, α = 1.0
Amplitude [Stress]
X-Axis
Y-Axis
σ1`, 2D Cross Section in 3D Grid, α = 1.0
Y-Axis
X-Axis
Amplitude [Stress]
P, 2D Cross Section in 3D Grid, α = 1.0
Amplitude [Stress]
X-Axis
Y-Axis
P, 2D Cross Section in 3D Grid, α = 1.0
Y-Axis
X-Axis
Amplitude [Stress]

Figure 3.2 c)

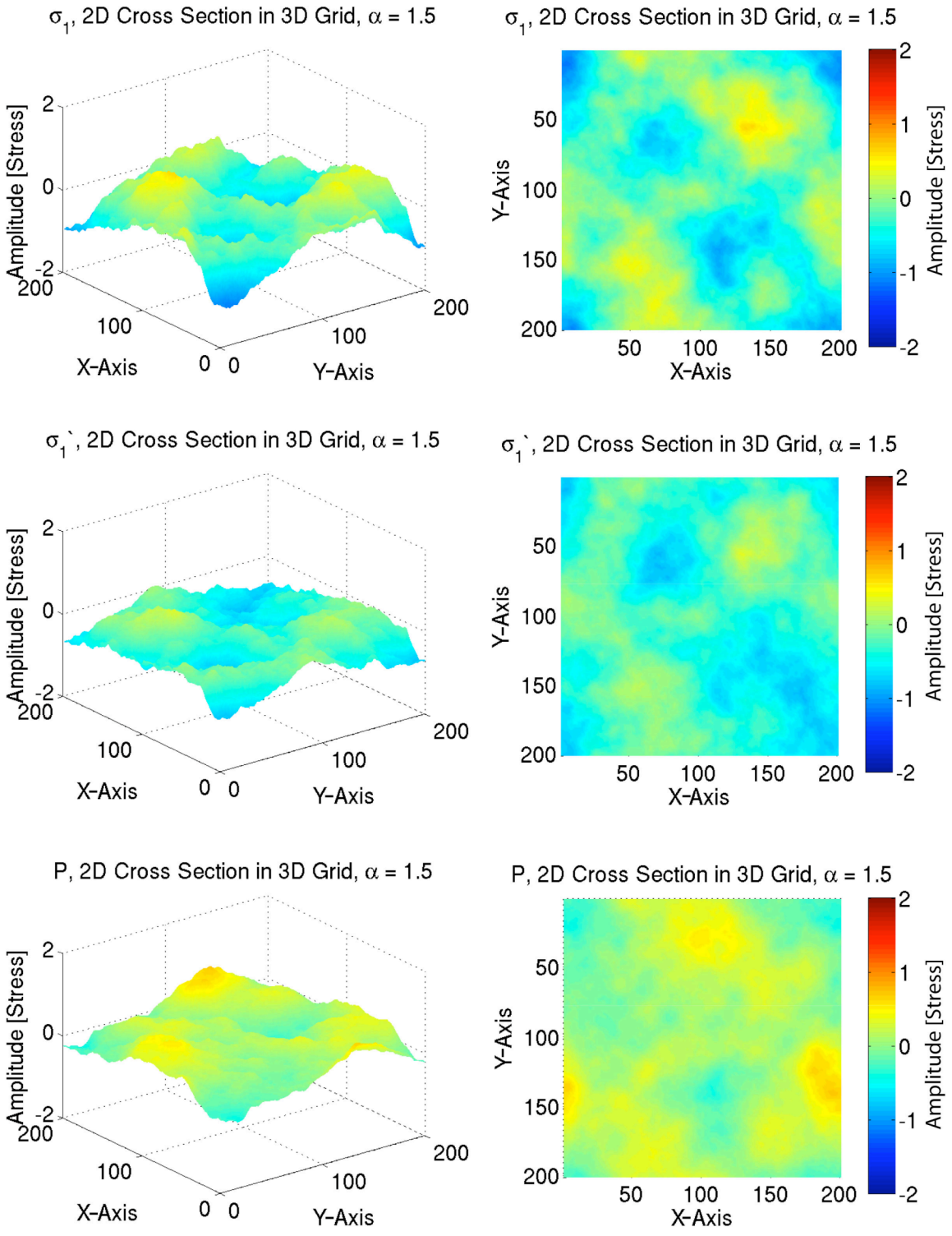
σ1, 2D Cross Section in 3D Grid, α = 1.5
Amplitude [Stress]
X-Axis
Y-Axis
σ1, 2D Cross Section in 3D Grid, α = 1.5
Y-Axis
X-Axis
Amplitude [Stress]
σ1`, 2D Cross Section in 3D Grid, α = 1.5
Amplitude [Stress]
X-Axis
Y-Axis
σ1`, 2D Cross Section in 3D Grid, α = 1.5
Y-Axis
X-Axis
Amplitude [Stress]
P, 2D Cross Section in 3D Grid, α = 1.5
Amplitude [Stress]
X-Axis
Y-Axis
P, 2D Cross Section in 3D Grid, α = 1.5
Y-Axis
X-Axis
Amplitude [Stress]

Figure 3.2 d)

Figure 3.2. *Plots of filtered scalar invariants,* σ_1, σ_1', *and* p *for 2D cross sections of 3D grids. The original 3D grids are 201x201x201; therefore, the 2D cross sections are 201x201 points. The cross sections are x-y planes at* $z = 101$, *approximately the center of the grid. We start with Gaussian white noise and apply the filtering strategy from Chapter 2 to produce filtered scalar invariants with spectral 1D falloffs of* α. *In* ***a)*** $\alpha = 0.0$ *is applied, which means no filtering of the Gaussian white noise,* ***b)*** $\alpha = 0.5$ *is applied,* ***c)*** $\alpha = 1.0$ *is applied, and* ***d)*** $\alpha = 1.5$ *is applied. On the left are surface plots of the filtered scalars where the 2 spatial dimensions of the 2D cross section are represented by the x and y axes and the amplitude of the scalar quantities is represented by the vertical height and color. On the right, are map view plots of the same 2D cross sections where the scalar amplitude is represented by color. The same color scale is used for the left and right hand plots, which goes from -2.5 to 2.5 for* $\alpha = 0.0$, $\alpha = 0.5$, *and* $\alpha = 1.0$ *and from -2.0 to 2.0 for* $\alpha = 1.5$.

Upon inspection one can notice a few features. The principal stress, σ_1, tends to have a larger amplitude than the deviatoric principal stress, σ_1', but similar spatial smoothing. By design as the value of α increases so does the spatial smoothing. Since Figure 3.2 shows only 2D cross sections through a 3D grid, and the mean is set to zero for the entire 3D grid, the means of the 2D cross sections are not necessarily zero; in fact, the means of the 2D cross sections are often non-zero.

Orientation Filtering

The next three quantities we wish to consider filtering are the three angles describing the orientation of the stress tensor. There are several sets of three angles we could choose. We could choose

- Three Euler angles that describe the rotation of a stress tensor relative to a reference orientation. This would be analogous to the strike, dip, and rake of slip vector on a fault plane.
- Azimuth and plunge of the P axis plus an angle describing the orientation of the T axis about the P axis
- A total rotation angle, ω, about a rotation axis, $[\theta,\phi]$ that represents a single rotation from a reference stress orientation to our desired point stress orientation.

The representation we prefer to use is the third one, a total rotation angle, ω, about a rotation axis, $[\theta,\phi]$. This seems to be the most natural set of three angles to filter if our intended goal is to filter stress tensor orientations. Namely, when we filter ω, we are simply filtering the amplitude of the rotation (amplitude of the spherical linear interpolation from the reference orientation to our desired orientation). When we filter

the angles in the rotation axis, $[\theta,\phi]$, we are filtering the axis about which the rotation takes place, where $[\theta,\phi]$ describe the path of the spherical linear interpolation. So by filtering these three quantities $(\omega,[\theta,\phi])$, we smooth out in space the total 3D orientation of the stress tensor. See Figures 3.3 and 3.4 for graphical explanations of this representation. Figure 3.3 explains how the rotation axis is defined; it passes from the origin through the point with colatitude, θ, and longitude, ϕ (this point is called the pole of rotation). Figure 3.4 shows how once the rotation axis is defined with $[\theta,\phi]$, we can then apply our single rotation of amplitude ω, about this axis, $[\theta,\phi]$.

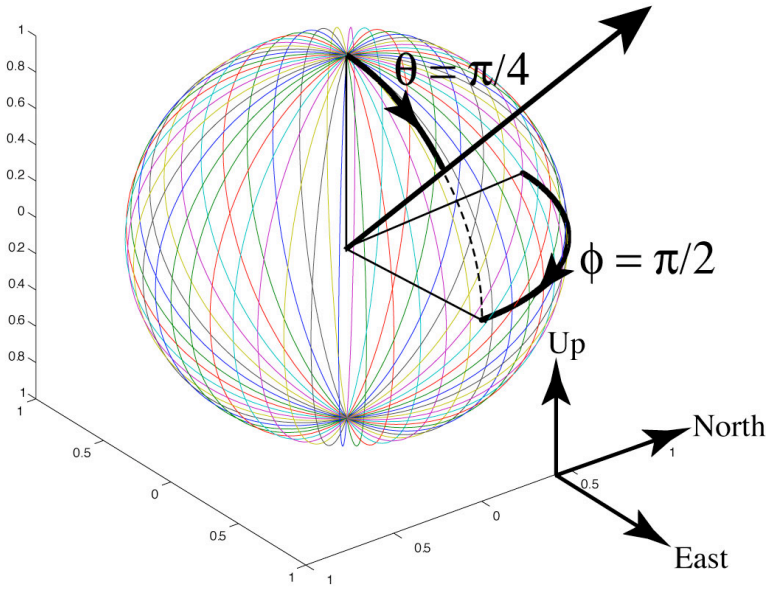

Figure 3.3. *How the rotation axis, $[\theta,\phi]$, is defined. The rotation axis, is the thick black arrow projecting out of the unit sphere. θ is the colatitude of the rotation axis, the angle between the Up vector and the rotation vector, while ϕ is the longitude of the rotation axis, the angle between the North vector and the horizontal projection of the rotation axis, in a right-hand coordinate system about the Up vector.*

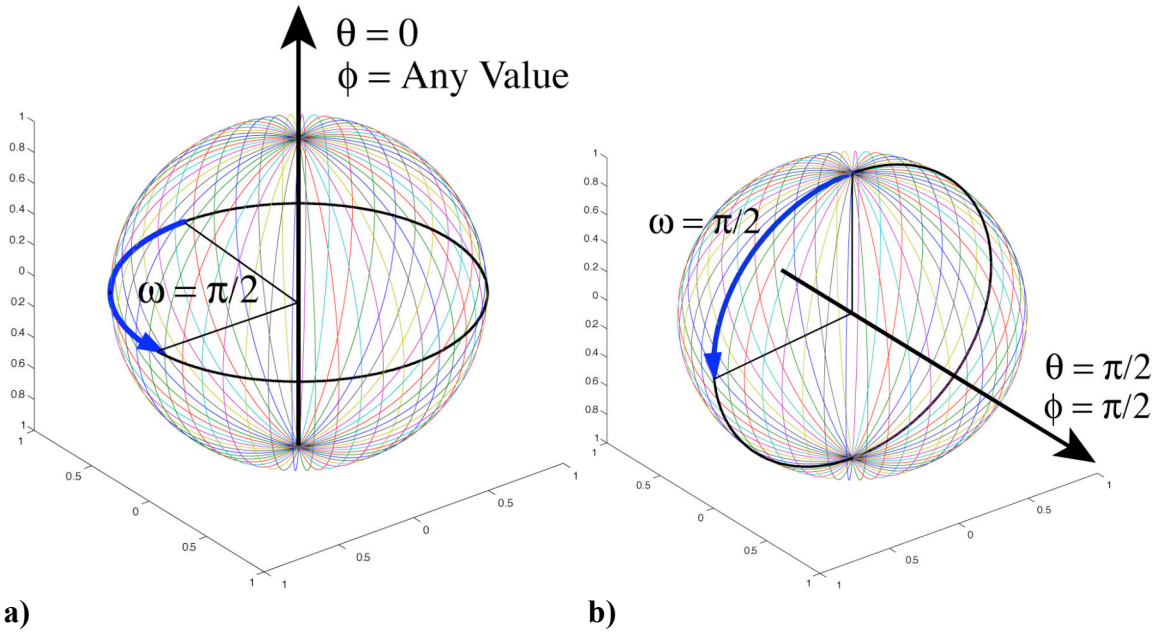

Figure 3.4. *Two examples of our* $(\omega,[\theta,\phi])$ *representation of 3D rotations. In* ***a)*** *we have* $\theta = 0$ *and* $\phi =$ *any value for the rotation axis. For* ***b)*** *we have* $\theta = \pi/2$ *and* $\phi = \pi/2$ *for the rotation axis. Both* ***a)*** *and* ***b)*** *have an* $\omega = \pi/2$ *rotation about their respective rotation axes.*

Now that we have defined the three scalar angles we wish to filter, an amplitude, ω, plus a rotation axis, $[\theta,\phi]$, how do we go about filtering them? We first wish to generate completely random sets of $(\omega,[\theta,\phi])$, then filter the three angles. Random sets of $(\omega,[\theta,\phi])$ are $(\omega,[\theta,\phi])$ such that the summation of N stress tensors as $N \to \infty$ combined with random σ_1', σ_2', and σ_3', produces an expected value of

$\boldsymbol{\sigma}' = \begin{pmatrix} 0.0 & 0.0 & 0.0 \\ 0.0 & 0.0 & 0.0 \\ 0.0 & 0.0 & 0.0 \end{pmatrix}$, i.e., $E\langle\boldsymbol{\sigma}'\rangle = 0$. This is important because when we create our filtered heterogeneous component of the stress tensor, there should be no net orientation to the deviatoric, heterogeneous term in 3D.

$$E\left\langle\boldsymbol{\sigma}'_{Heterogeneous}\right\rangle = 0 \tag{3.11}$$

To create truly random sets of $(\omega,[\theta,\phi])$, it is helpful to work in quaternion space, producing random quaternions, then transform them back to $(\omega,[\theta,\phi])$ space.

A quaternion is simply a four-component vector that represents a 3D rotation. Analogy can be used to understand this. To describe a point on a 3D unit sphere, there are two different ways to represent the position. One representation would be a three-component vector, $\vec{u} = [u_x, u_y, u_z]$, with the constraint that $|\vec{u}| = \sqrt{u_x^2 + u_y^2 + u_z^2} = 1$, so that the point lies on the surface of the 3D unit sphere. This reduces the degrees of freedom from three to two. Another representation would be in terms of two angles, θ and ϕ. In the case of a 4D unit hypersphere, we again have two possible analogous representations. We can use a four-component vector, a quaternion, $\vec{q} = [q_0, q_1, q_2, q_3]$, with the constraint that $|\vec{q}| = \sqrt{q_0^2 + q_1^2 + q_2^2 + q_3^2} = 1$, so that the point lies on the surface of the 4D unit sphere and the degrees of freedom reduce from four to three. Alternatively, we can use three angles, ω, θ, and ϕ. Thus this problem of producing random $(\omega,[\theta,\phi])$ reduces to the problem of choosing completely random points on the surface of a unit 4D hypersphere, which was solved by Marsaglia [1972].

The method of Marsaglia [1972] for picking random points on a 4D hypersphere, which produces unbiased 3D orientations, is summarized at the following web link http://mathworld.wolfram.com/HyperspherePointPicking.html [*Weisstein*]. In this method, one uses a uniform random number generator to pick pairs of points (x_1, x_2) and (x_3, x_4), keeping only those pairs that satisfy the following constraints, $x_1^2 + x_2^2 < 1$ and $x_3^2 + x_4^2 < 1$. For each set of points that are retained, one calculates the random quaternion, $\vec{q}^{\,R} = \left[q_0^R, q_1^R, q_2^R, q_3^R\right]$, as follows,

$$\begin{aligned} q_0^R &= x_4\sqrt{\frac{1-x_1^2-x_2^2}{x_3^2+x_4^2}} \\ q_1^R &= x_1 \\ q_2^R &= x_2 \\ q_3^R &= x_3\sqrt{\frac{1-x_1^2-x_2^2}{x_3^2+x_4^2}} \end{aligned} \quad . \tag{3.12}$$

Once the random unit quaternions are calculated, we then transform the four-vectors into their equivalent angles, $(\omega, [\theta, \phi])$. We use the standard relation between a quaternion, $\vec{q} = \left[q_0, q_1, q_2, q_3\right]$, and our set of angles, $(\omega, [\theta, \phi])$

$$\begin{aligned} q_0 &= \cos(\omega/2) \\ q_1 &= \sin(\omega/2)\sin(\theta)\cos(\phi) \\ q_2 &= \sin(\omega/2)\sin(\theta)\sin(\phi) \\ q_3 &= \sin(\omega/2)\cos(\theta) \end{aligned} \tag{3.13}$$

where

$$|\vec{q}| = \sqrt{q_0^2 + q_1^2 + q_2^2 + q_3^2} = 1.$$

Conversely, we can turn the quaternions into our three angles, ω, θ, and ϕ.

$$\begin{aligned}\omega &= 2\cos^{-1}\left(q_0\right)\\ \theta &= \cos^{-1}\left(q_3 / \sin\left(\omega/2\right)\right)\\ \phi &= \tan^{-1}\left(q_2/q_1\right)\end{aligned} \tag{3.14}$$

where $0° \le \omega \le 360°$, $0° \le \theta \le 180°$, and $0° \le \phi \le 360°$.

After generating random points on the 4D hypersphere (quaternions) and transforming these points into our orientation representation, $\left(\omega,[\theta,\phi]\right)$, we can now filter these three angles separately using the scalar filtering technique outlined in the previous chapter. As we will show in Figures 3.11, the filtering process introduces an orientation bias. We remove this bias by stacking at least 10–20 simulations where a random rotation has been added to the orientations in each simulation. Any orientation bias cancels out in the stacking process also seen in Figure 3.11.

To add a random rotation to our stress orientations, we again employ quaternions. Quaternions allow rotations to be added algebraically. For example, if we have a stress tensor orientation represented by the quaternion $\vec{q}^{\,A} = \left[q_0^A, q_1^A, q_2^A, q_3^A\right]$ and we wish to add on the 3D rotation represented by quaternion $\vec{q}^{\,B} = \left[q_0^B, q_1^B, q_2^B, q_3^B\right]$ to produce a final orientation represented by quaternion $\vec{q}^{\,C} = \left[q_0^C, q_1^C, q_2^C, q_3^C\right]$, the algebra would simply be (adapted from http://www.mathworks.com/access/helpdesk/help/toolbox/aeroblks/aeroblks.html, Quaternion Multiplication) [*Mathworks*, 1994-2006],

$$\begin{aligned}q_0^C &= q_0^B q_0^A - q_1^B q_1^A - q_2^B q_2^A - q_3^B q_3^A\\ q_1^C &= q_0^B q_1^A + q_1^B q_0^A - q_2^B q_3^A + q_3^B q_2^A\\ q_2^C &= q_0^B q_2^A + q_1^B q_3^A + q_2^B q_0^A - q_3^B q_1^A\\ q_3^C &= q_0^B q_3^A - q_1^B q_2^A + q_2^B q_1^A + q_3^B q_0^A.\end{aligned} \tag{3.15}$$

As expected, the order of rotations is important, i.e., rotations are noncommutative.

Figure 3.6 shows 1D plots of our filtered orientation angles, $(\omega,[\theta,\phi])$, before and after random rotations have been added. The amplitude angles, ω, are plotted on the left as a function of 1D linear distance, and the rotation axes, $[\theta,\phi]$, are plotted on the right as points on an equal area plot where $0° < \omega < 360°$, $0° < \theta < 180°$, and $0° < \phi < 360°$. The longitude, ϕ, is represented by the azimuthal angle about the circular, equal area plot as shown in Figure 3.5, and θ is represented by the radial distance from the center of the circle. $\theta = 0°$ at the center, and $\theta = 180°$ at the circumference. At first this may seem like an odd representation until one thinks about the plot in terms of latitude, $\lambda = 90° - \theta$, instead of the colatitude, θ. In terms of the latitude, λ, $\lambda = 90°$ at the center and $\lambda = –90°$ at the circumference, which is similar to an equal area P-T plot that shows the full plunge range of $\pm\ 90°$.

The top and bottom rows show $(\omega,[\theta,\phi])$, where random orientations have been filtered with an α then multiplied with a reference quaternion. The top row shows the unrotated $(\omega,[\theta,\phi])$, and the bottom row shows the rotated $(\omega,[\theta,\phi])$. When the reference quaternion is $[q_0 = 1, q_1 = 0, q_2 = 0, q_3 = 0]$, as seen in the top row, $(\omega,[\theta,\phi])$ is unchanged upon multiplication, because $[q_0 = 1, q_1 = 0, q_2 = 0, q_3 = 0]$ produces no rotation; $\omega = 2\cos^{-1}(q_0) = 2\cos^{-1}(1.0) = 0°$. When the reference quaternion is something other than $[q_0 = 1, q_1 = 0, q_2 = 0, q_3 = 0]$, as seen in the bottom row, $(\omega,[\theta,\phi])$ is rotated upon quaternion multiplication.

If there is no filtering, $\alpha = 0.0$, then our $(\omega,[\theta,\phi])$s are produced using the random unit quaternion generator, and the rotation axes, $[\theta,\phi]$, are uniformly distributed on the equal area plot as seen in Figure 3.6 a). As the filtering constant, α, increases, the spatial smoothing of $(\omega,[\theta,\phi])$ increases: 1) ω becomes smoother as a function of distance. 2) The rotation axes, $[\theta,\phi]$, at first clump for $\alpha = 0.5$ and $\alpha = 1.0$, then track a clearly distinguishable linear path on the equal area plot for $\alpha = 1.5$. The rotated and unrotated cases have fairly similar properties (degree of spatial smoothing, clumping, etc.); therefore, we should be able to stack the filtered and randomly rotated $(\omega,[\theta,\phi])$s to produce no net orientation, while maintaining to first order, the α-filtered properties of each individual run.

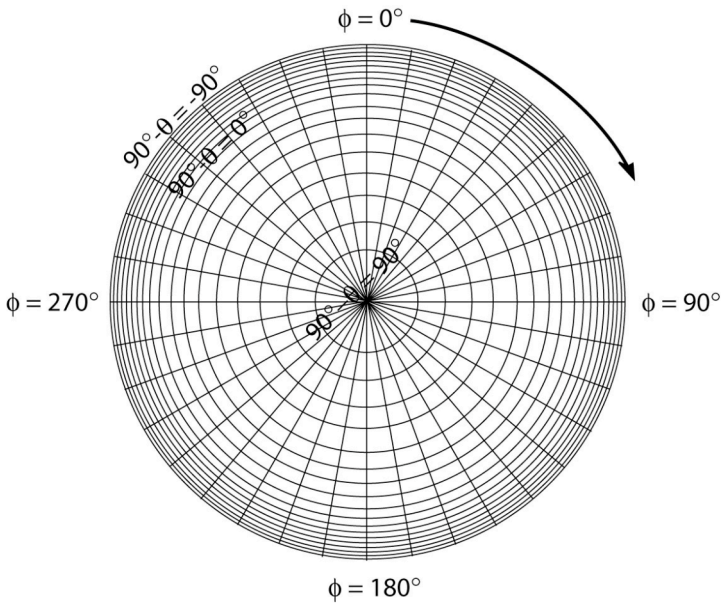

Figure 3.5. *A cartoon of the equal area plots used in Figure 3.6 for the rotation axes,* $[\theta,\phi]$. *The longitude,* ϕ*, is the azimuth of the circle, and latitude,* $\lambda = 90° - \theta$*, is plotted as a function of radial distance where,* $\lambda = 90° - \theta = 90°$ *at the center and* $\lambda = 90° - \theta = -90°$*, at the circumference. Note the cartoon is not necessarily to scale.*

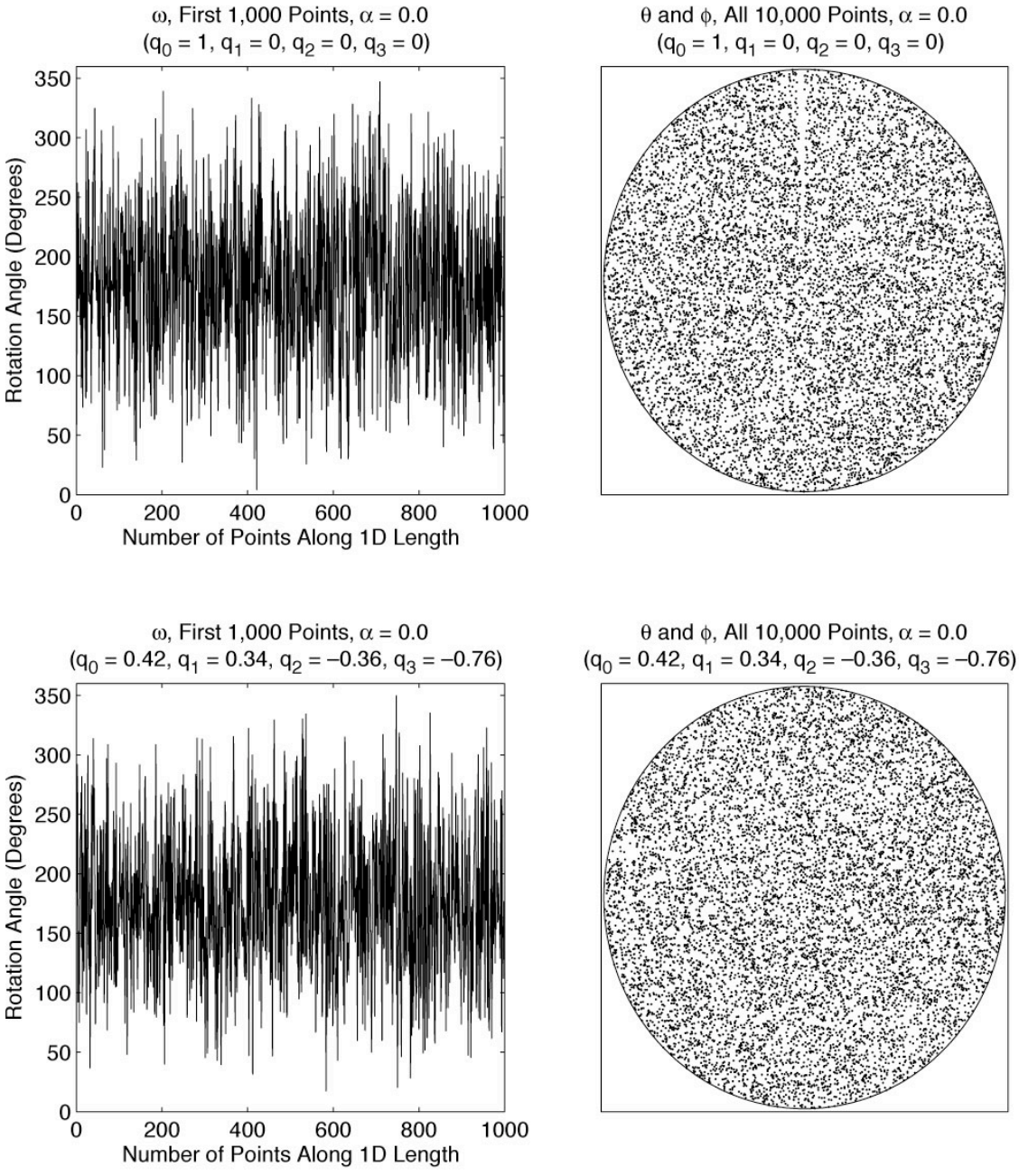
ω, First 1,000 Points, α = 0.0
(q0 = 1, q1 = 0, q2 = 0, q3 = 0)
θ and ϕ, All 10,000 Points, α = 0.0
(q0 = 1, q1 = 0, q2 = 0, q3 = 0)
Rotation Angle (Degrees)
Number of Points Along 1D Length
ω, First 1,000 Points, α = 0.0
(q0 = 0.42, q1 = 0.34, q2 = –0.36, q3 = –0.76)
θ and ϕ, All 10,000 Points, α = 0.0
(q0 = 0.42, q1 = 0.34, q2 = –0.36, q3 = –0.76)
Rotation Angle (Degrees)
Number of Points Along 1D Length

Figure 3.6 a)

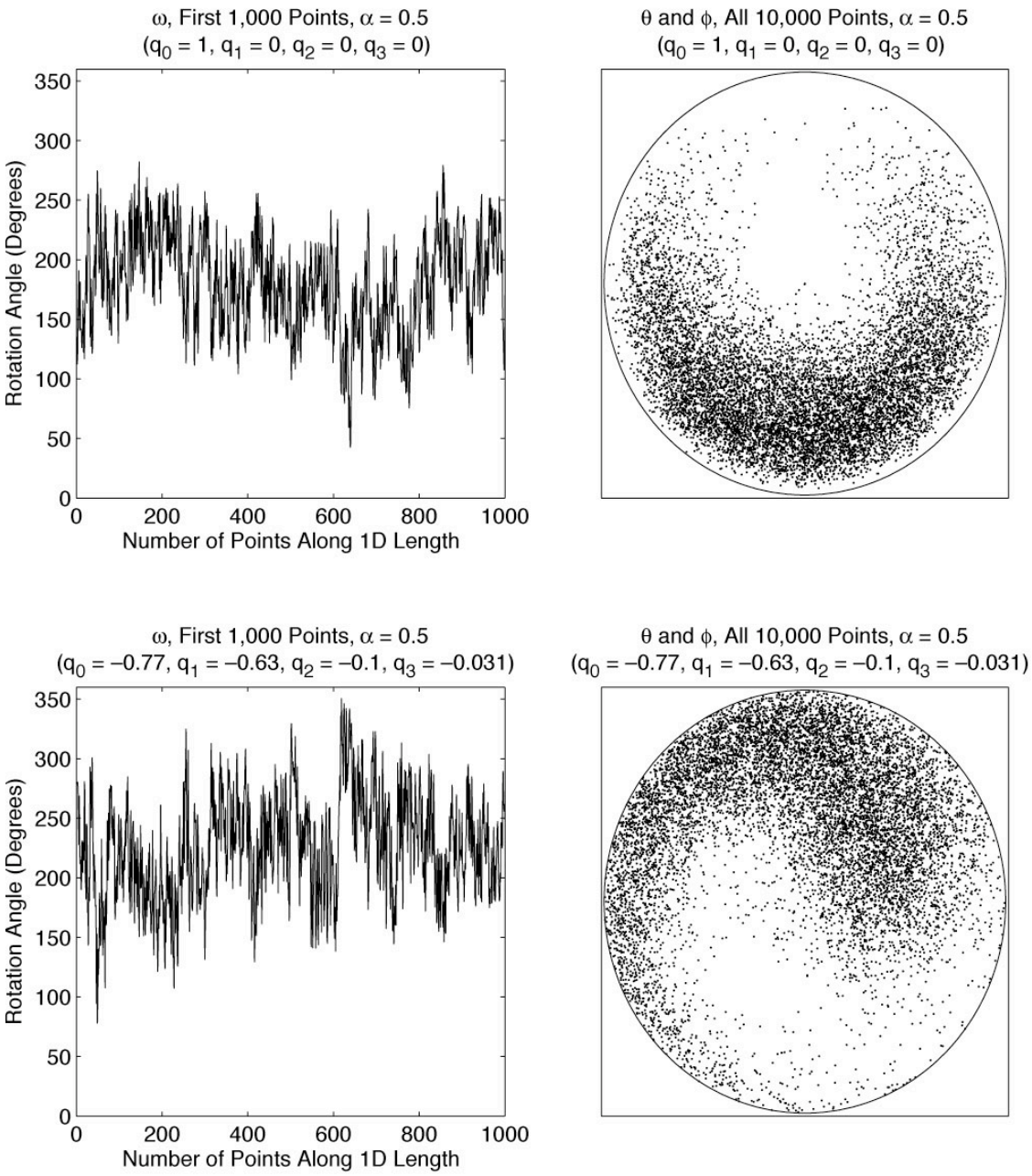
ω, First 1,000 Points, α = 0.5
(q0 = 1, q1 = 0, q2 = 0, q3 = 0)
θ and ϕ, All 10,000 Points, α = 0.5
(q0 = 1, q1 = 0, q2 = 0, q3 = 0)
Rotation Angle (Degrees)
Number of Points Along 1D Length
ω, First 1,000 Points, α = 0.5
(q0 = −0.77, q1 = −0.63, q2 = −0.1, q3 = −0.031)
θ and ϕ, All 10,000 Points, α = 0.5
(q0 = −0.77, q1 = −0.63, q2 = −0.1, q3 = −0.031)
Rotation Angle (Degrees)
Number of Points Along 1D Length

Figure 3.6 b)

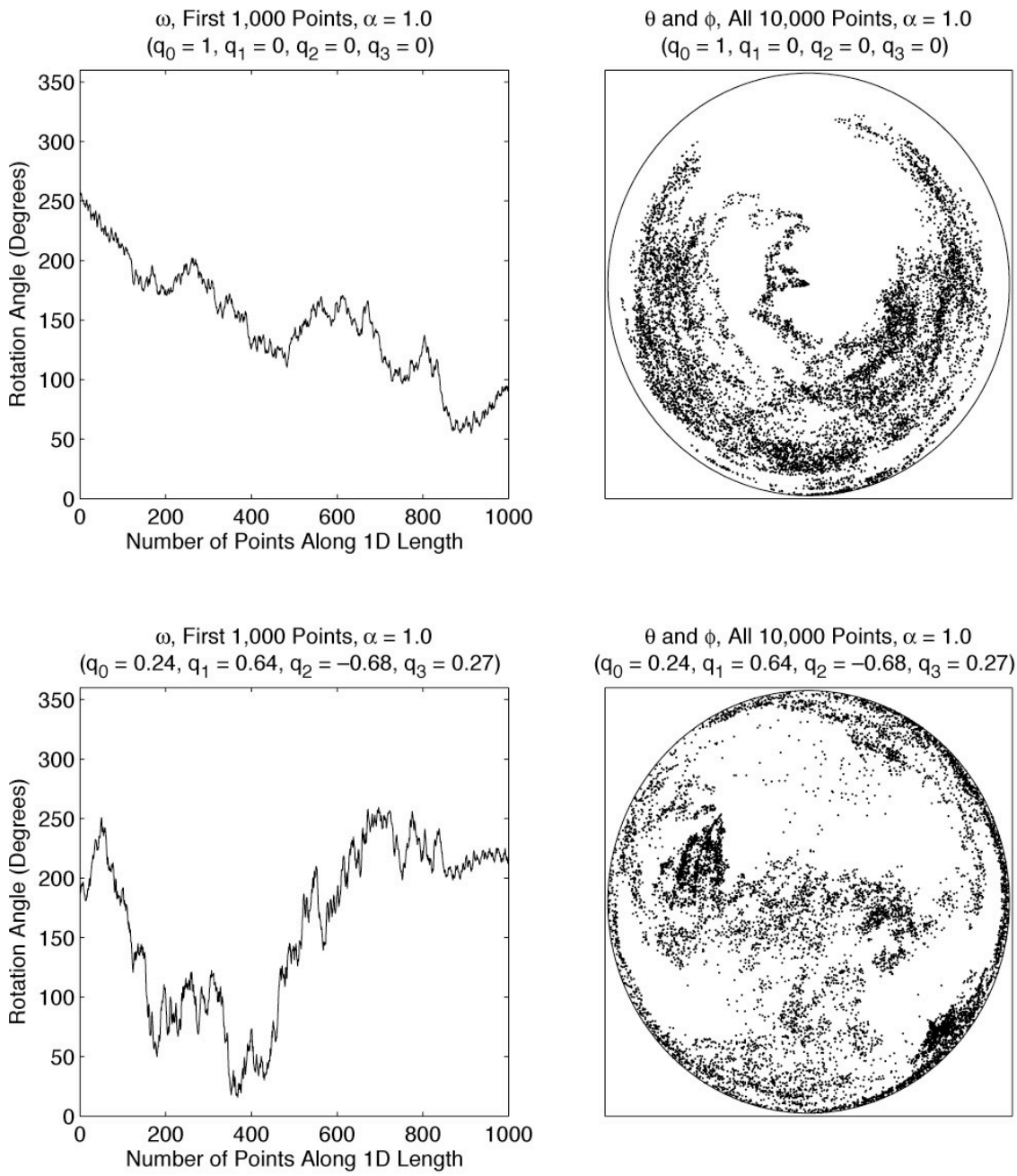
ω, First 1,000 Points, α = 1.0
(q0 = 1, q1 = 0, q2 = 0, q3 = 0)
θ and ϕ, All 10,000 Points, α = 1.0
(q0 = 1, q1 = 0, q2 = 0, q3 = 0)
Rotation Angle (Degrees)
Number of Points Along 1D Length
ω, First 1,000 Points, α = 1.0
(q0 = 0.24, q1 = 0.64, q2 = −0.68, q3 = 0.27)
θ and ϕ, All 10,000 Points, α = 1.0
(q0 = 0.24, q1 = 0.64, q2 = −0.68, q3 = 0.27)
Rotation Angle (Degrees)
Number of Points Along 1D Length

Figure 3.6 c)

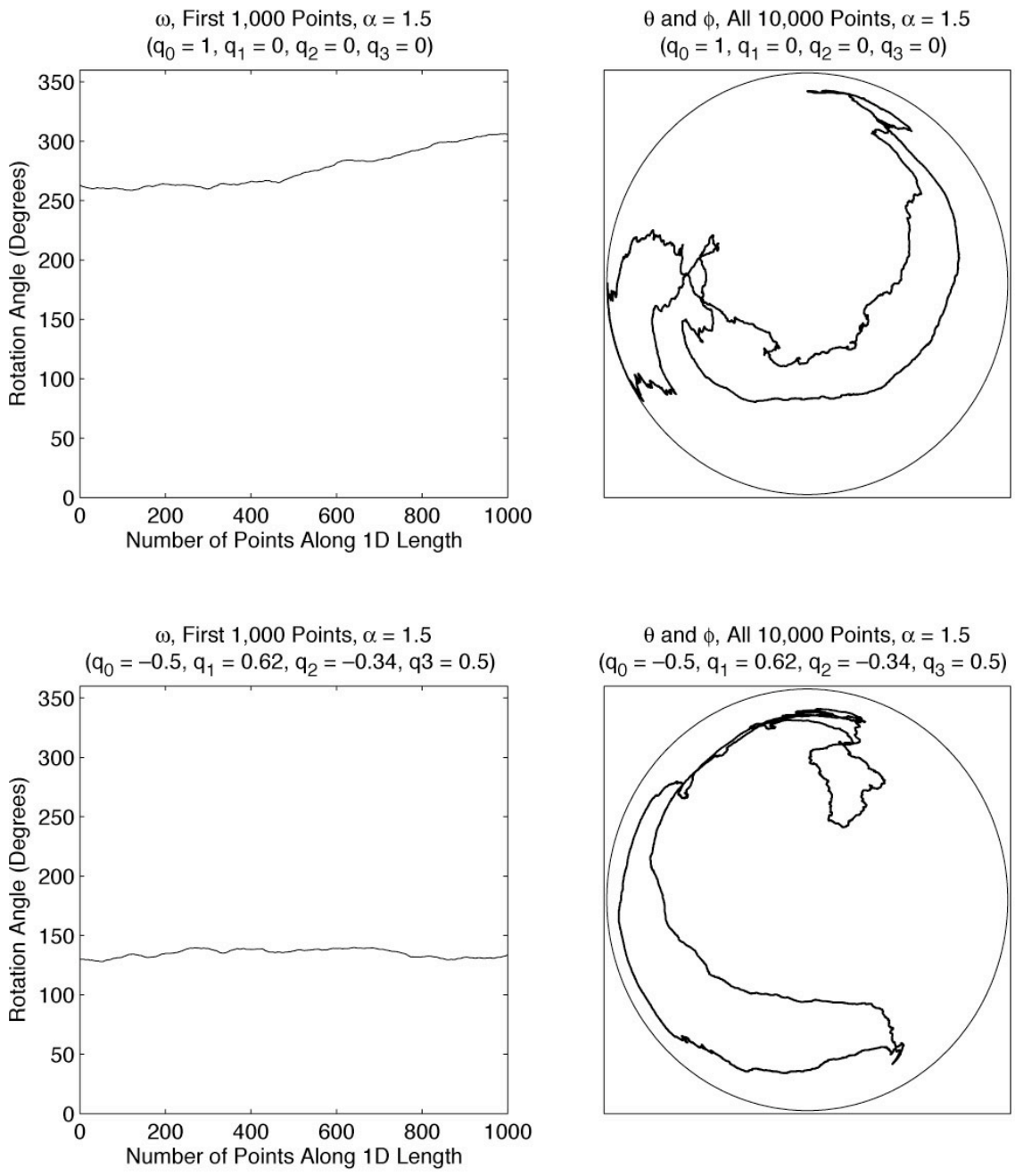
ω, First 1,000 Points, α = 1.5
(q0 = 1, q1 = 0, q2 = 0, q3 = 0)
θ and ϕ, All 10,000 Points, α = 1.5
(q0 = 1, q1 = 0, q2 = 0, q3 = 0)
Rotation Angle (Degrees)
Number of Points Along 1D Length
ω, First 1,000 Points, α = 1.5
(q0 = –0.5, q1 = 0.62, q2 = –0.34, q3 = 0.5)
θ and ϕ, All 10,000 Points, α = 1.5
(q0 = –0.5, q1 = 0.62, q2 = –0.34, q3 = 0.5)
Rotation Angle (Degrees)
Number of Points Along 1D Length

Figure 3.6 d)

Figure 3.6. *A series of 1D simulations are shown with different degrees of smoothing, α, applied where* ***a)*** $\alpha = 0.0$, ***b)*** $\alpha = 0.5$, ***c)*** $\alpha = 1.0$, *and* ***d)*** $\alpha = 1.5$. *Each simulation is approximately 10,000 points. For each α, there are a total of four subplots. On the top left is a 1,000-points-long segment of the filtered rotation angle, ω. As expected, as α increases, the spatial smoothness of the rotation angle, ω, increases. On the bottom left is again ω, but after a random rotation has been applied to the orientation angles. It appears to maintain its filtered properties to first order upon inspection. See Figure 3.8 for a more thorough evaluation of what happens to the spectral properties upon rotation of coordinate system. On the top right is an equal area plot with the rotation axes, $[\theta,\phi]$, plotted as black dots. On the bottom right is another equal area plot of the rotation poles, $[\theta,\phi]$, after a random rotation has been applied. Again the spatially smoothed rotation poles maintain their spectral properties to first order.*

For $\alpha = 0.0$, no spatial smoothing or completely random orientations produce completely random rotation poles on our equal area plot. This unbiased distribution remains unchanged upon rotation of coordinate systems. As α increases, the rotation poles begin clumping together until they form 1D lines, representing the wander of the 1D data set.

In Figure 3.7, our three orientation angles, $(\omega,[\theta,\phi])$, for 1D simulations are visualized in a different way. 3D unit spheres have been plotted with a wire mesh, then the position of the rotation axes, $[\theta,\phi]$, are plotted as points on the sphere. Last, the color of the points represents the amplitude angle, ω according to the horizontal color bars underneath. On the left, are the unrotated, $(\omega,[\theta,\phi])$, and on the right are the rotated, $(\omega,[\theta,\phi])$. When there is no filtering, $\alpha = 0.0$, the rotation axes, $[\theta,\phi]$, are uniformly distributed over the sphere, and the color, which represents the amplitude, ω, is random. Additionally, when $\alpha = 0.0$ the angles, $(\omega,[\theta,\phi])$, appear to be unchanged upon rotation. There is the same random pattern after rotation as before. As the filtering, α, increases, the spatial smoothing of the points on the sphere increases, and the spatial smoothing of the colors increases, representing the smoothing of the three angles, $(\omega,[\theta,\phi])$, until at $\alpha = 1.5$ the data form clear demarcated linear tracks. The rotated data on the right have similar smoothness as the unrotated data to first order.

The spectral properties of the unrotated and rotated ω are plotted in Figure 3.8 to examine how closely our filtered angles approach the desired α spectral falloff. While not shown, the rotation axes, $[\theta,\phi]$, have similar properties, but ϕ is more difficult to plot because one needs to wrap the phase appropriately before calculating the spectral properties. The plots on the left in Figure 3.8 show the angle ω as a function of 1D length, and the plots on the right in Figure 3.8 show the Fourier transform of the angle ω as a function of spatial frequency. The right-hand plots also have a thick black line, which shows the desired α spectral falloff. To first order, ω, follows the desired α spectral falloff for both the rotated and unrotated cases with the lowest frequencies

sometimes a little underrepresented. The exact spectral falloff for our three orientation angles, $(\omega,[\theta,\phi])$, is calculated in Table 3.1, where the spectral falloffs for 200 1D simulations, approximately 10,000 points each is averaged for different values of α. Then the results of Table 3.1 are plotted in Figure 3.9. We find that indeed the unrotated, $(\omega,[\theta,\phi])$, has exactly the spectral falloff we want, α, but the rotated angles, are slightly rougher for $\alpha < 0.6$.

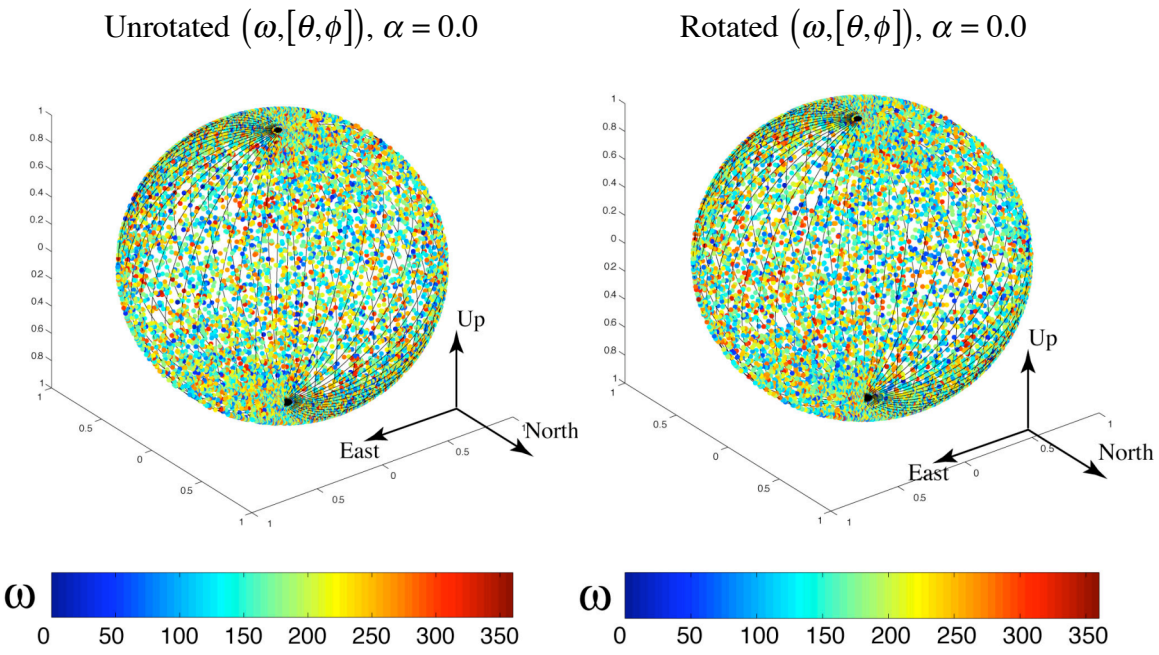

Figure 3.7 a)

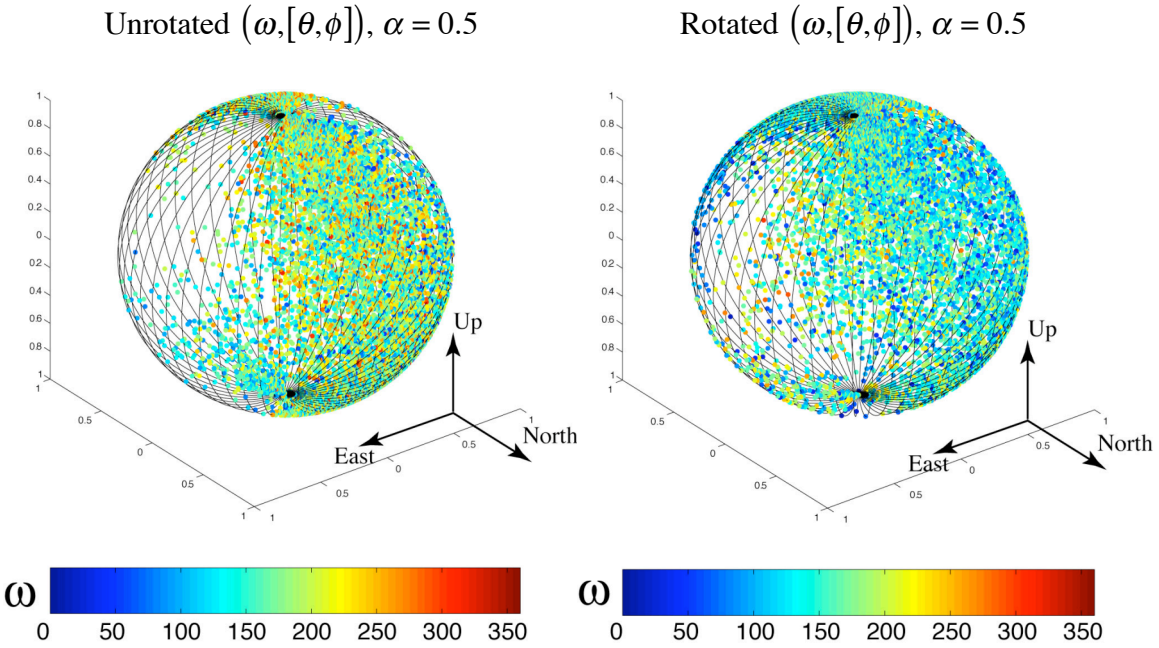

Figure 3.7 b)

Unrotated $(\omega,[\theta,\phi])$, $\alpha = 1.0$ Rotated $(\omega,[\theta,\phi])$, $\alpha = 1.0$

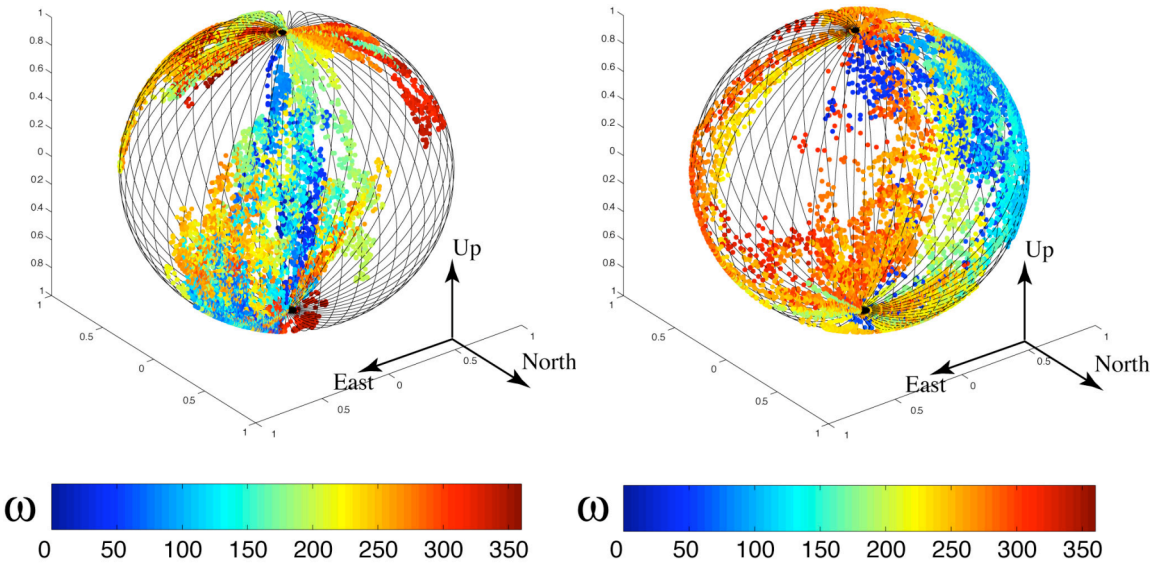

Figure 3.7 c)

Unrotated $(\omega,[\theta,\phi])$, $\alpha = 1.5$ Rotated $(\omega,[\theta,\phi])$, $\alpha = 1.5$

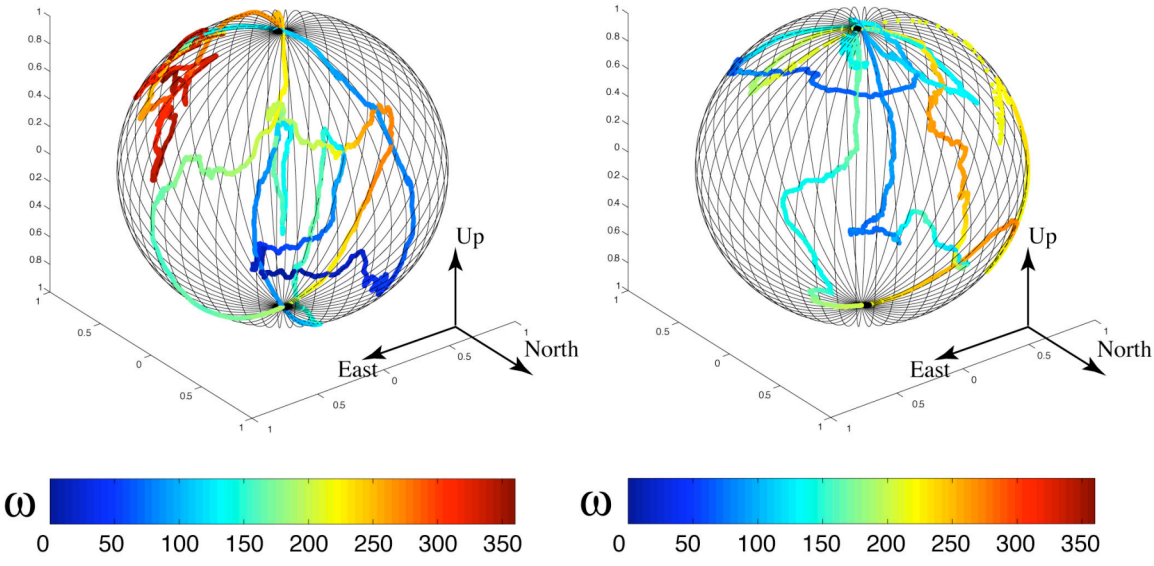

Figure 3.7 d)

Figure 3.7. *This is another way to visualize our filtered orientation data. The position of the plotted points on the 3D spheres represents the rotation axes* $[\theta,\phi]$*, and the color represents the rotation about the poles,* ω*, where* $blue = 0°$ *and* $red = 360°$*. Of course, for* $\alpha = 0.0$*, there are random positions of the points and random colors, representing the random 3D orientations,* $(\omega,[\theta,\phi])$*. As* α *increases, the spatial smoothing of point locations increases until there are linear tracks. Concurrently, as* α *increases, the spatial smoothing of color increases until the color changes smoothly from one to another along the 1D lines for* $\alpha = 1.5$*. This demonstrates that we have successfully smoothed the three orientation angles,* $(\omega,[\theta,\phi])$*, together. On the left, we plot* $(\omega,[\theta,\phi])$ *without the random rotation added, and on the right, we plot* $(\omega,[\theta,\phi])$ *with the random rotation added. These show that* $(\omega,[\theta,\phi])$ *still has similar properties regardless of the random rotation added.*

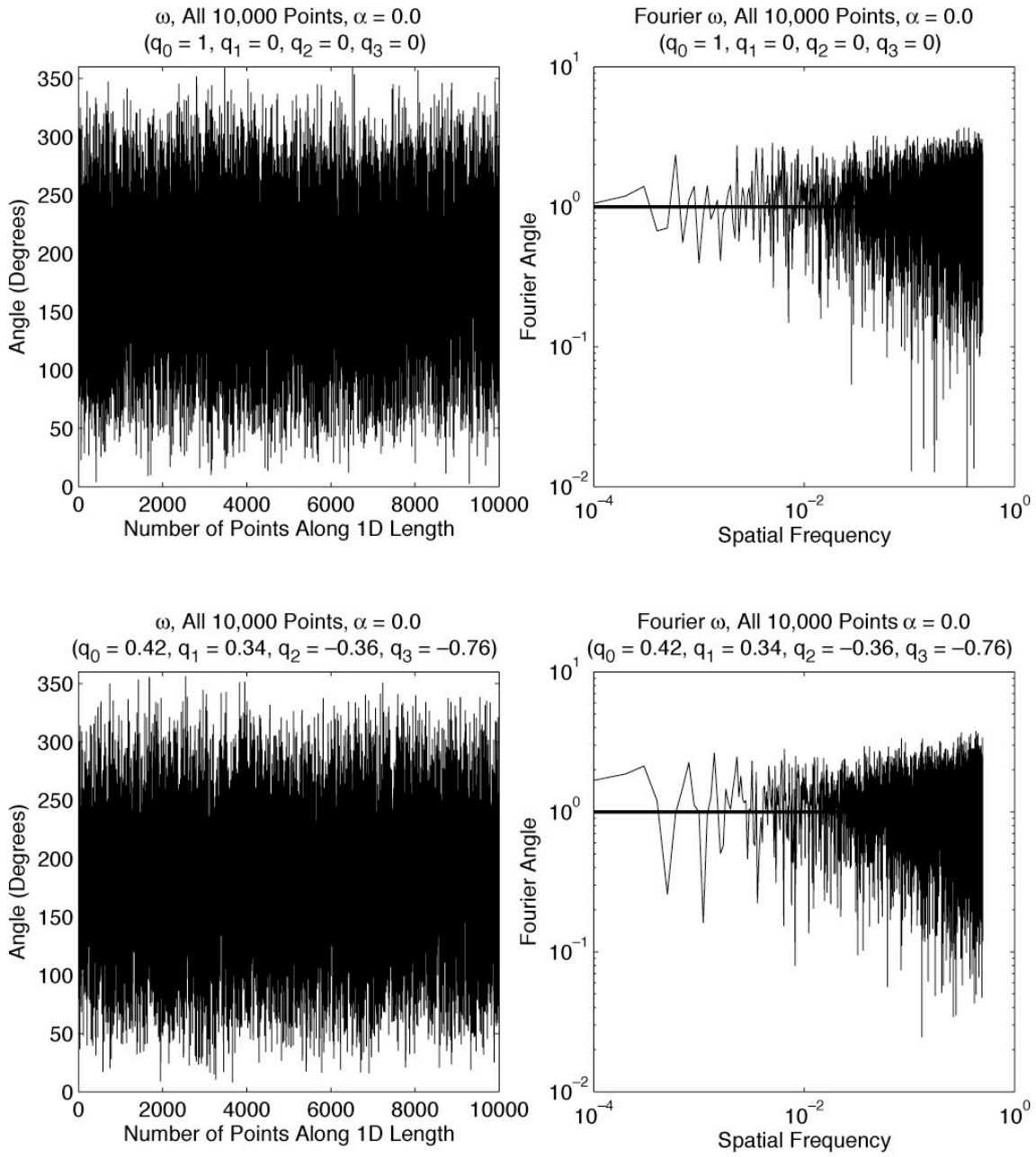
ω, All 10,000 Points, α = 0.0
(q0 = 1, q1 = 0, q2 = 0, q3 = 0)
Angle (Degrees)
Number of Points Along 1D Length
Fourier ω, All 10,000 Points, α = 0.0
(q0 = 1, q1 = 0, q2 = 0, q3 = 0)
Fourier Angle
Spatial Frequency
ω, All 10,000 Points, α = 0.0
(q0 = 0.42, q1 = 0.34, q2 = −0.36, q3 = −0.76)
Angle (Degrees)
Number of Points Along 1D Length
Fourier ω, All 10,000 Points α = 0.0
(q0 = 0.42, q1 = 0.34, q2 = −0.36, q3 = −0.76)
Fourier Angle
Spatial Frequency

Figure 3.8 a)

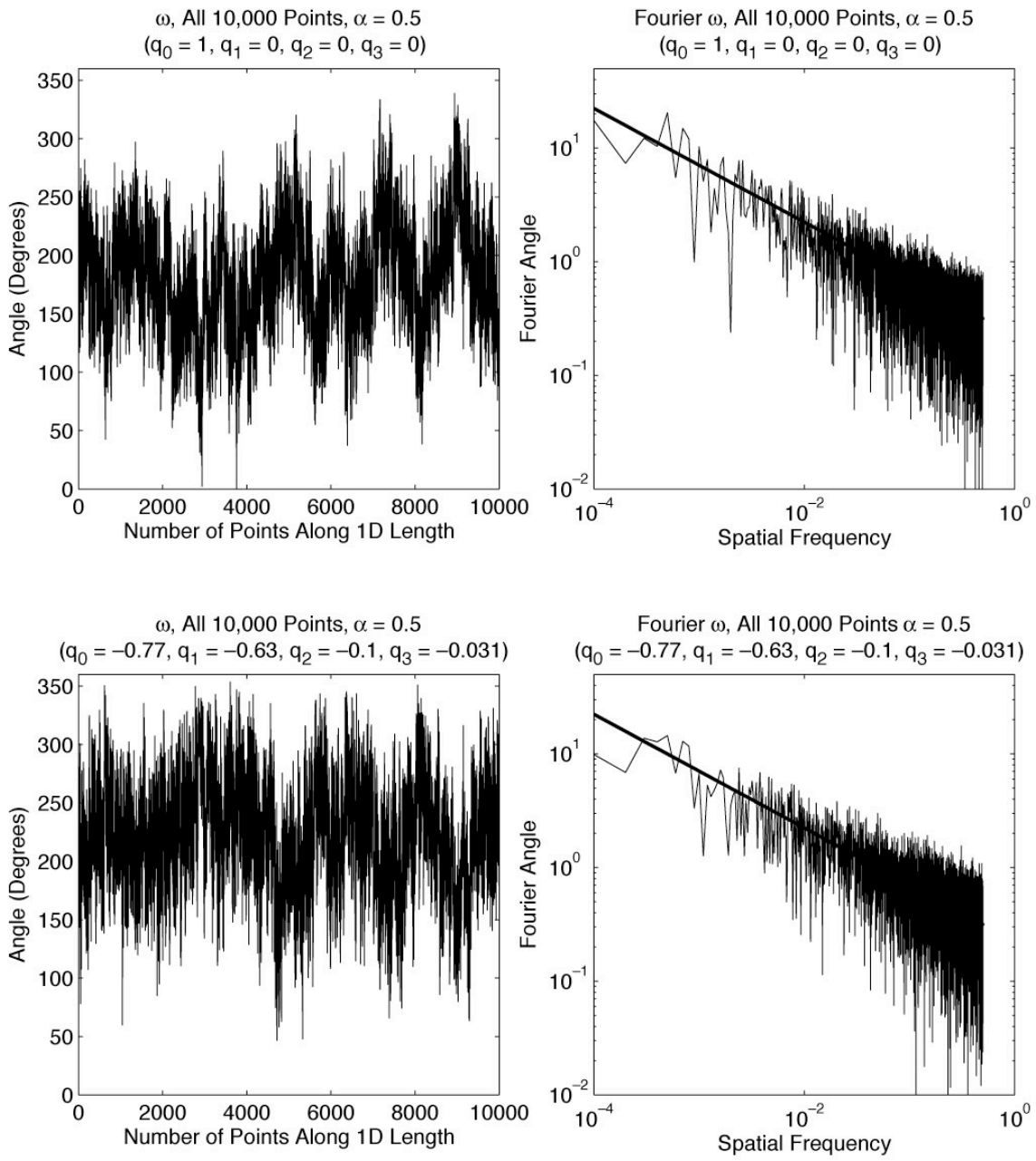
ω, All 10,000 Points, α = 0.5
(q0 = 1, q1 = 0, q2 = 0, q3 = 0)
Angle (Degrees)
Number of Points Along 1D Length
Fourier ω, All 10,000 Points, α = 0.5
(q0 = 1, q1 = 0, q2 = 0, q3 = 0)
Fourier Angle
Spatial Frequency
ω, All 10,000 Points, α = 0.5
(q0 = −0.77, q1 = −0.63, q2 = −0.1, q3 = −0.031)
Angle (Degrees)
Number of Points Along 1D Length
Fourier ω, All 10,000 Points α = 0.5
(q0 = −0.77, q1 = −0.63, q2 = −0.1, q3 = −0.031)
Fourier Angle
Spatial Frequency

Figure 3.8 b)

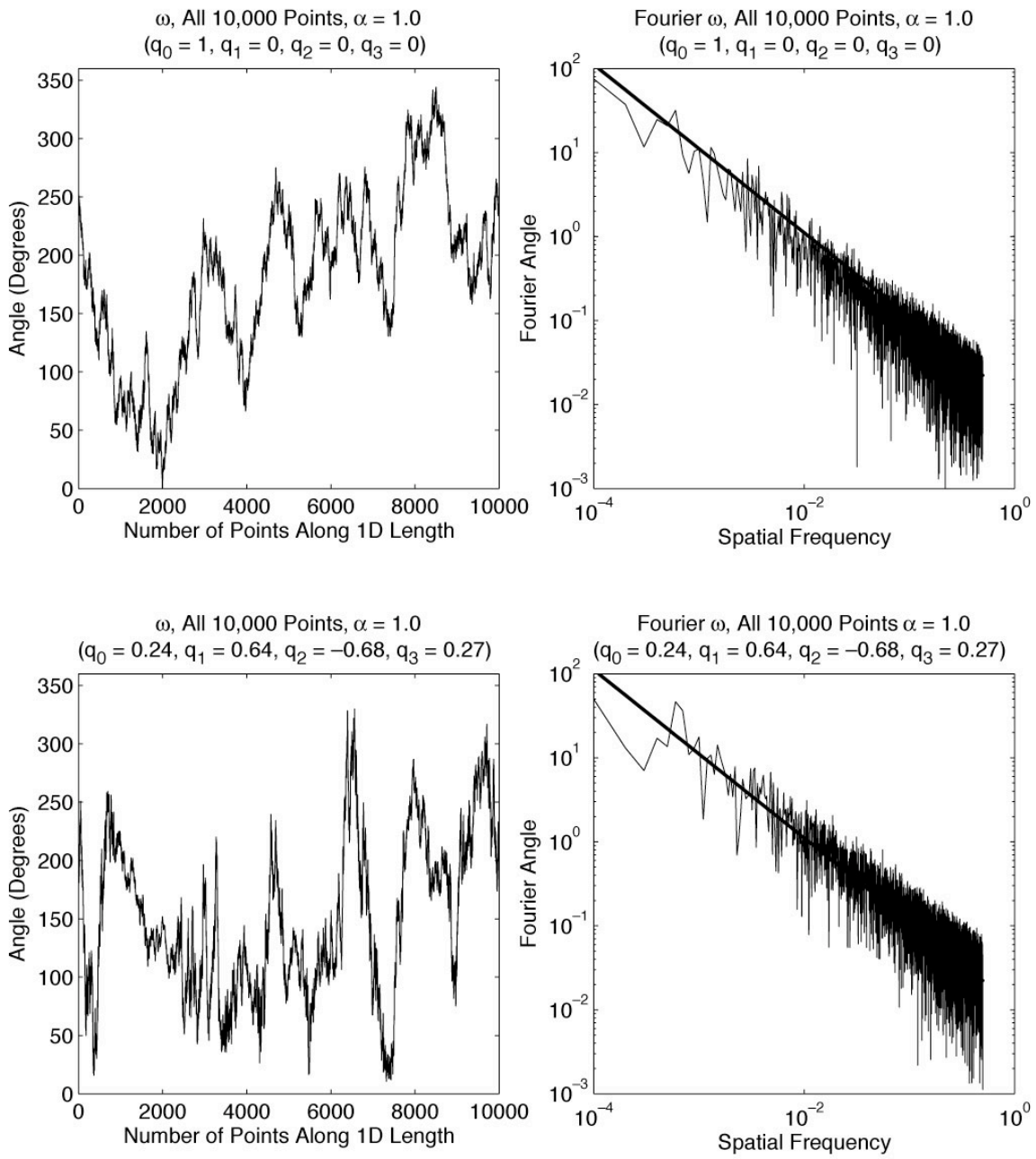
ω, All 10,000 Points, α = 1.0
(q0 = 1, q1 = 0, q2 = 0, q3 = 0)
Angle (Degrees)
Number of Points Along 1D Length
Fourier ω, All 10,000 Points, α = 1.0
(q0 = 1, q1 = 0, q2 = 0, q3 = 0)
Fourier Angle
Spatial Frequency
ω, All 10,000 Points, α = 1.0
(q0 = 0.24, q1 = 0.64, q2 = –0.68, q3 = 0.27)
Angle (Degrees)
Number of Points Along 1D Length
Fourier ω, All 10,000 Points α = 1.0
(q0 = 0.24, q1 = 0.64, q2 = –0.68, q3 = 0.27)
Fourier Angle
Spatial Frequency

Figure 3.8 c)

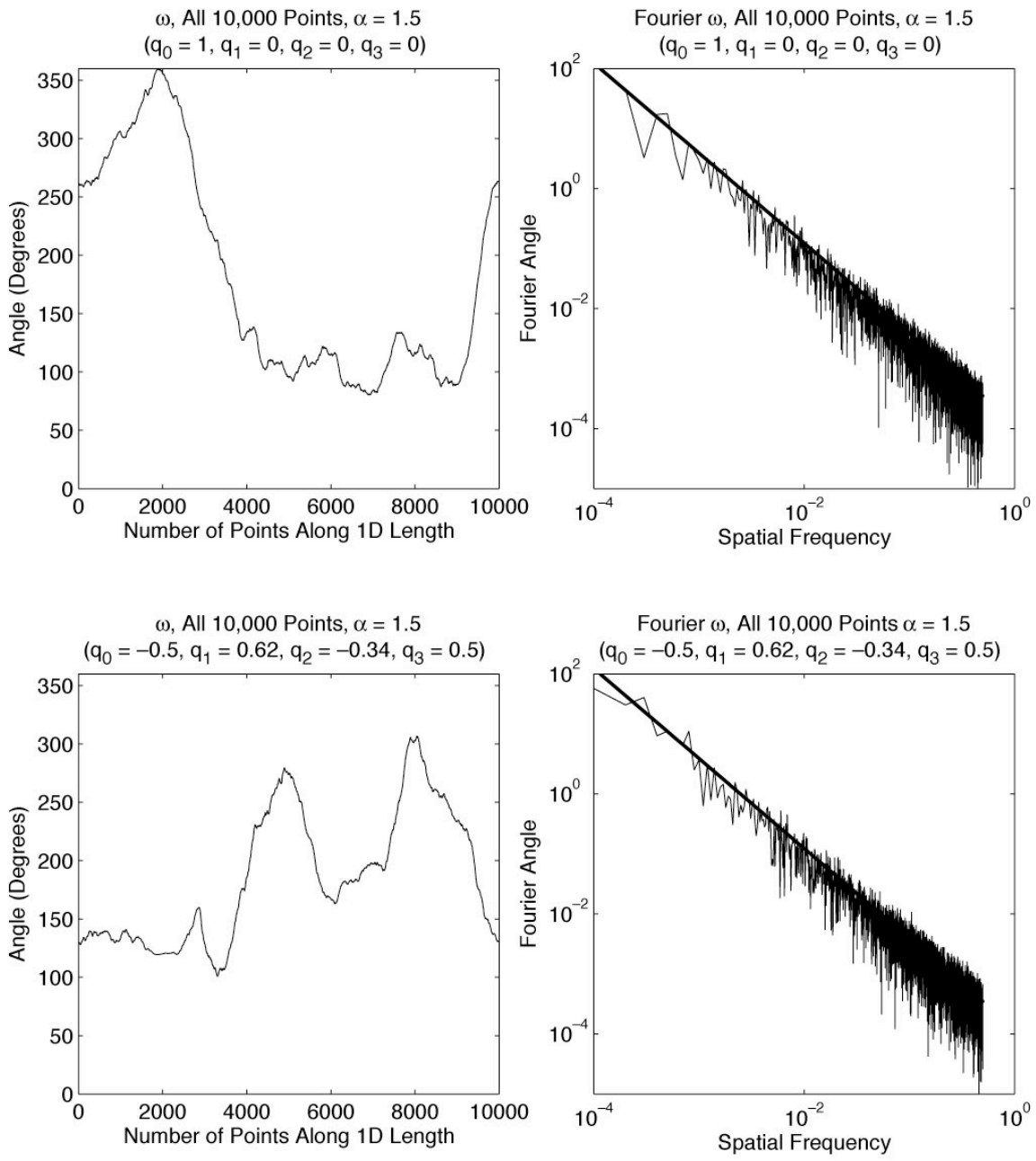
ω, All 10,000 Points, α = 1.5
(q0 = 1, q1 = 0, q2 = 0, q3 = 0)
Angle (Degrees)
Number of Points Along 1D Length
Fourier ω, All 10,000 Points, α = 1.5
(q0 = 1, q1 = 0, q2 = 0, q3 = 0)
Fourier Angle
Spatial Frequency
ω, All 10,000 Points, α = 1.5
(q0 = −0.5, q1 = 0.62, q2 = −0.34, q3 = 0.5)
Angle (Degrees)
Number of Points Along 1D Length
Fourier ω, All 10,000 Points α = 1.5
(q0 = −0.5, q1 = 0.62, q2 = −0.34, q3 = 0.5)
Fourier Angle
Spatial Frequency

Figure 3.8 d)

Figure 3.8. *A series of 1D simulations are shown with different degrees of smoothing, α, applied where* ***a)*** $\alpha = 0.0$, ***b)*** $\alpha = 0.5$, ***c)*** $\alpha = 1.0$, *and* ***d)*** $\alpha = 1.5$. *Each simulation is approximately 10,000 points. In this figure, ω is plotted for all 10,000 points on the left, and its spectral falloff is plotted on the right. The top plots represent ω before the random rotation is added, and the bottom plots represent ω after the random rotation is added. The main feature to notice is that ω does indeed have the approximately the appropriate spectral falloff both before and after the random rotation. The thick black line represents the expected α falloff, and the smoothed ω data for all the cases we tried between $0.0 < \alpha < 1.5$ approximately follows this expected thick black line. Sometimes, the very low frequencies are a little underrepresented, but overall this works quite well.*

Table 3.1. The Spectral Falloff Calculated for Each Filtered Angle as a Function of α

α	ω **Unrotated Falloff**	θ **Unrotated Falloff**	ϕ **Unrotated Falloff**	ω **Rotated Falloff**	θ **Rotated Falloff**
0	-4.16E-03	-2.79E-03	-1.62E-03	-4.85E-03	1.19E-03
0.1	0.1020	0.1016	0.0978	0.0548	0.0489
0.2	0.2010	0.2016	0.2008	0.1358	0.1317
0.3	0.2985	0.2951	0.3039	0.2299	0.2211
0.35	0.3480	0.3525	0.3461	0.2796	0.2645
0.4	0.4011	0.4003	0.4019	0.3459	0.3301
0.5	0.5003	0.5008	0.5021	0.4623	0.4352
0.6	0.6001	0.6006	0.6007	0.5841	0.5475
0.7	0.7016	0.7006	0.7005	0.6872	0.6609
0.8	0.8008	0.7987	0.8066	0.8009	0.7778
0.9	0.8999	0.8999	0.8970	0.8987	0.8822
1	1.0000	1.0051	1.0030	1.0023	1.0028
1.1	1.0986	1.0980	1.0969	1.0924	1.1060
1.2	1.2026	1.1982	1.1961	1.2031	1.2030
1.3	1.2963	1.3026	1.2996	1.2984	1.2964
1.4	1.3960	1.4012	1.4020	1.4002	1.3977
1.5	1.5033	1.4986	1.4989	1.4980	1.4944

If everything is working properly, the spectral falloff should $\approx \alpha$. *For each* α, *we*

- *generate 200 1D simulations, approximately 10,000 points each,*
- *determine the spectral falloff for the log-log plots of the data,*
- *then average the slopes for all 200 simulations.*

As expected, the spectral falloff of the unrotated angles, ω, θ, *and* ϕ *equals* α *for* $0.0 \le \alpha \le 1.5$. *The rotated simulations have spectral falloffs close to* α, *but tend to be a little spatially rougher, especially for* $\alpha < 0.6$ *(Figure 3.9). We calculate the spectral falloff of only the* ω *and* θ *rotated angles because the jumps in* ϕ *for a rotated simulation make it difficult to accurately assess a new spatial roughness.*

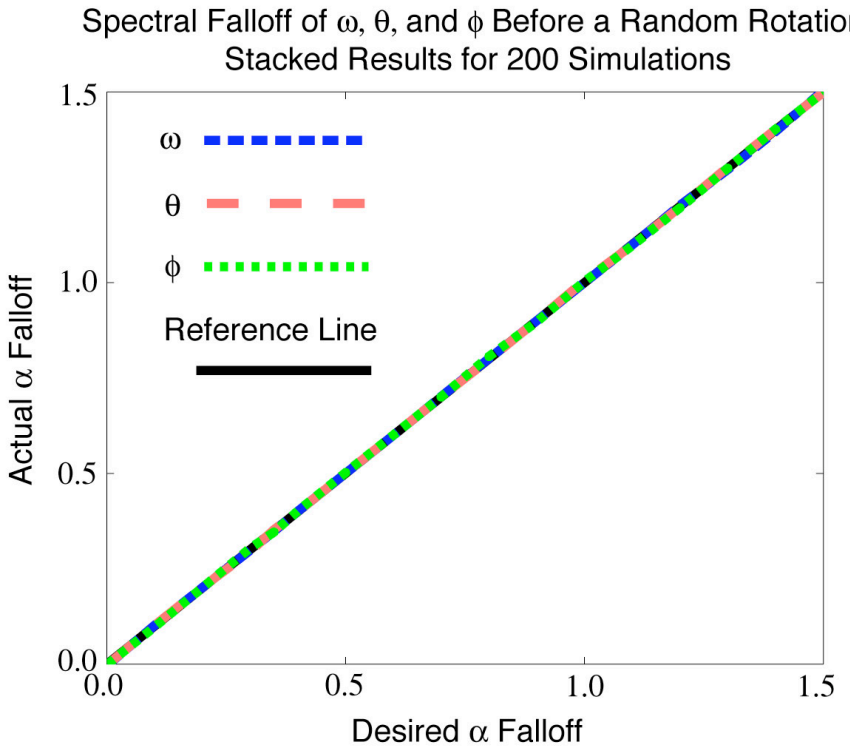
Spectral Falloff of ω, θ, and ϕ Before a Random Rotation
Stacked Results for 200 Simulations
ω
θ
ϕ
Reference Line
Actual α Falloff
Desired α Falloff
0.0
0.5
1.0
1.5

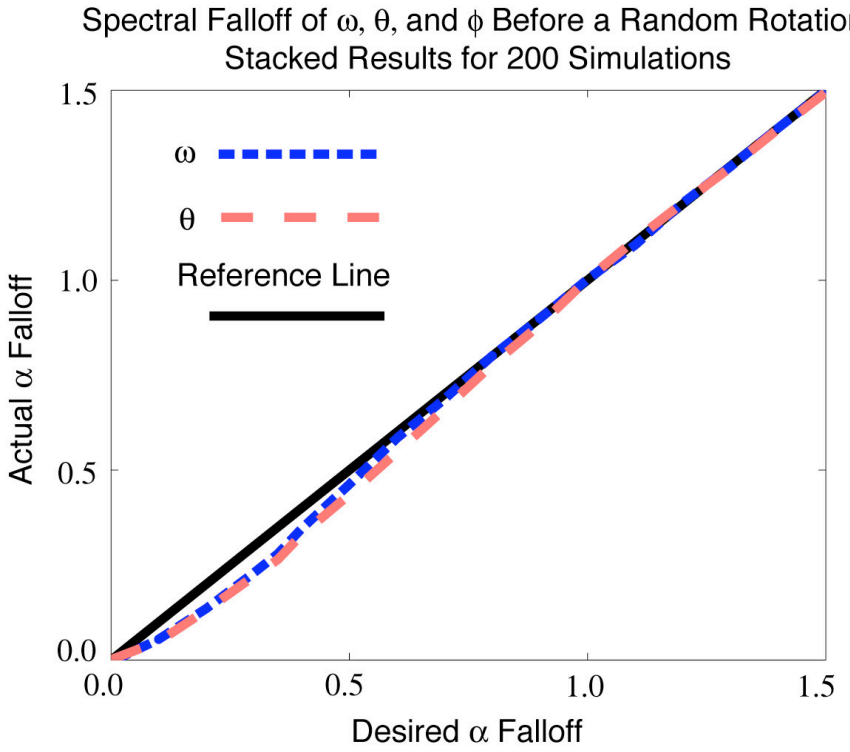
Spectral Falloff of ω, θ, and ϕ Before a Random Rotation
Stacked Results for 200 Simulations
ω
θ
Reference Line
Actual α Falloff
Desired α Falloff
0.0
0.5
1.0
1.5

Figure 3.9. *Plots of Table 3.1 data. The top plot shows spectral falloff as a function of* α *for the unrotated data, and the bottom plot shows the spectral falloff as a function of* α *for the rotated data. In both cases, the desired relationship is a linear line with a slope of 1.0 and an intercept of 0.0, indicated by a thick black line. In the top plot, the unrotated,* ω *(in blue),* θ *(in red), and* ϕ *(in green) plot directly on top of the desired black line. In the bottom plot, the rotated* ω *(in blue) and* θ *(in red) tend to be slightly rougher spatially for* $\alpha < 0.6$*, which produces spectral falloff values (negative slopes on a log-log plot) that are slightly less than* α*.*

Now that we have determined how to create filtered, approximately random, heterogeneous stress tensor orientations in terms of our three angles $(\omega,[\theta,\phi])$ and thoroughly examined their spectral properties, we can convert $(\omega,[\theta,\phi])$ into strike, dip, and rake, (Θ,δ,λ). Last, we will combine (Θ,δ,λ) with filtered σ_1, σ_2, and σ_3 to produce our full-filtered heterogeneous stress tensor. Technically, in the code used for this thesis, once $(\omega,[\theta,\phi])$ has been filtered, we convert it first into the associated quaternion vectors, $\vec{q}^{\,F} = \left[q_0^F, q_1^F, q_2^F, q_3^F\right]$, where F stands for filtered, then calculate (Θ,δ,λ). Using the derived equations in Appendix B, we have,

$$\tan\lambda = \frac{q_0^F\ q_1^F + q_2^F\ q_3^F}{q_0^F\ q_2^F - q_1^F\ q_3^F} \tag{3.16}$$

$$\tan\Theta = \frac{q_0^F\ q_1^F - q_2^F\ q_3^F}{q_0^F\ q_2^F + q_1^F\ q_3^F} \tag{3.17}$$

$$\tan\delta = \frac{2\left(q_0^F\ q_1^F + q_2^F\ q_3^F\right)/\sin\lambda}{q_0^F\ q_0^F - q_1^F\ q_1^F - q_2^F\ q_2^F + q_3^F\ q_3^F}\ . \tag{3.18}$$

Appendix A describes how to combine (Θ,δ,λ) with σ_1, σ_2, and σ_3 to produce the full heterogeneous stress tensor. It also explains how to convert (Θ,δ,λ) into the azimuth and plunge of the P-T axes, (θ_P,δ_P) and (θ_T,δ_T).

Plots of (θ_P,δ_P) and (θ_T,δ_T) from filtered 1D heterogeneous orientations, $(\omega,[\theta,\phi])$, are shown in Figure 3.11 for four different levels of smoothing, $\alpha = 0.0$, 0.5, 1.0, and 1.5. (θ_P,δ_P) and (θ_T,δ_T) are plotted on equal area plots for a plunge range of $\pm\ 90°$ as diagrammed in Figure 3.10. Typically, P-T equal area plots only have a plunge range of $0° - 90°$, because if for example, $\delta_P < 0$, then one can just apply the following transformation, $\delta_P' = -\delta_P$ and $\theta_P' = \theta_P + \pi$, to create a vector with a non-negative plunge that produces the same stress tensor. However, in our simulations, when $\alpha = 1.5$, it is interesting to see the unbroken linear track of the 1D simulation in P-T space, and this can only be seen if we use the full range of $\pm\ 90°$. In the top row, the P-T angles, (θ_P,δ_P) and (θ_T,δ_T), are plotted for filtered, unrotated $(\omega,[\theta,\phi])$, and in the bottom row the same data are plotted after a rotation. The quaternion vector listed for each plot is the quaternion that is multiplied with $(\omega,[\theta,\phi])$, where, $[q_0 = 1, q_1 = 0, q_2 = 0, q_3 = 0]$ produces no rotation, and $\vec{q} \neq [q_0 = 1, q_1 = 0, q_2 = 0, q_3 = 0]$ produces a rotation. For $\alpha = 0.0$, the points in P-T space on the equal area plots are uniformly distributed. This means that indeed, the random quaternion generator does

produce random orientations in 3D. Last, as the spatial smoothing, α, increases, the smoothing in P-T space increases. Thus, it would appear that the spatial smoothing of our orientations $(\omega,[\theta,\phi])$ translates well into (θ_P,δ_P) and (θ_T,δ_T).

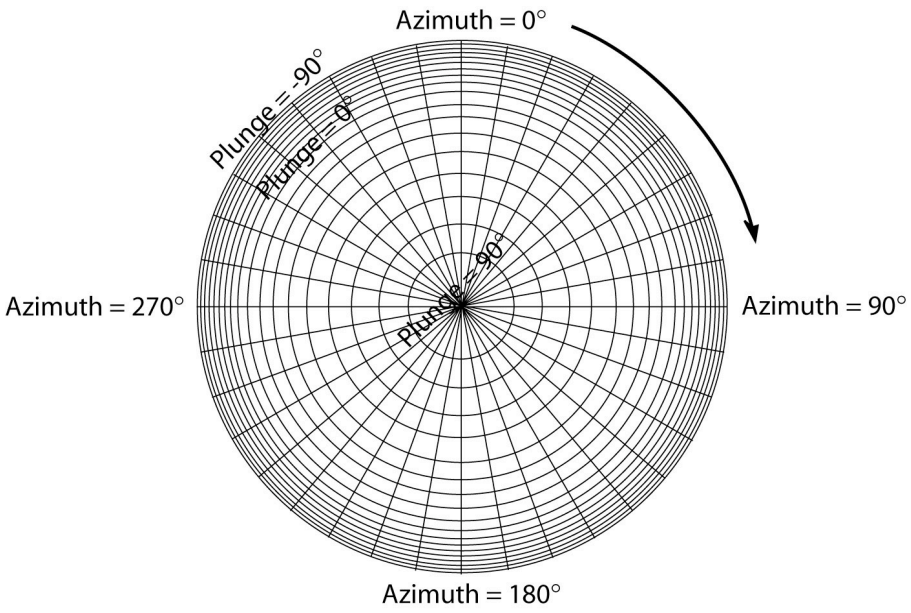

Figure 3.10. *A cartoon of the equal area plots used in Figure 3.11 for the P-T azimuths and plunges,* (θ_P,δ_P) and (θ_T,δ_T). *The longitude,* θ, *is the azimuth of the circle, and plunge,* δ, *is plotted as a function of radial distance where,* $\delta = 90°$ *at the center, and* $\delta = -90°$ *at the circumference. Note the radial lines are not necessarily to scale.*

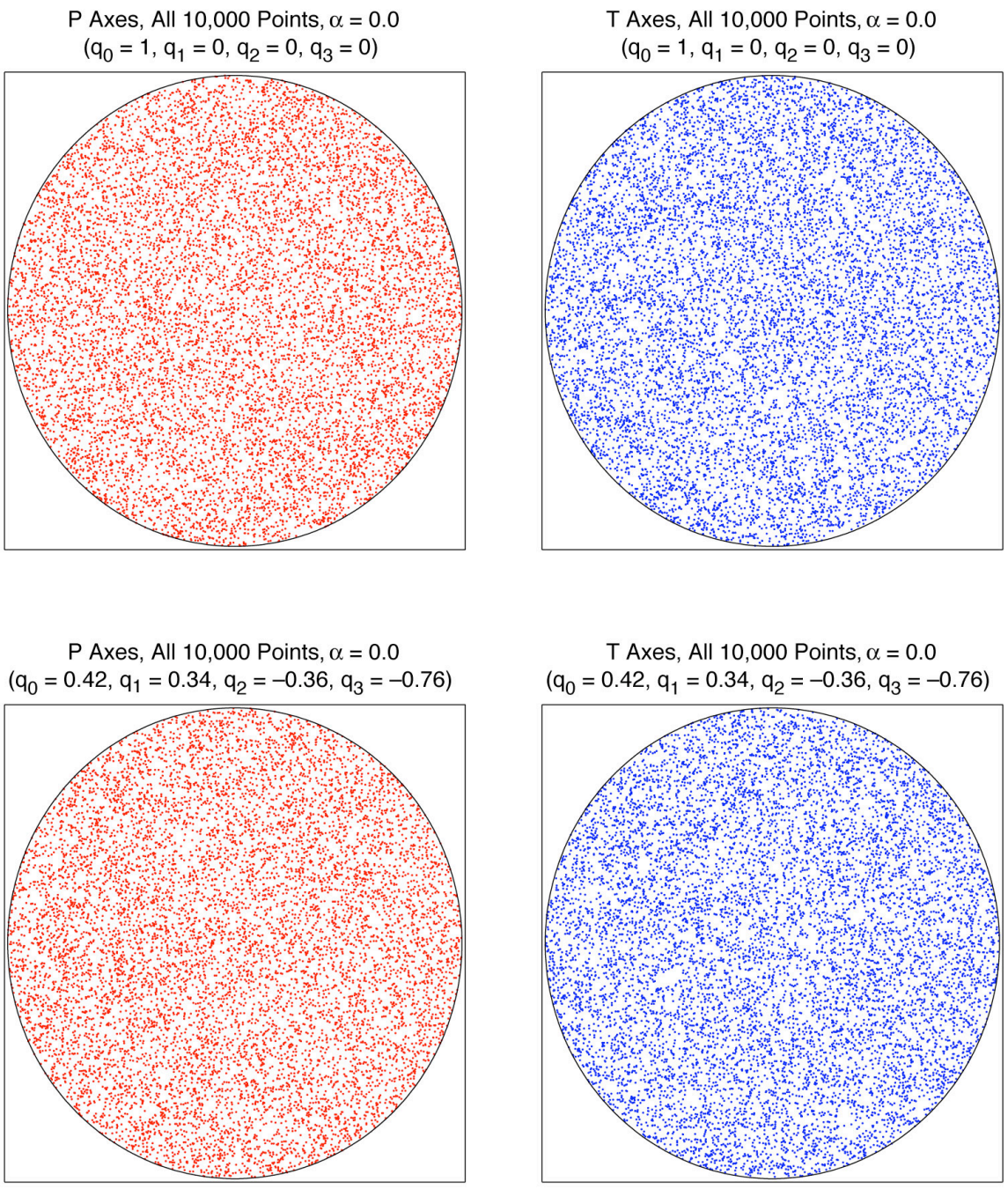
P Axes, All 10,000 Points, α = 0.0
(q0 = 1, q1 = 0, q2 = 0, q3 = 0)
T Axes, All 10,000 Points, α = 0.0
(q0 = 1, q1 = 0, q2 = 0, q3 = 0)
P Axes, All 10,000 Points, α = 0.0
(q0 = 0.42, q1 = 0.34, q2 = –0.36, q3 = –0.76)
T Axes, All 10,000 Points, α = 0.0
(q0 = 0.42, q1 = 0.34, q2 = –0.36, q3 = –0.76)

Figure 3.11 a)

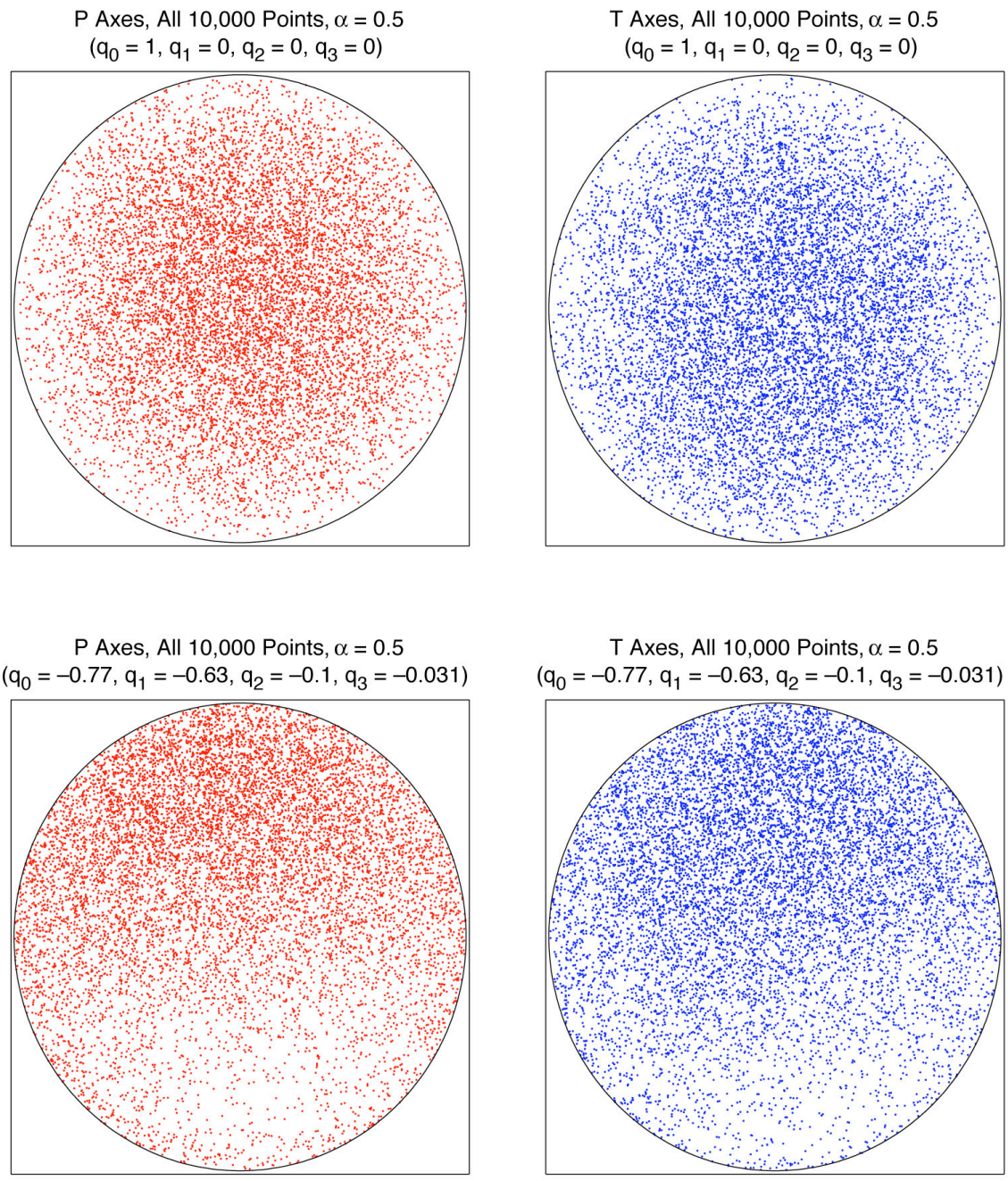
P Axes, All 10,000 Points, α = 0.5
(q0 = 1, q1 = 0, q2 = 0, q3 = 0)
T Axes, All 10,000 Points, α = 0.5
(q0 = 1, q1 = 0, q2 = 0, q3 = 0)
P Axes, All 10,000 Points, α = 0.5
(q0 = –0.77, q1 = –0.63, q2 = –0.1, q3 = –0.031)
T Axes, All 10,000 Points, α = 0.5
(q0 = –0.77, q1 = –0.63, q2 = –0.1, q3 = –0.031)

Figure 3.11 b)

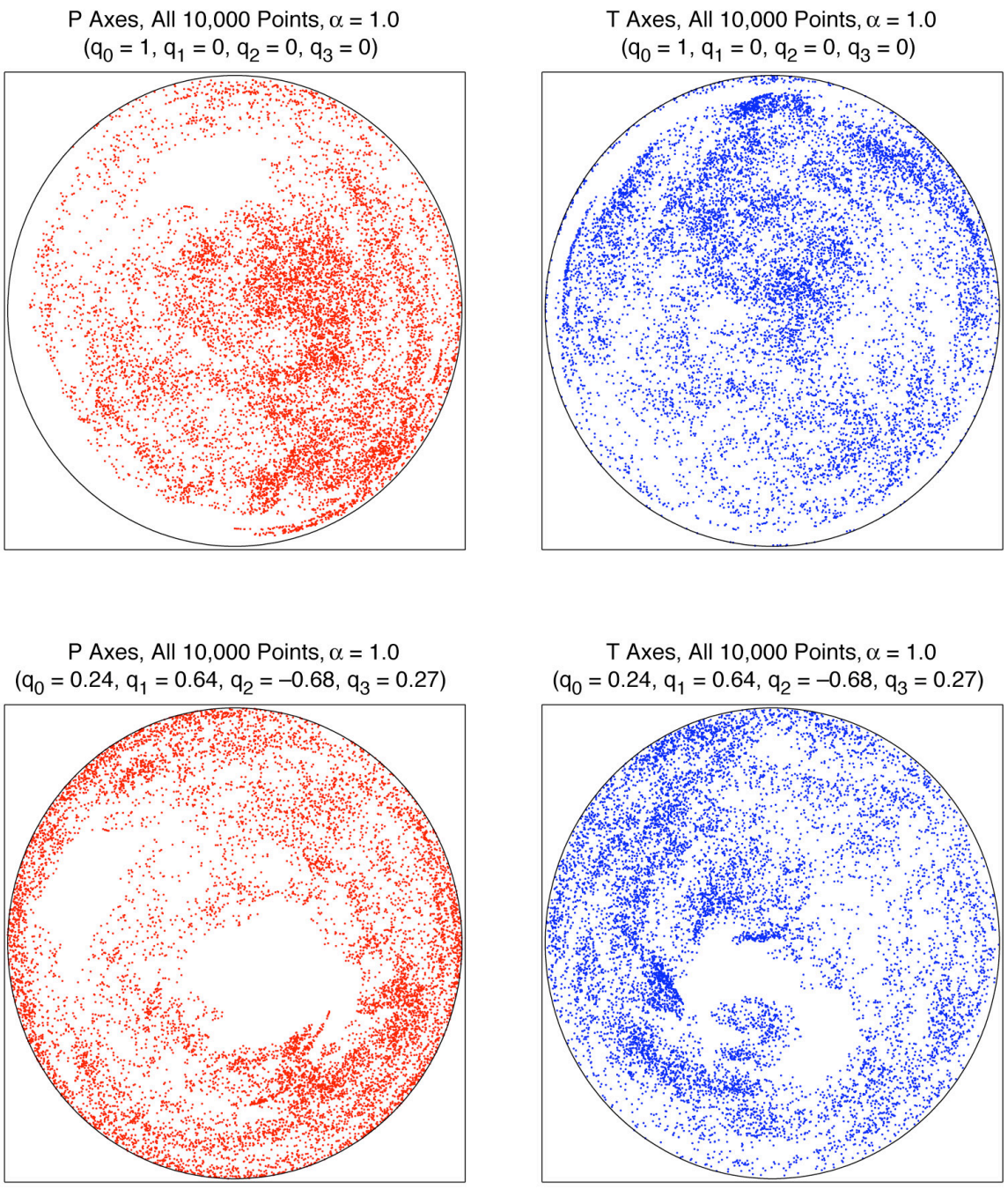
P Axes, All 10,000 Points, α = 1.0
(q0 = 1, q1 = 0, q2 = 0, q3 = 0)
T Axes, All 10,000 Points, α = 1.0
(q0 = 1, q1 = 0, q2 = 0, q3 = 0)
P Axes, All 10,000 Points, α = 1.0
(q0 = 0.24, q1 = 0.64, q2 = –0.68, q3 = 0.27)
T Axes, All 10,000 Points, α = 1.0
(q0 = 0.24, q1 = 0.64, q2 = –0.68, q3 = 0.27)

Figure 3.11 c)

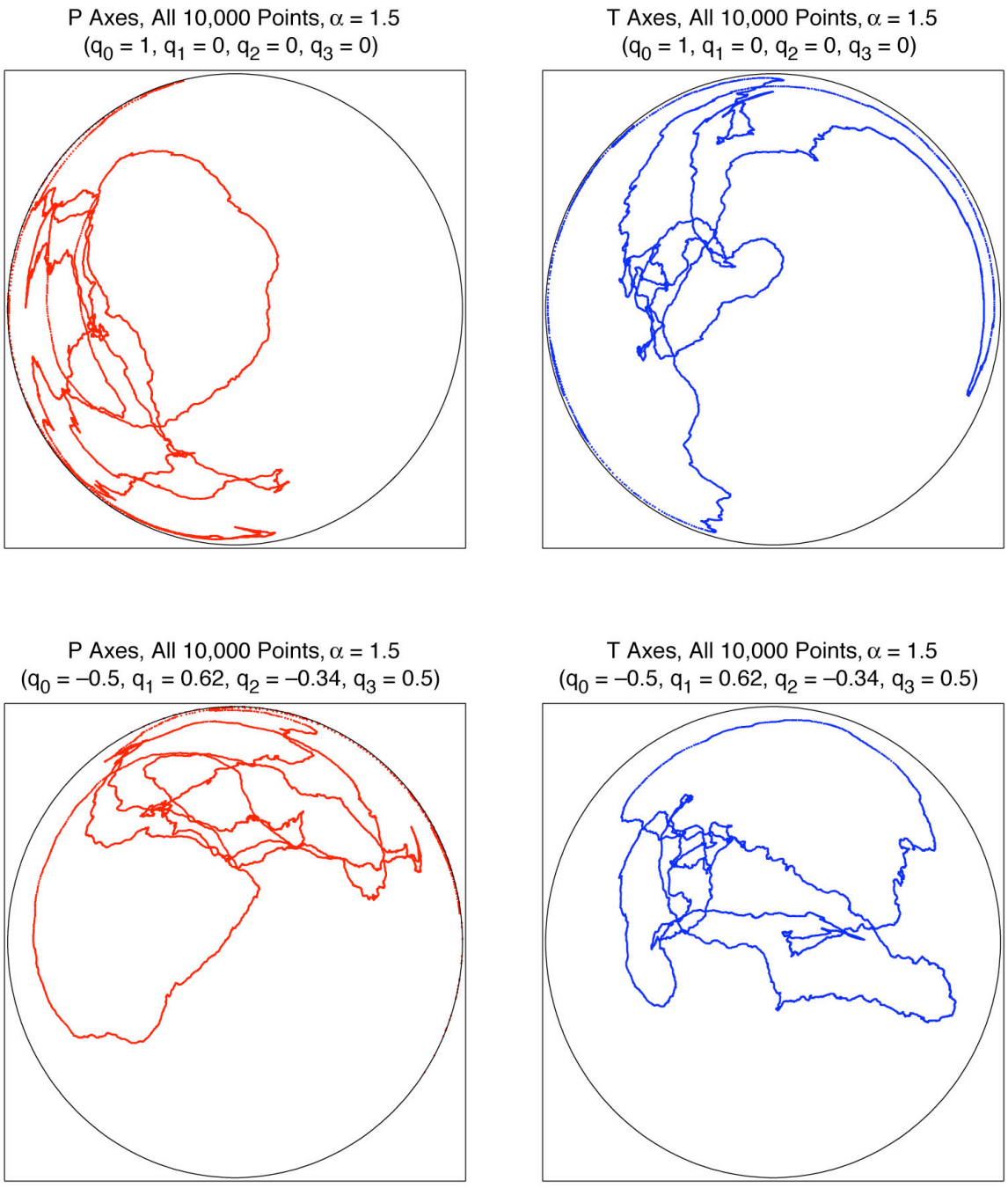
P Axes, All 10,000 Points, α = 1.5
(q0 = 1, q1 = 0, q2 = 0, q3 = 0)
T Axes, All 10,000 Points, α = 1.5
(q0 = 1, q1 = 0, q2 = 0, q3 = 0)
P Axes, All 10,000 Points, α = 1.5
(q0 = –0.5, q1 = 0.62, q2 = –0.34, q3 = 0.5)
T Axes, All 10,000 Points, α = 1.5
(q0 = –0.5, q1 = 0.62, q2 = –0.34, q3 = 0.5)

Figure 3.11 d)

Figure 3.11. *The Principal Compression Axes (P axes) and Principal Tension Axes (T axes) are plotted as on equal area plots for a series of simulations. The P axes are red on the left, and the T axes are blue on the right. The plunge range is* $\pm 90°$ *on the equal area plots instead of the usual* $0° - 90°$*, so that when* $\alpha = 1.5$ *one can more easily track the linear track of the data in P-T space. The top rows show P-T angles,* (θ_P, δ_P) *and* (θ_T, δ_T)*, for the filtered and unrotated,* $(\omega, [\theta, \phi])$*, and the bottom row shows the same data except that* $(\omega, [\theta, \phi])$ *were rotated. The quaternion by which the data* $(\omega, [\theta, \phi])$ *were multiplied is listed on each plot, where* $[q_0 = 1, q_1 = 0, q_2 = 0, q_3 = 0]$ *produces no rotation, and* $\vec{q} \neq [q_0 = 1, q_1 = 0, q_2 = 0, q_3 = 0]$ *produces a rotation.*

Note that for ***a)*** $\alpha = 0.0$ *the P-T axes are evenly and randomly distributed on the equal area plots for both the unrotated and rotated cases. This indicates there is no orientation bias for* $\alpha = 0.0$*, which is not surprising since our unfiltered orientations were by design generated randomly. For* ***b)*** $\alpha = 0.5$ *one can see that the axes are still somewhat randomly distributed, but there is a slight radial clumping for the unrotated P-T plots, and this clumping of orientations is rotated for the bottom P-T plots. As* α *increases further, to* ***c)*** $\alpha = 1.0$*, more fine-scale structure and orientational clumping arises, and it still has some orientational bias. Last, when* ***d)*** $\alpha = 1.5$*, the orientations smoothly vary from one point to another such that it forms a continuous, wandering line in P-T space. One can see that for* $\alpha > 0.0$*, a single filtered simulation may not generate randomly orientated data; hence, this is why we wish to stack many simulations where each data set has been given a random rotation. Figure 3.13 shows the efficacy of this approach.*

While the filtering of the orientation angles, $(\omega,[\theta,\phi])$, works quite well in producing filtered, P-T axes angles, (θ_P,δ_P) and (θ_T,δ_T), it also produces an orientation bias. Since we wish to generate heterogeneous stress with no orientation bias, we employ the strategy mentioned previously. Generate at least 10–20 filtered data sets, add a random rotation to each data set, then stack the data sets. Figure 3.13 compares the stacking of multiple data sets with and without the random rotations to demonstrate the necessity of randomly rotating the data sets before stacking them. P-T axes are plotted in Figure 3.13, using the typical $0° - 90°$ plunge range for P-T equal area plots. This typical plunge range is diagrammed in the Figure 3.12 cartoon. In Figure 3.13, the top row of P-T equal area plots for each α has stacked 200 1D simulations, each 1,001 points long, without any random rotations applied to $(\omega,[\theta,\phi])$. The bottom row of P-T equal area plots for each α has stacked 200 1D simulations, each 1,001 points long, with a random rotation applied to $(\omega,[\theta,\phi])$ for each simulation.

One finds that stacking the data alone (top rows), without any random rotations applied, helps, but still produces an average bias in the P-T orientations; one can visually see this in Figure 3.13 with the uneven coverage of the equal area plots especially for $\alpha = 1.5$. When one adds a random rotation to each simulation and then stacks multiple simulations (bottom rows), the P-T orientations begin to average out until the equal area plots are fairly uniformly covered, and there is little to no orientation bias.

Underneath each set of P-T plots, we have also listed the component-wise mean heterogeneous stress tensor, that is calculated as follows:

$$\boldsymbol{\sigma}'_{HeterogeneousMean} = \frac{1}{N1\ N2}\sum_{j=1}^{N2}\sum_{i=1}^{N1}\boldsymbol{\sigma}'^{ij}_{Heterogeneous}\left(\sigma_1'^{ij},\sigma_2'^{ij},\sigma_3'^{ij},\omega^{ij},\theta^{ij},\phi^{ij}\right) \qquad (3.19)$$

where $N1$ is the number of points in each simulation and $N2$ is the number of simulations. Note, filtered deviatoric principal stresses, σ_1', σ_2', and σ_3' have been combined with our orientation angles $(\omega,[\theta,\phi])$, to generate $\boldsymbol{\sigma}'_{Heterogeneous}$ for each simulation; then the above component-wise mean equation above is applied. Last, the square root of the second invariant of the deviatoric stress tensor, $\sqrt{I_2'}$, is calculated for the component-wise mean heterogeneous stress tensor. In Chapter 4, we will see why $I_2' = \sigma_{11}'^2 + \sigma_{22}'^2 + \sigma_{33}'^2 + 2\sigma_{12}'^2 + 2\sigma_{23}'^2 + 2\sigma_{13}'^2$, is so important; I_2' is an invariant measure of the maximum shear stress and is the quantity used to determine when points fail for our grid. Also, as mentioned in Chapter 1, $\sqrt{I_2'}$ is used in calculating the ratio of heterogeneous stress to background stress. Therefore, $\sqrt{I'_{2\ HeterogeneousMean}}$ is a natural way of measuring the size of the residual average stress tensor. The smaller the $\sqrt{I'_{2\ HeterogeneousMean}}$ the better when attempting to produce heterogeneous deviatoric stress tensors with an approximately zero component-wise mean. We find that in Figure 3.13 indeed, stacking the data alone is insufficient to produce approximately zero mean stress tensors; adding a rotation to each simulation then stacking is necessary if one wishes to have a zero mean stress tensor for any filtering power, α.

Our last figure with filtered 1D data, is Figure 3.14, which shows one component of the filtered deviatoric stress tensor, σ_{11}', and its spectral properties. The other components of the deviatoric stress tensor, σ_{22}', σ_{33}', σ_{12}', σ_{23}', and σ_{13}', have similar spectral properties and are not shown. The main point of Figure 3.14 is to show that even if the orientations $(\omega,[\theta,\phi])$ and the principal stresses, σ_1', σ_2', and σ_3' are all filtered

with an $\alpha > 0.0$, the components of the stress tensor in a Cartesian coordinate system, σ'_{11}, σ'_{22}, σ'_{33}, σ'_{12}, σ'_{23}, and σ'_{13} do not have the α spectral falloff. To create our stress tensor, we have rotated principal stresses at each point into their specified reference frames. The simple act of rotating principal stresses into different reference frames, even using smoothed rotations, causes the symmetric stress tensor to not have the same α smoothing as the principal stresses. Even if one started with a Cartesian stress tensor and smoothed each component separately, then rotated to another reference frame, one loses all the α smoothing spectral properties. So Figure 3.14 helps demonstrate why we choose not to filter the components of a stress tensor for a particular reference frame but instead choose to filter the principal stresses and orientation angles.

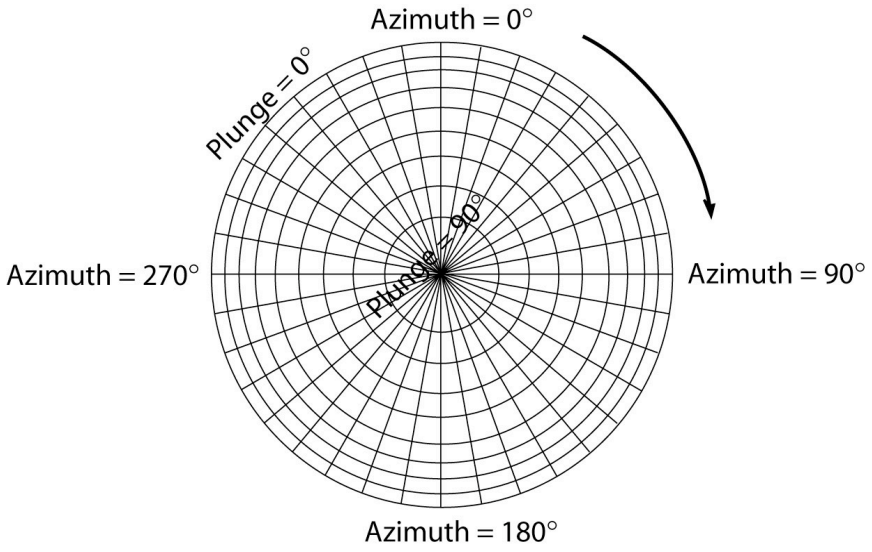

Figure 3.12. *A cartoon of the equal area plots used in Figure 3.13 for the P-T azimuths and plunges,* (θ_P, δ_P) and (θ_T, δ_T). *The longitude,* θ, *is the azimuth of the circle, and plunge,* δ, *is plotted as a function of radial distance where* $\delta = 90°$ *at the center, and* $\delta = 0°$ *at the circumference. Note the radial lines are not necessarily to scale.*

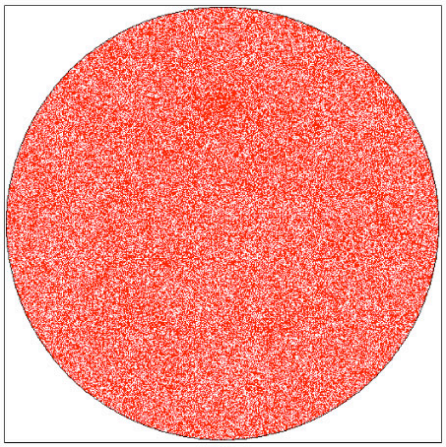

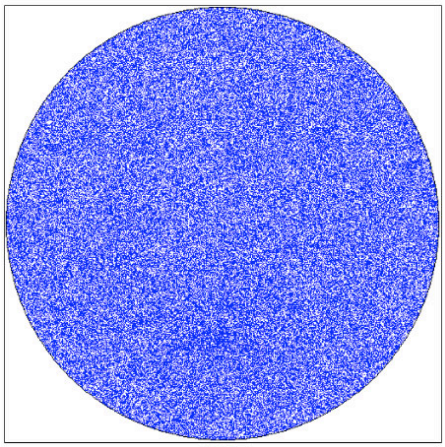

$$\boldsymbol{\sigma}'_{HeterogeneousMean} = \begin{pmatrix} 0.0009 & 0.0006 & -0.0007 \\ 0.0006 & -0.0013 & 0.0081 \\ -0.0007 & 0.0081 & 0.0004 \end{pmatrix} \text{ for 200 runs, 1,001 points each}$$

$$\sqrt{I'_{2\ HeterogeneousMean}} = 0.0117$$

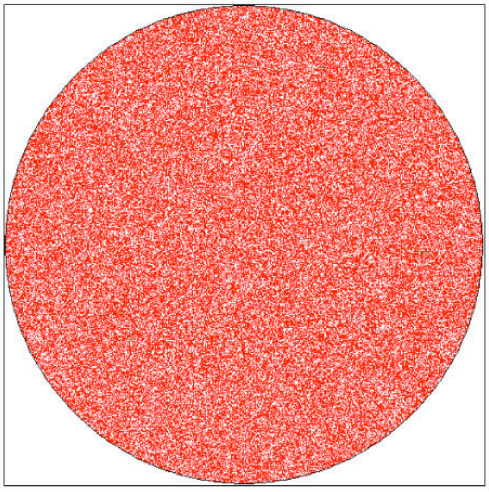

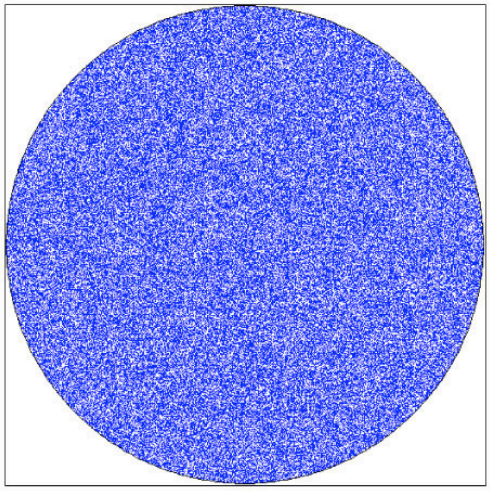

$$\boldsymbol{\sigma}'_{HeterogeneousMean} = \begin{pmatrix} -0.0010 & 0.0001 & -0.0002 \\ 0.0001 & 0.0013 & -0.0011 \\ -0.0002 & -0.0011 & -0.0003 \end{pmatrix} \text{ for 200 runs, 1,001 points each}$$

$$\sqrt{I'_{2\ HeterogeneousMean}} = 0.0023$$

Figure 3.13 a)

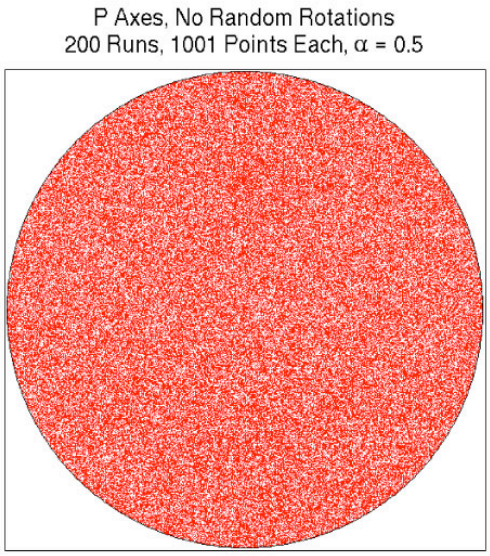

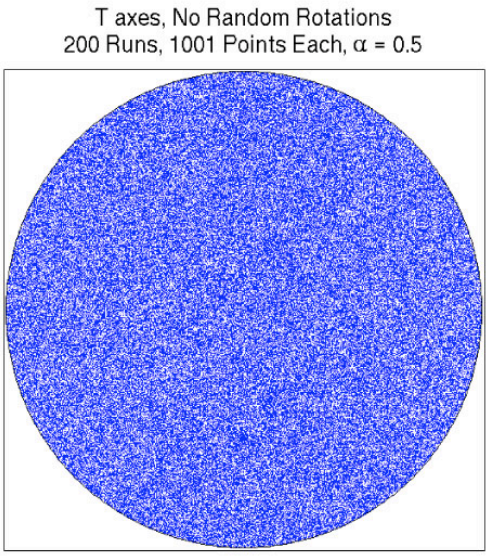

$$\boldsymbol{\sigma}'_{HeterogeneousMean} = \begin{pmatrix} -0.0013 & 0.0001 & -0.0008 \\ 0.0001 & -0.0002 & -0.0013 \\ -0.0008 & -0.0013 & 0.0015 \end{pmatrix}$$ for 200 runs, 1,001 points each

$$\sqrt{I'_{2\ HeterogeneousMean}} = 0.0030$$

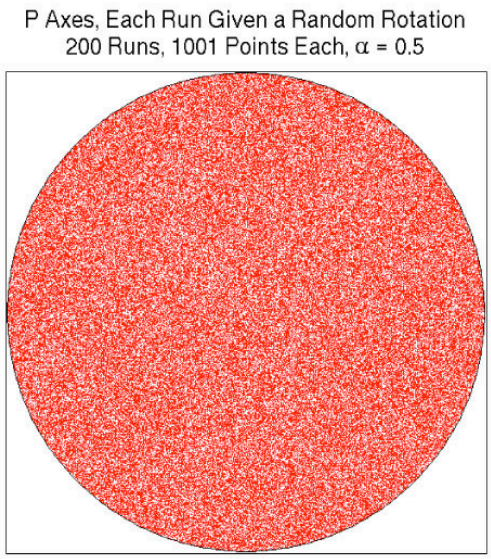

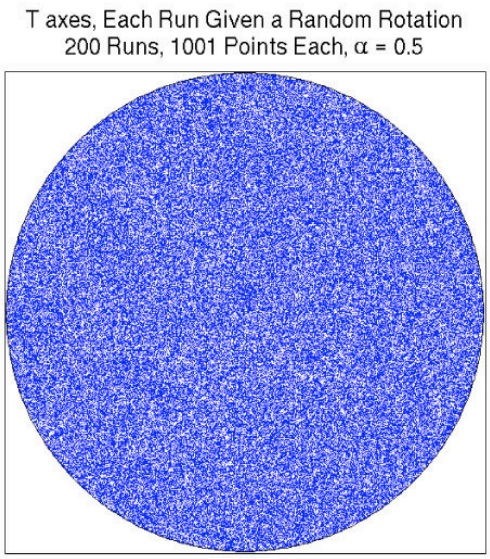

$$\boldsymbol{\sigma}'_{HeterogeneousMean} = \begin{pmatrix} 0.0003 & -0.0000 & 0.0007 \\ -0.0000 & -0.0016 & 0.0001 \\ 0.0007 & 0.0001 & 0.0013 \end{pmatrix}$$ for 200 runs, 1,001 points each

$$\sqrt{I'_{2\ HeterogeneousMean}} = 0.0023$$

Figure 3.13 b)

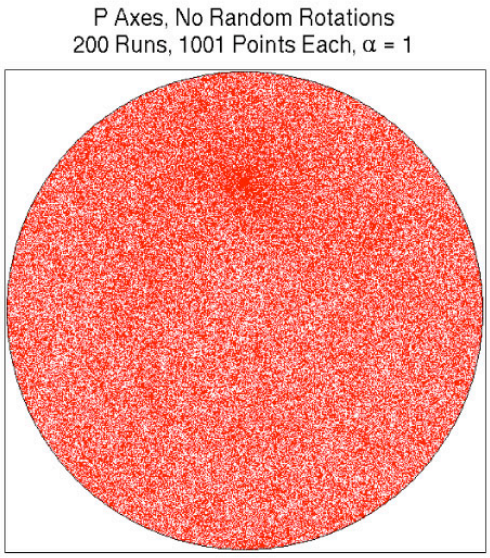

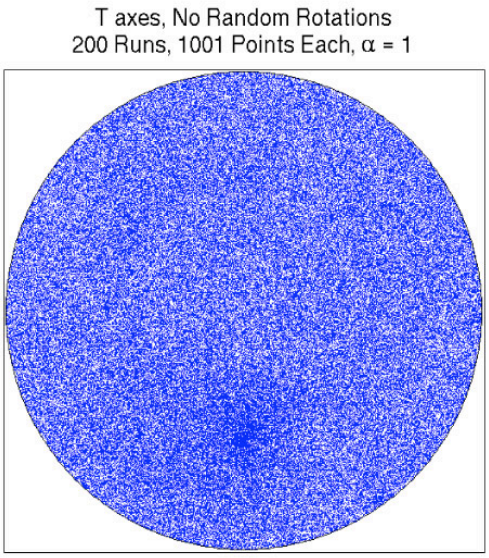

$$\boldsymbol{\sigma}'_{HeterogeneousMean} = \begin{pmatrix} -0.0011 & 0.0022 & 0.0006 \\ 0.0022 & -0.0036 & 0.0216 \\ 0.0006 & 0.0216 & 0.0047 \end{pmatrix} \text{ for 200 runs, 1,001 points each}$$

$$\sqrt{I'_{2\ HeterogeneousMean}} = 0.0314$$

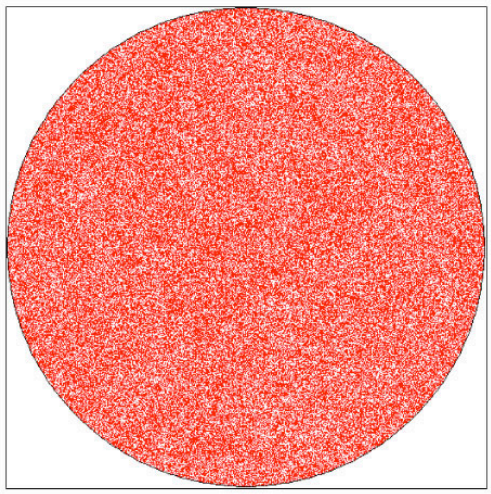

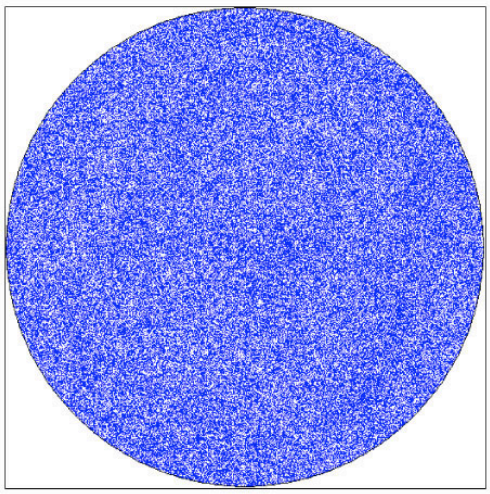

$$\boldsymbol{\sigma}'_{HeterogeneousMean} = \begin{pmatrix} 0.0022 & -0.0012 & 0.0003 \\ -0.0012 & -0.0019 & -0.0024 \\ 0.0003 & -0.0024 & -0.0004 \end{pmatrix} \text{ for 200 runs, 1,001 points each}$$

$$\sqrt{I'_{2\ HeterogeneousMean}} = 0.0048$$

Figure 3.13 c)

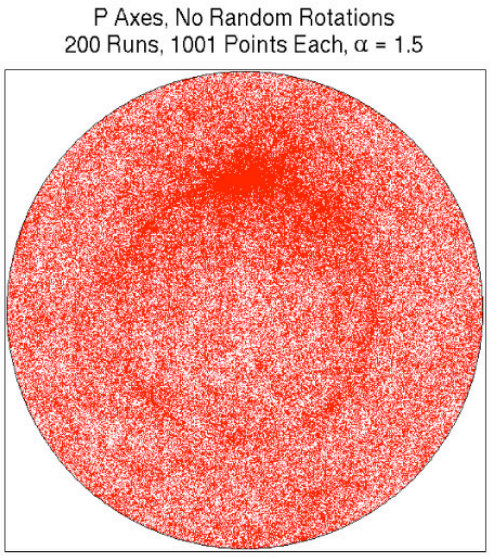

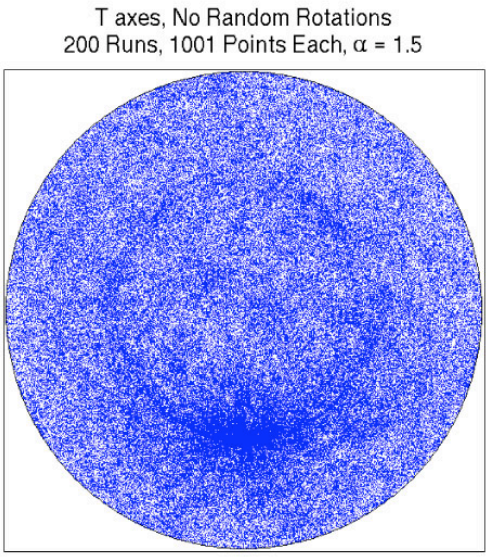

$$\boldsymbol{\sigma}'_{HeterogeneousMean} = \begin{pmatrix} -0.0009 & -0.0060 & 0.0035 \\ -0.0060 & -0.0128 & 0.0753 \\ 0.0035 & 0.0753 & 0.0137 \end{pmatrix} \text{ for 200 runs, 1,001 points each}$$

$$\sqrt{I'_{2\ HeterogeneousMean}} = 0.1086$$

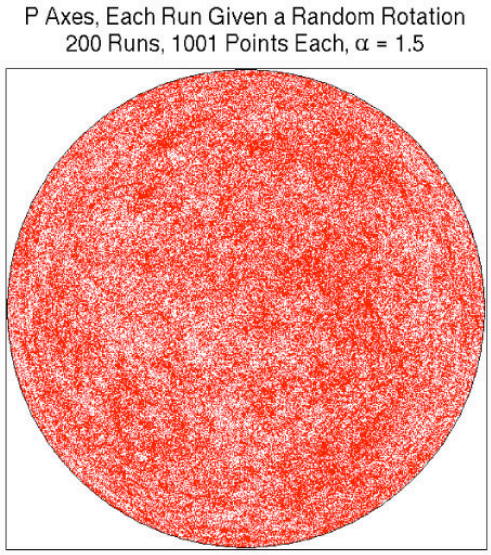

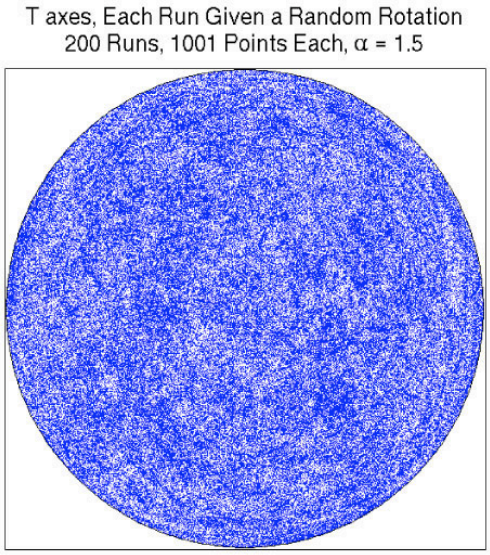

$$\boldsymbol{\sigma}'_{HeterogeneousMean} = \begin{pmatrix} 0.0022 & -0.0021 & 0.0081 \\ -0.0021 & -0.0023 & 0.0053 \\ 0.0081 & 0.0053 & 0.0001 \end{pmatrix} \text{ for 200 runs, 1,001 points each}$$

$$\sqrt{I'_{2\ HeterogeneousMean}} = 0.0117$$

Figure 3.13 d)

Figure 3.13. *For 4 different levels of smoothing,* ***a)*** $\alpha = 0.0$, ***b)*** $\alpha = 0.5$, ***c)*** $\alpha = 1.0$, *and* ***d)*** $\alpha = 1.5$**,** *we stack the results of 200 simulations, 1D length of 1,001 points each, and inspect whether or not there still is an orientation bias. In the top row, each simulation's three orientation angles,* $(\omega,[\theta,\phi])$, *are filtered, converted to the P-T angles,* (θ_P,δ_P) *and* (θ_T,δ_T), *then stacked. In the top row each simulation's three orientation angles,* $(\omega,[\theta,\phi])$, *are filtered, given a random rotation, converted to the P-T angles,* (θ_P,δ_P) *and* (θ_T,δ_T), *then stacked. Below each set of P-T equal area plots is an associated* $\boldsymbol{\sigma}'_{HeterogeneousMean}$ *stress tensor. This is calculated as follows. For each simulation, filtered principal stresses,* σ'_1, σ'_2, *and* σ'_3 *with* $\sqrt{I'_2} = 1.0$, *are combined with the unrotated or rotated angles,* $(\omega,[\theta,\phi])$, *to produce filtered heterogeneous stress tensors. Then all the stress tensors from all the simulations are averaged component-wise to create,* $\boldsymbol{\sigma}'_{HeterogeneousMean}$. *Last,* $\sqrt{I'_{2\ HeterogeneousMean}}$, *is shown as a measure of the size of* $\boldsymbol{\sigma}'_{HeterogeneousMean}$. *It shows the extent to which the components of* $\boldsymbol{\sigma}'_{HeterogeneousMean}$ *have not canceled out in the stacked simulations, and there is still a bias in the heterogeneous stress. Ideally, we want stacked simulations that have the following properties: 1) P and T equal area plots with uniform distributions of points (indicating no orientation bias) 2)* $\boldsymbol{\sigma}'_{HeterogeneousMean}$ *with each component approaching zero; therefore,* $\sqrt{I'_{2\ HeterogeneousMean}} \to 0$ *as the number of stacked runs* $\to \infty$. *We find that stacking filtered data alone is insufficient (the top row), that one needs to both randomly rotate each simulation and then stack the data to produce heterogeneous stress with no orientation bias and a* $\sqrt{I'_{2\ HeterogeneousMean}} \approx 0$ *for all* α.

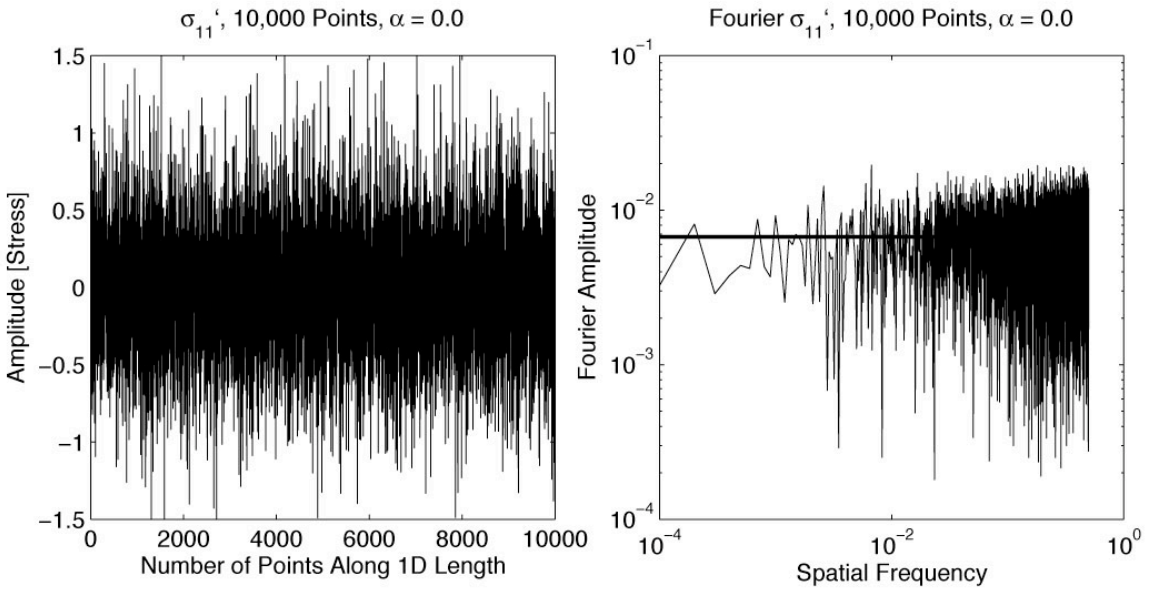

Figure 3.14 a)

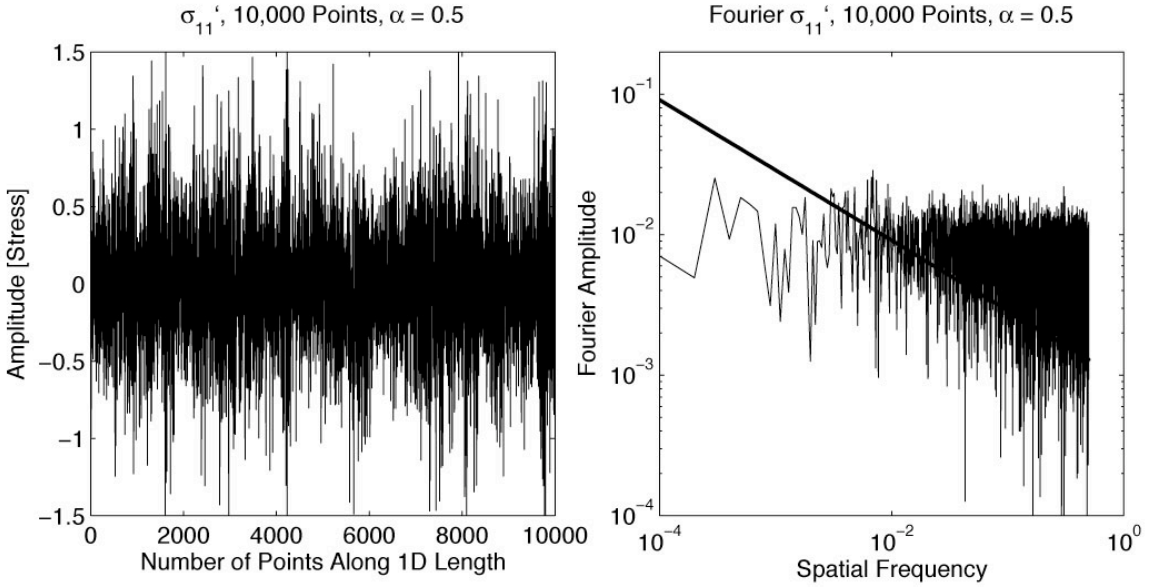

Figure 3.14 b)

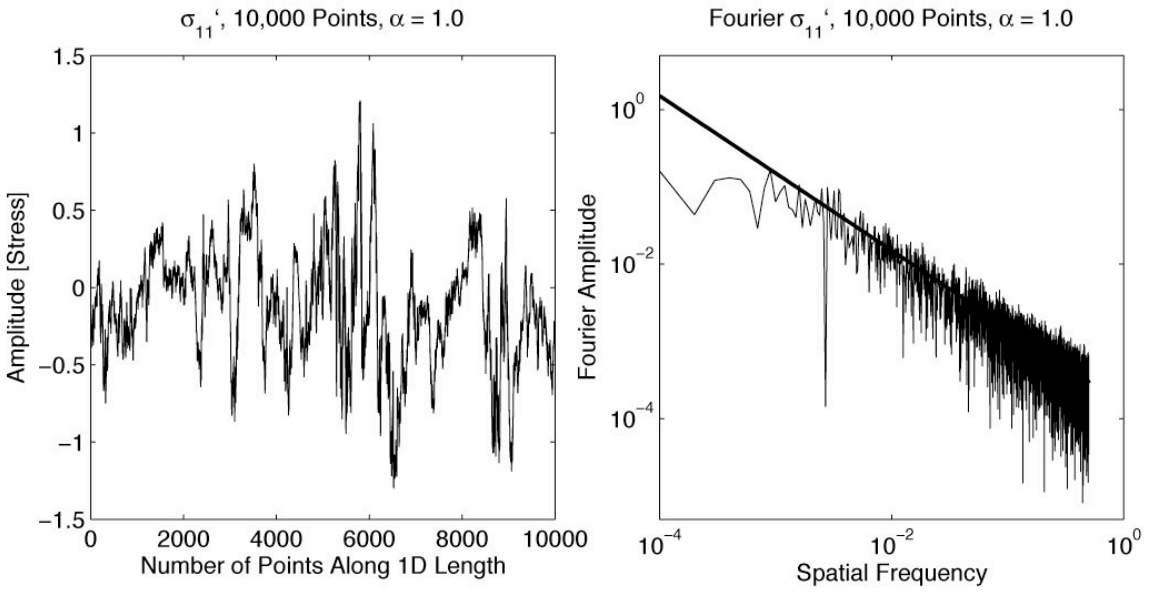

Figure 3.14 c)

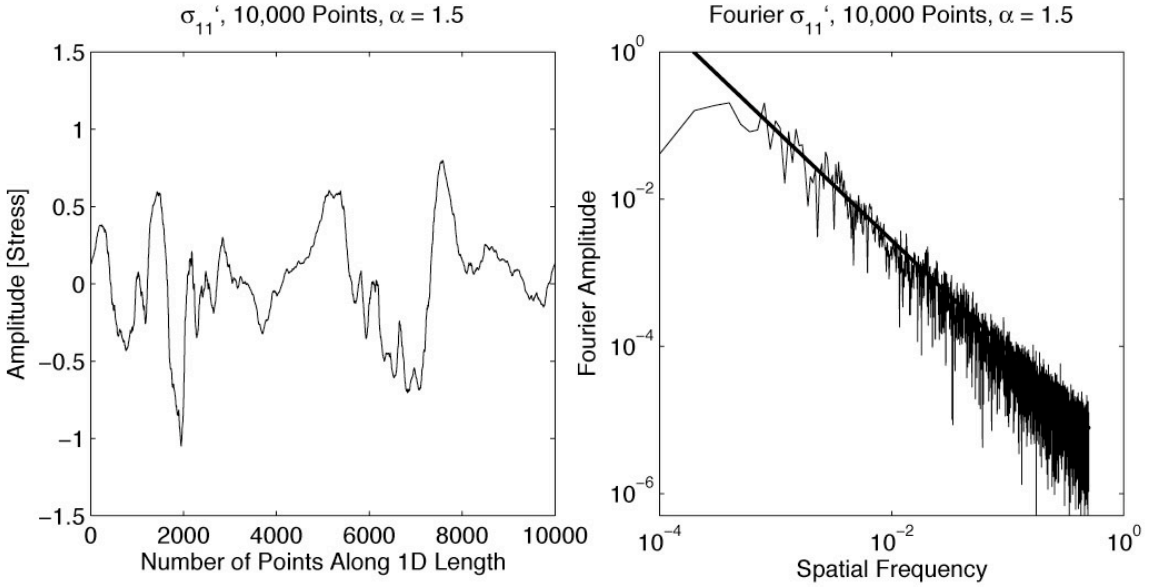

Figure 3.14 d)

Figure 3.14. *We plot the one component of a stress tensor for different levels of* α *smoothing. The other components of the stress tensor have similar spectral properties. Smoothed orientation angles,* $(\omega,[\theta,\phi])$*, and smoothed principal stresses,* σ_1', σ_2'*, and* σ_3'*, are combined together to produce a symmetric stress tensor in a particular reference frame. Note that the independent components of the stress tensor are much rougher than the smoothed orientation angles and principal stresses. When the smoothed principal stresses,* σ_1', σ_2'*, and* σ_3'*, are rotated into their respective reference frames using the smoothed angles,* $(\omega,[\theta,\phi])$*, to produce the Cartesian stress tensor components, much of the* α *smoothing is lost. This occurs because the symmetric stress tensor is defined for a Cartesian coordinate system in a particular reference frame, and stress components can lose their spectral properties upon rotation. This property is the reason we chose to filter the principal stresses and orientation angles rather than components of the Cartesian stress tensor in a particular reference frame.*

The last few plots show results for our 201x201x201 3D grids. Figures 3.15–3.18 show 2D slices through our filtered 3D grids at the $Z = 100$ height, midway through the 3D grids. The quantities shown in Figures 3.15–3.18 are shown for four different levels of smoothing, $\alpha = 0.0$, 0.5, 1.0, and 1.5 . In Figures 3.15–3.17, we find plots of the filtered and rotated 3D orientation angles, $\left(\omega[\theta,\phi]\right)$. Note for each α , a different random seed is used to create the 3D grid prior to filtering, and a different random rotation is applied to each grid. Random rotations can change the mean values of $\left(\omega[\theta,\phi]\right)$; hence, the 2D slices of $\left(\omega[\theta,\phi]\right)$, shown in Figures 3.15–3.17, have different mean levels for different α . This has nothing to do with the filtering. It is simply a function of the different random rotations that are applied.

In Figure 3.18 we have plots of σ'_{11}, the first diagonal component of the deviatoric stress tensor. The 3D deviatoric stress tensor is calculated by combining the filtered, and rotated 3D orientation angles, $\left(\omega[\theta,\phi]\right)$ with filtered 3D principal stresses, σ'_1, σ'_2, and σ'_3. We only show one component of the filtered 3D deviatoric stress tensor because the other components are similar. Again the components of the deviatoric stress tensor are not as spatially smooth as the orientation angles or principal stresses as we saw in the 1D. The only pattern we find within the filtered deviatoric stress tensor is that the standard deviations of the off-diagonal components tend to be ≈14% smaller than the standard deviations of the diagonal components.

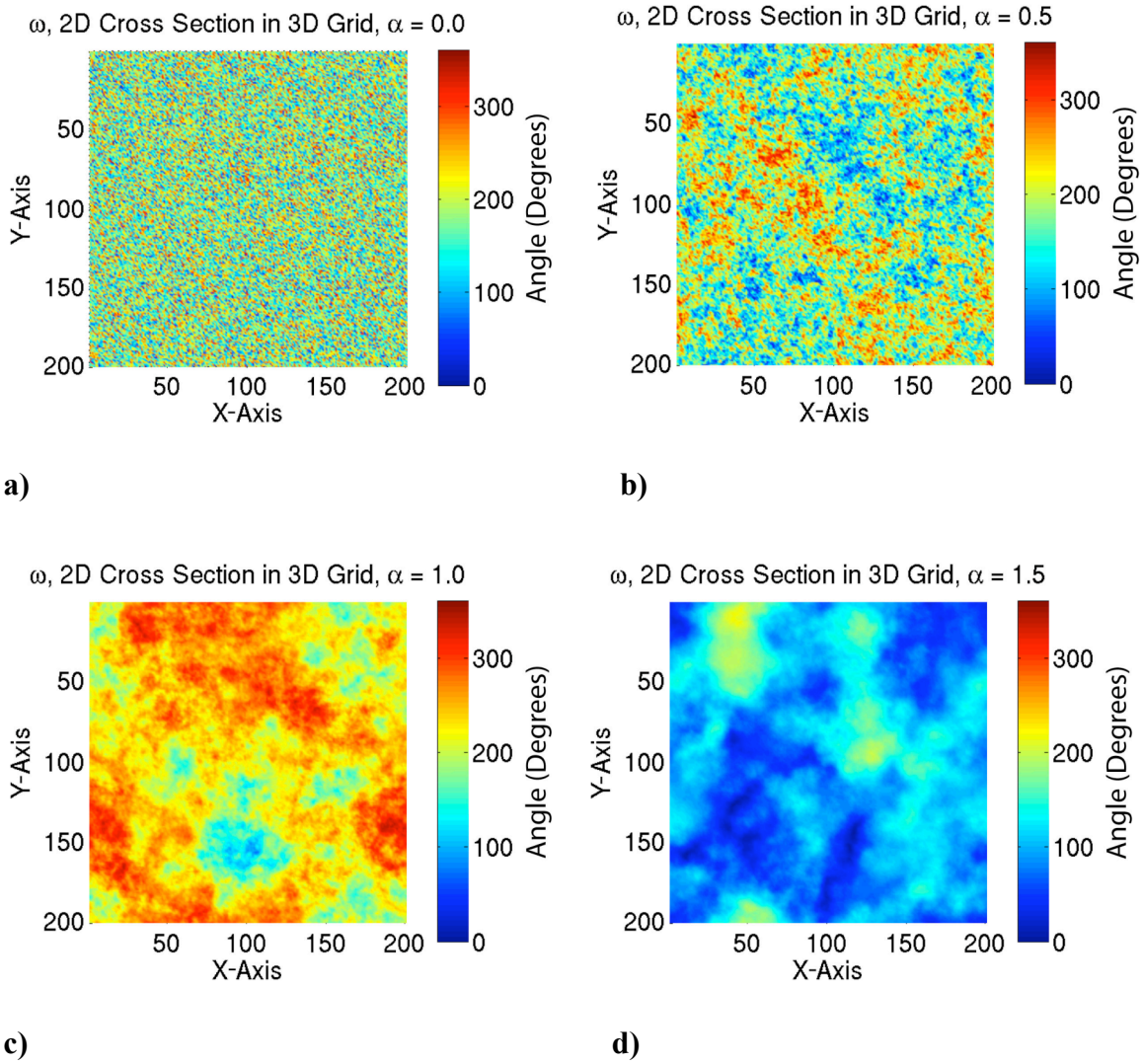

Figure 3.15. *2D slices of the angle, ω, through a 3D grid for four different levels of smoothing,* ***a)*** $\alpha = 0.0$, ***b)*** $\alpha = 0.5$, ***c)*** $\alpha = 1.0$, *and* ***d)*** $\alpha = 1.5$. *Each grid is 201x201x201 points, for a total of over 8 million grid points. The 2D slices shown are in the x-y plane approximately halfway through the grid at z = 100. All the planes exhibit similar spatial smoothing. Since it is a different simulation for each α, with a different random rotation of the angles $(\omega,[\theta,\phi])$ for each simulation, the mean value of the angle, ω, is different from simulation to simulation.*

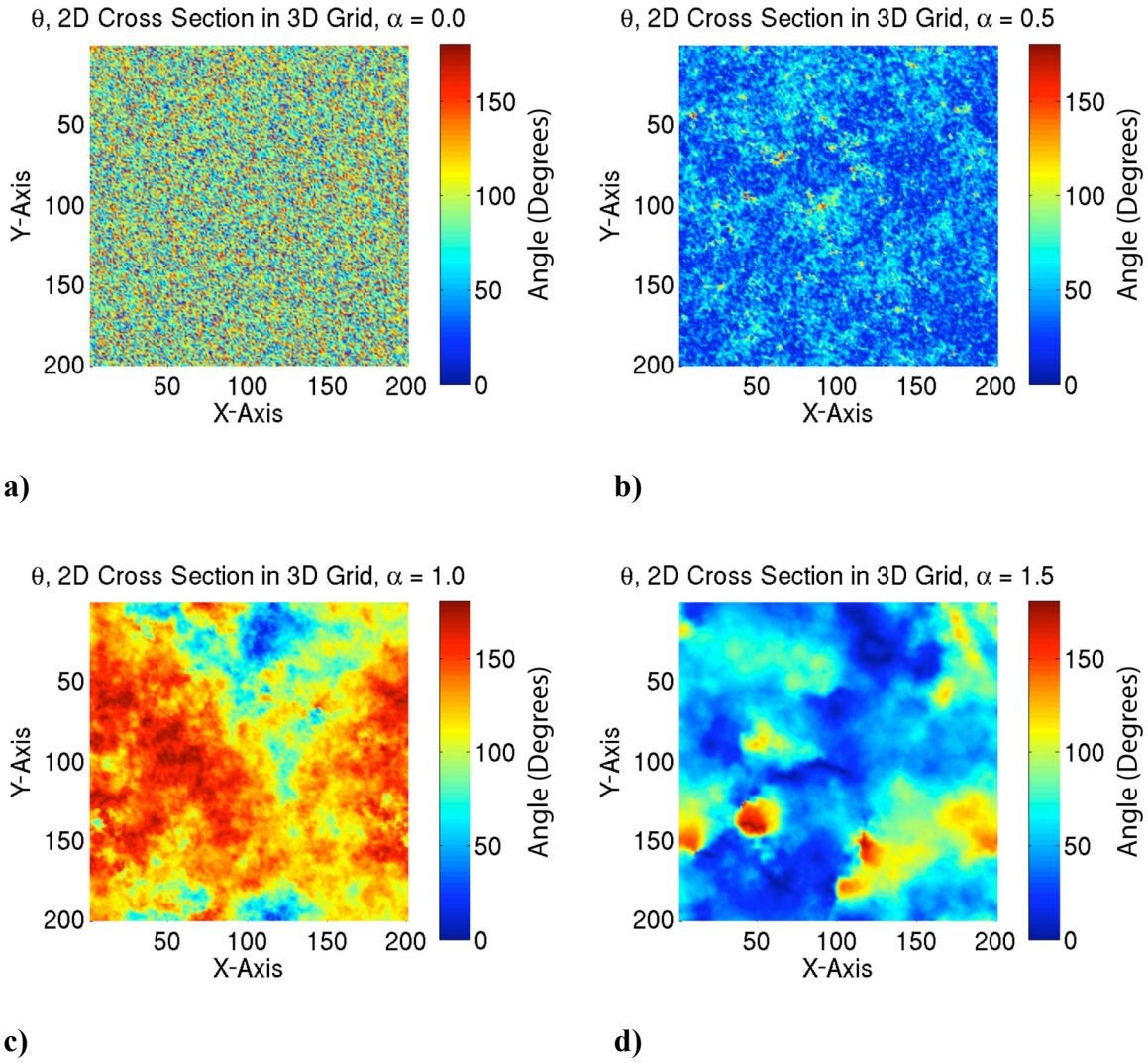

Figure 3.16. *2D slices of the angle, θ, through a 3D grid for four different levels of smoothing,* ***a)*** $\alpha = 0.0$, ***b)*** $\alpha = 0.5$, ***c)*** $\alpha = 1.0$, *and* ***d)*** $\alpha = 1.5$. *The 2D slices shown are in the x-y plane approximately halfway through the grid at z = 100. All the planes exhibit similar spatial smoothing. Since it is a different simulation for each α, with a different random rotation of the angles $(\omega,[\theta,\phi])$ for each simulation, the mean value of the angle, θ, is different from simulation to simulation.*

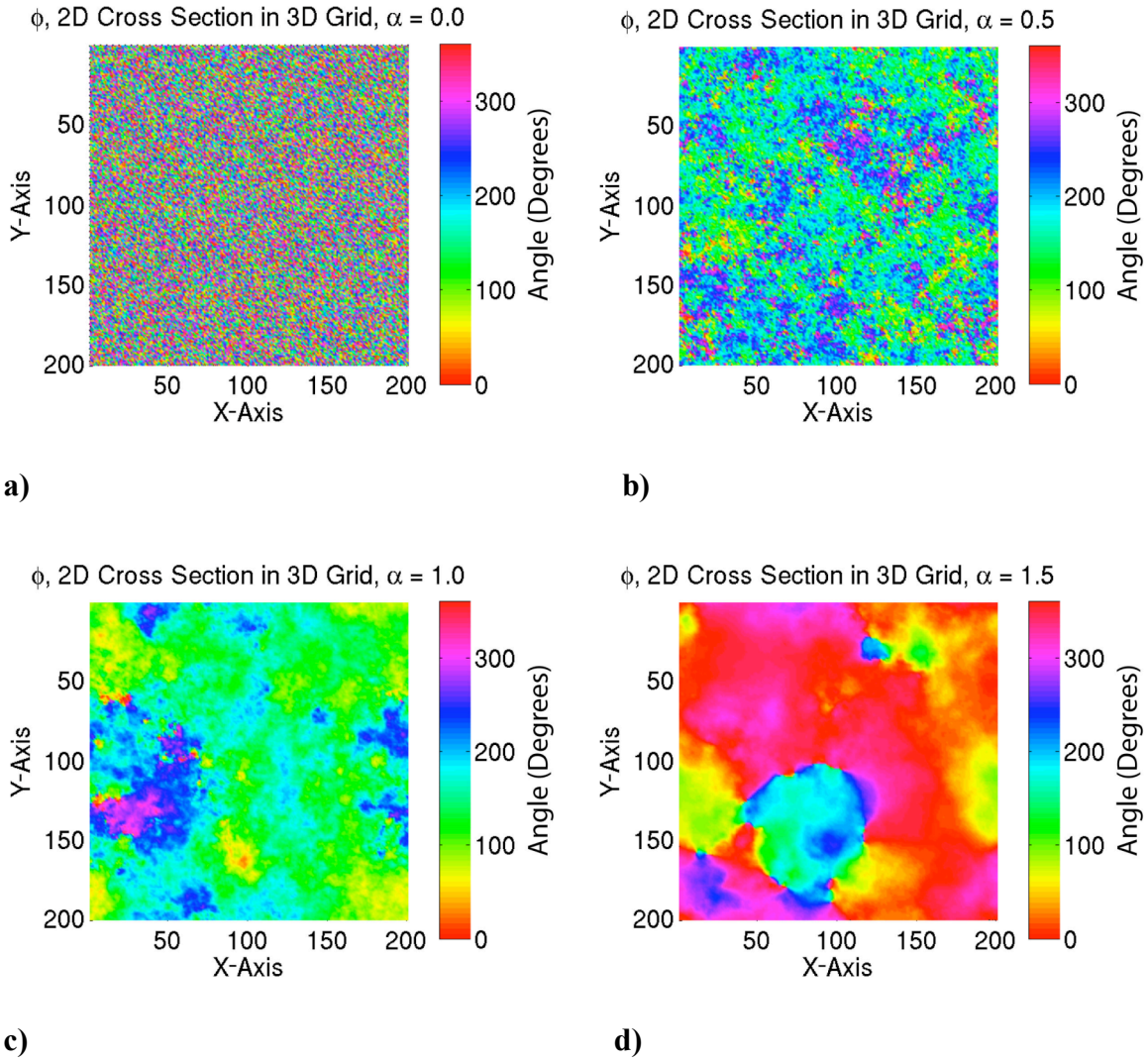

Figure 3.17. *2D slices of the angle, ϕ, through a 3D grid for four different levels of smoothing,* ***a)*** $\alpha = 0.0$, ***b)*** $\alpha = 0.5$, ***c)*** $\alpha = 1.0$, *and* ***d)*** $\alpha = 1.5$. *The 2D slices shown are in the x-y plane approximately halfway through the grid at z = 100. All the planes exhibit similar spatial smoothing. Since it is a different simulation for each α, with a different random rotation of the angles $(\omega,[\theta,\phi])$ for each simulation, the mean value of the angle, ϕ, is different from simulation to simulation.*

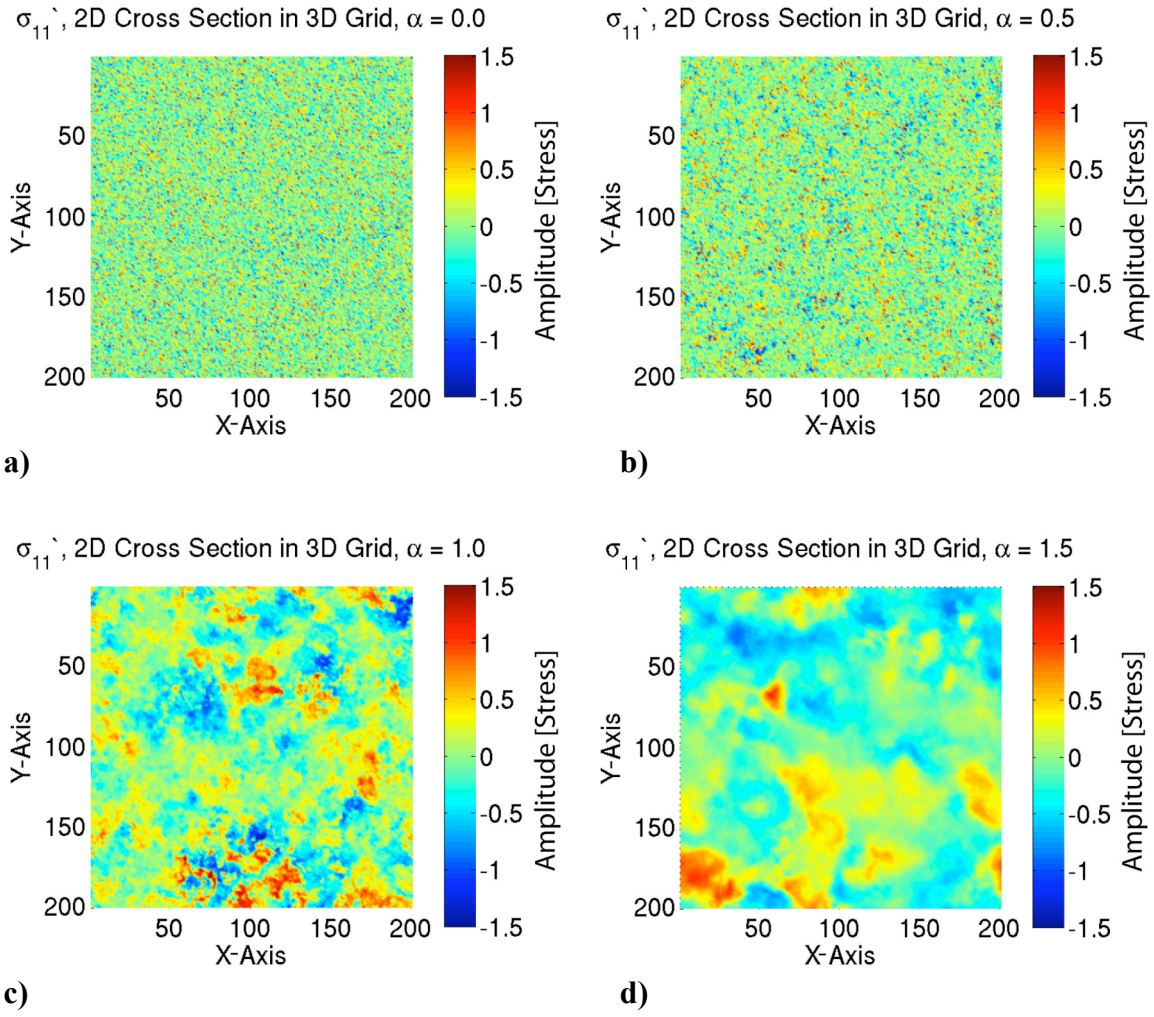

Figure 3.18. *2D slices of the first diagonal component of the deviatoric stress tensor,* σ'_{11}*, through a 3D grid for four different levels of smoothing,* ***a)*** $\alpha = 0.0$*,* ***b)*** $\alpha = 0.5$*,* ***c)*** $\alpha = 1.0$*, and* ***d)*** $\alpha = 1.5$*. The 2D slices shown are in the x-y plane approximately halfway through the grid at z = 100.* σ'_{11} *is rougher than the smoothed principal stresses,* σ'_1*,* σ'_2*,* and σ'_3*, or smoothed orientation angles* $(\omega,[\theta,\phi])$*. See Figure 3.14, the 1D example, for an explanation. The other components of the deviatoric stress tensor show similar spectral properties, i.e., degree of spatial smoothing.*

The next question we ask is how random are our 3D grids for different levels of spatial smoothing, α. Figure 3.19 explores this. Using the azimuth and plunge ranges illustrated in the Figure 3.12 cartoon, Figure 3.19 plots the P-T axes from randomly selected points within our 3D grids for four different levels of α. For each α, 100,000 points are randomly selected and plotted, a component-wise mean stress tensor, $\boldsymbol{\sigma}'_{HeterogeneousMean}$, is calculated, and its associated $\sqrt{I'_{2\ HeterogeneousMean}}$ (a measure of the size of $\boldsymbol{\sigma}'_{HeterogeneousMean}$) is shown. If the 3D grid has unbiased orientations, we would expect to see a uniform coverage of the equal area P-T plots as we see in Figure 3.19 a) and if the stress heterogeneity has a zero mean (which is what we are trying to design), we would expect the components of $\boldsymbol{\sigma}'_{HeterogeneousMean}$ to be close to zero and $\sqrt{I'_{2\ HeterogeneousMean}}$ to be very small. For comparison, the deviatoric principal stresses used in creating the stress tensor, have an $\sqrt{I'_2} = 1.0$. We find that for the $\alpha = 0.0$ case, Figure 3.19 a), the P-T equal area plots are uniformly covered with points as one might expect for no filtering. As α increases, the spatial clumping of data on the P-T plots increases. Interestingly, $\sqrt{I'_{2\ HeterogeneousMean}}$ is quite small for both $\alpha = 0.0$ and $\alpha = 0.5$, less than 1% when compared to the size of the input principal stresses, $\sqrt{I'_2} = 1.0$. As α increases, eventually, $\sqrt{I'_{2\ HeterogeneousMean}}$ increases to $\approx 2\%$ for $\alpha = 1.0$ and $\sqrt{I'_{2\ HeterogeneousMean}} \approx 8\%$ for $\alpha = 1.5$. Consequently, if one remains within the range of $0.0 \le \alpha < 1.0$, there will be less than 2% bias within the heterogeneity stress tensor for our 3D grids.

For first order calculations, a single filtered 3D heterogeneous stress grid should be sufficient to approximate heterogeneous stress with zero mean for $0.0 \le \alpha < 1.0$ if one averages over the entire grid. For $1.0 \le \alpha \le 1.5$, other issues will arise. Namely, as α

increases and the heterogeneous stress is increasingly smoothed, there will develop regions within the grid that will be more likely to fail than others (large I_2'), which can produce an average orientation bias in simulations that generate synthetic focal mechanisms. Again the answer will be to stack results from simulations with different 3D heterogeneous stress grids. See Chapter 4 for an explanation as to why regions with large I_2' are more likely to fail.

Figure 3.19 demonstrates that there is little to no bias when one averages over our entire 3D grids, but what happens if one averages over only a subregion of our 3D grids? This is another subject unto itself [*Heaton*, 2006, in preparation], but for now we just want to show that as the spatial smoothing, α, increases, there is increased clustering of orientations in P-T space, and the stress tensor has a significant non-zero mean for subregions. Also some subregions will be more likely to fail than others, those with larger I_2'. Figure 3.20 diagrams how we divide our grid into subregions (with the unprimed numbers) and the subdivide into sub-subregions (with the primed numbers). Figure 3.21 shows P-T plots, $\boldsymbol{\sigma}'_{HeterogeneousMean}$, and $\sqrt{I'_{2\ HeterogeneousMean}}$ for sample subregions and sub-subregions. The azimuthal and plunge ranges are the same as in Figure 3.19. For each α, one subregion, (1,1,1), containing 100,000 points and one sub-subregion, (1',1',1'), containing 1,000 points are plotted. As expected, for $\alpha = 0.0$, it is still uniform, random, even in the subdivisions of the grid. For $\alpha = 0.5$, a little spatial clumping begins. It is for $\alpha = 1.0$ and $\alpha = 1.5$, that we begin to notice marked differences between the average orientations of subdivisions and the entire grid. For example, $\alpha = 1.0$, (1,1,1) has a $\sqrt{I'_{2\ HeterogeneousMean}} \approx 18\%$, and the sub-subregion (1',1',1')

has an $\sqrt{I'^2_{HeterogeneousMean}} \approx 43\%$. Compare that to the $\sqrt{I'^2_{HeterogeneousMean}} \approx 2\%$ for randomly selected points from the entire 3D grid in Figure 3.19. When $\alpha = 1.5$, the effect can become even more extreme. (1,1,1) has a $\sqrt{I'^2_{HeterogeneousMean}} \approx 29\%$, and the sub-subregion (1',1',1') has a $\sqrt{I'^2_{HeterogeneousMean}} \approx 160\%$ whereas $\sqrt{I'^2_{HeterogeneousMean}} \approx 8\%$ for randomly selected points in Figure 3.19.

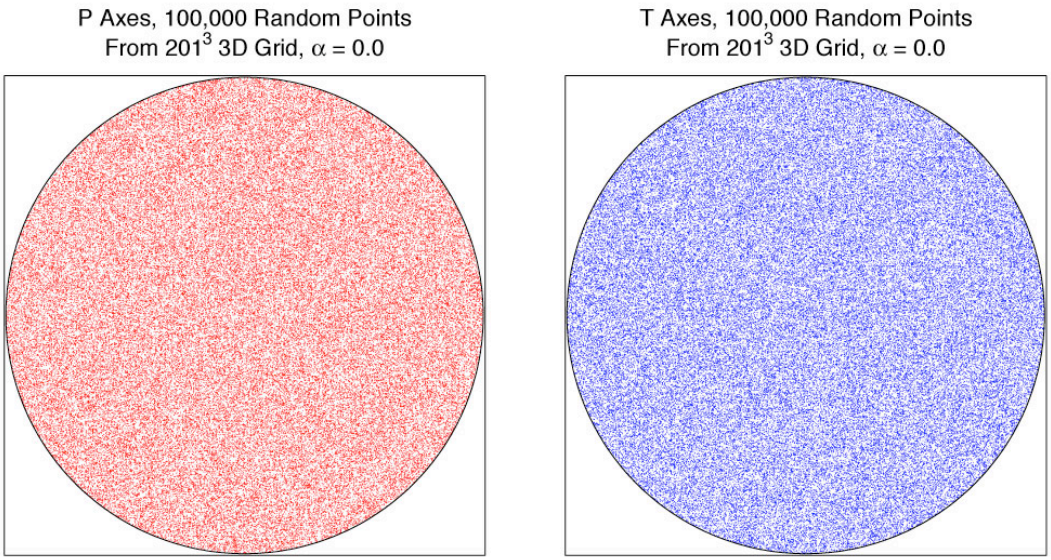

$$\boldsymbol{\sigma}'_{HeterogeneousMean} = \begin{pmatrix} -0.0012 & -0.0010 & -0.0016 \\ -0.0010 & -0.0004 & 0.0000 \\ -0.0016 & 0.0000 & 0.0016 \end{pmatrix} \text{ for 100,000 Random Points}$$

$$\sqrt{I'_{2\ HeterogeneousMean}} = 0.0033$$

Figure 3.19 a)

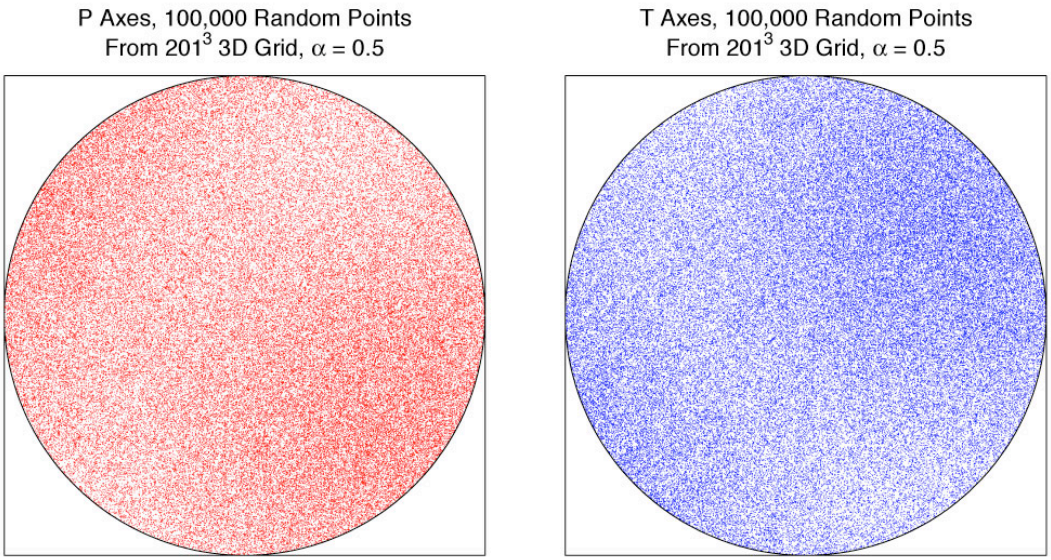

$$\boldsymbol{\sigma}'_{HeterogeneousMean} = \begin{pmatrix} 0.0015 & -0.0013 & 0.0006 \\ -0.0013 & -0.0011 & -0.0013 \\ 0.0006 & -0.0013 & -0.0004 \end{pmatrix} \text{ for 100,000 Random Points}$$

$$\sqrt{I'_{2\ HeterogeneousMean}} = 0.0033$$

Figure 3.19 b)

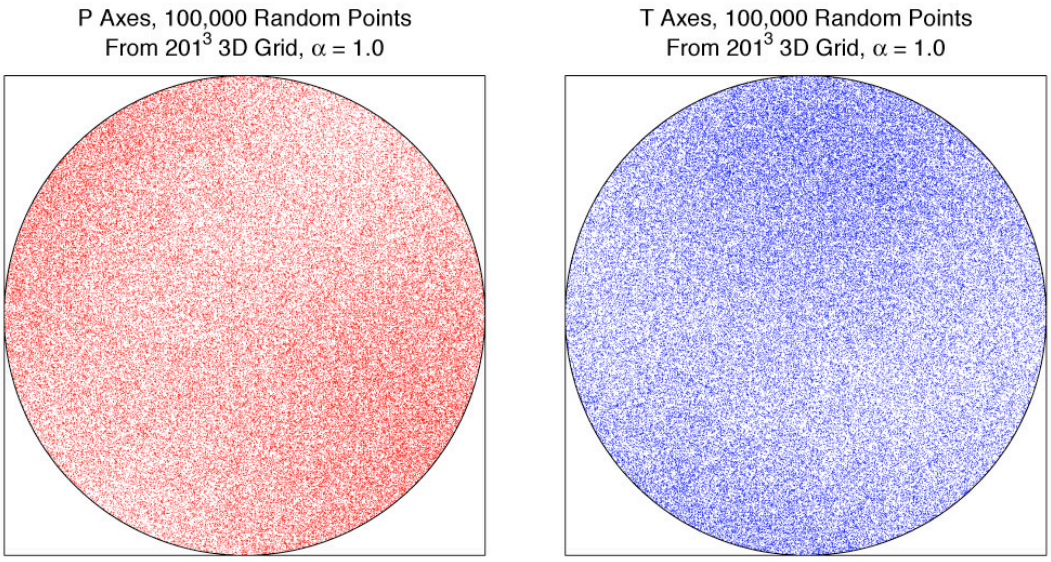

$$\boldsymbol{\sigma}'_{HeterogeneousMean} = \begin{pmatrix} 0.0110 & 0.0037 & 0.0042 \\ 0.0037 & -0.0107 & -0.0031 \\ 0.0042 & -0.0031 & -0.0003 \end{pmatrix} \text{ for 100,000 Random Points}$$

$$\sqrt{I'_{2\ HeterogeneousMean}} = 0.0178$$

Figure 3.19 c)

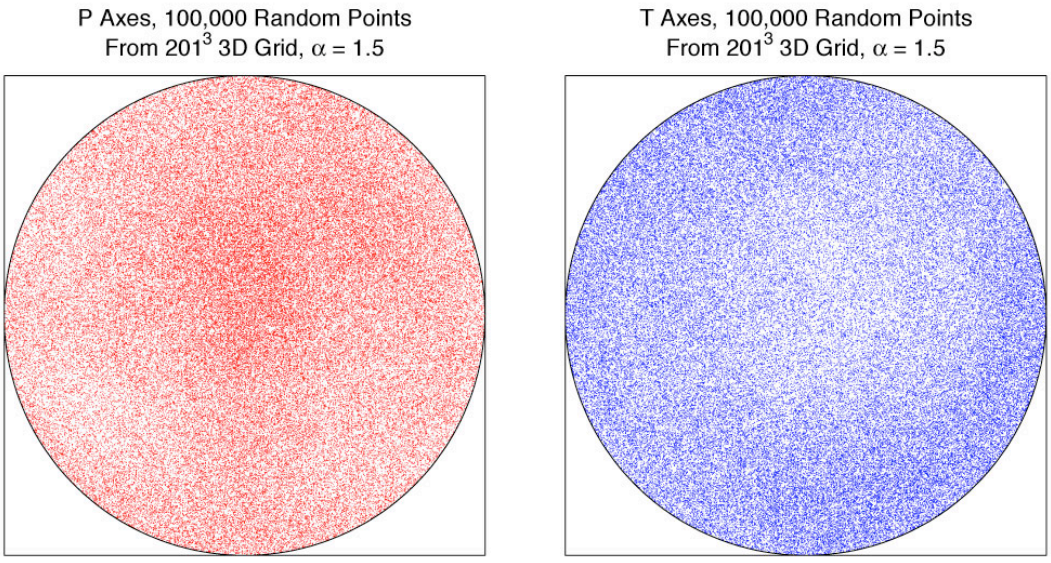

$$\boldsymbol{\sigma}'_{HeterogeneousMean} = \begin{pmatrix} -0.0241 & 0.0166 & -0.0151 \\ 0.0166 & 0.0515 & 0.0236 \\ -0.0151 & 0.0236 & -0.0274 \end{pmatrix} \text{ for 100,000 Random Points}$$

$$\sqrt{I'_{2\ HeterogeneousMean}} = 0.0781$$

Figure 3.19 d)

Figure 3.19. *We have P (Principal Compression Axis in red) and T (Principal Tension Axis in blue) plots for 3D, filtered, heterogeneous grids at four different levels of smoothing,* ***a)*** $\alpha = 0.0$, ***b)*** $\alpha = 0.5$, ***c)*** $\alpha = 1.0$, *and* ***d)*** $\alpha = 1.5$. *Each grid is 201x201x201 points for a total of over 8 million grid points. We randomly choose 100,000 points from the over 8 million possible points and plot their P and T Axes axes on equal area plots. For these P-T plots, we choose the conventional plunge range shown in Figure 3.12. For each* α, *we calculate the component-wise mean tensor for the 100,000 randomly selected points,* $\boldsymbol{\sigma}'_{HeterogeneousMean}$ *and its associated* $\sqrt{I'_{2\ HeterogeneousMean}}$, *which has units of stress. For comparison, the principal stresses that are used in creating, the stress tensors have a* $\sqrt{I'_2} = 1.0$. *In* ***a)*** $\alpha = 0.0$, *there is no clumping of the points on the P-T plots indicating that the heterogeneous stress is without any appreciable orientation bias and is uniformly distributed over orientation space. Also* $\sqrt{I'_{2\ HeterogeneousMean}}$, *a measure of the size of the stress bias, is quite small for* $\alpha = 0.0$, *less than 1%. As* α *increases, the spatial clumping of the points begins to appear to a small degree. In 3D simulations, this is a much smaller effect than in 1D if the entire 3D grid is being sampled. As* α *increases ,* $\sqrt{I'_{2\ HeterogeneousMean}}$ *also begins to increase to* $\approx 2\%$ *for* $\alpha = 1.0$ *and* $\approx 8\%$ *for* $\alpha = 1.5$.

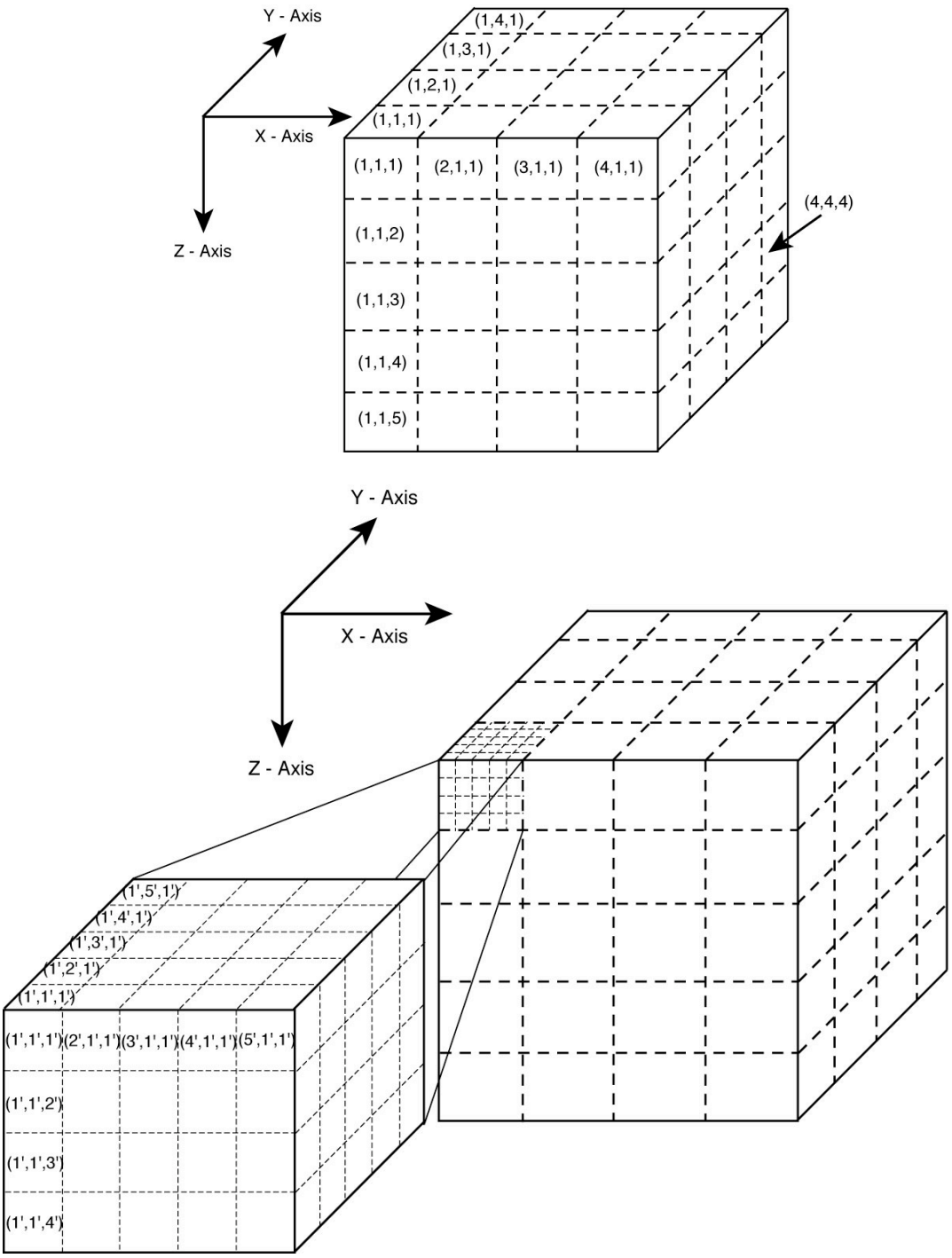

Figure 3.20. *A diagram of how we divide, then subdivide the 3D grid. The first division, produces subregions, approximately 100,000 points each. The second division produces sub-subregions, approximately 1,000 points each.*

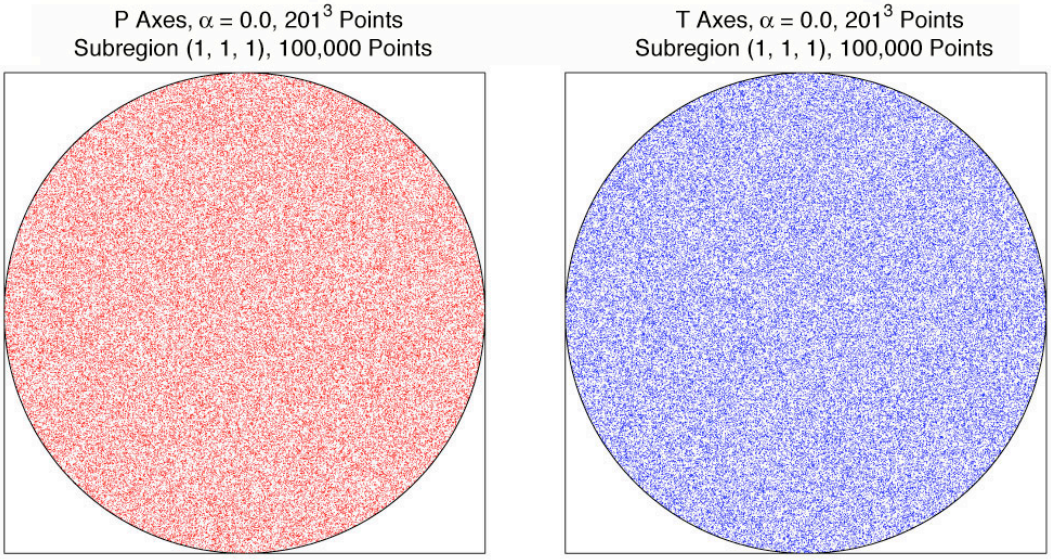

$$\boldsymbol{\sigma}'_{HeterogeneousMean} = \begin{pmatrix} -0.0011 & 0.0007 & -0.0012 \\ 0.0007 & 0.0013 & -0.0006 \\ -0.0012 & -0.0006 & -0.0002 \end{pmatrix} \text{ for 100,000 Points}$$

$$\sqrt{I'_{2\ HeterogeneousMean}} = 0.0027$$

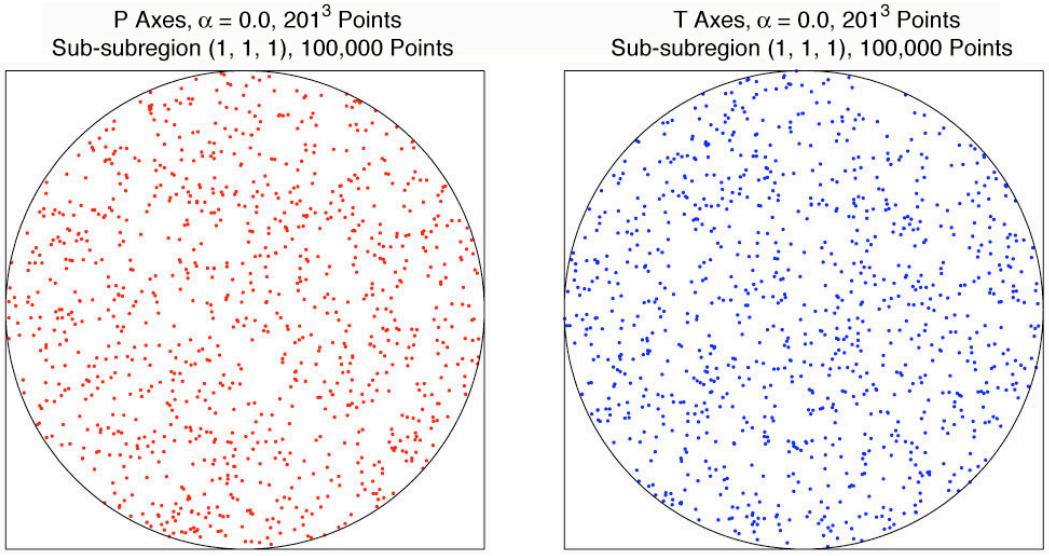

$$\boldsymbol{\sigma}'_{HeterogeneousMean} = \begin{pmatrix} 0.0023 & 0.0093 & -0.0079 \\ 0.0093 & -0.0236 & 0.0066 \\ -0.0079 & 0.0066 & 0.0213 \end{pmatrix} \text{ for 1,000 Points}$$

$$\sqrt{I'_{2\ HeterogeneousMean}} = 0.0374$$

Figure 3.21 a)

$$\boldsymbol{\sigma}'_{HeterogeneousMean} = \begin{pmatrix} -0.0220 & -0.0163 & 0.0169 \\ -0.0163 & 0.0175 & 0.0057 \\ 0.0169 & 0.0057 & 0.0045 \end{pmatrix} \text{ for 100,000 Points}$$

$$\sqrt{I'_{2\ HeterogeneousMean}} = 0.0447$$

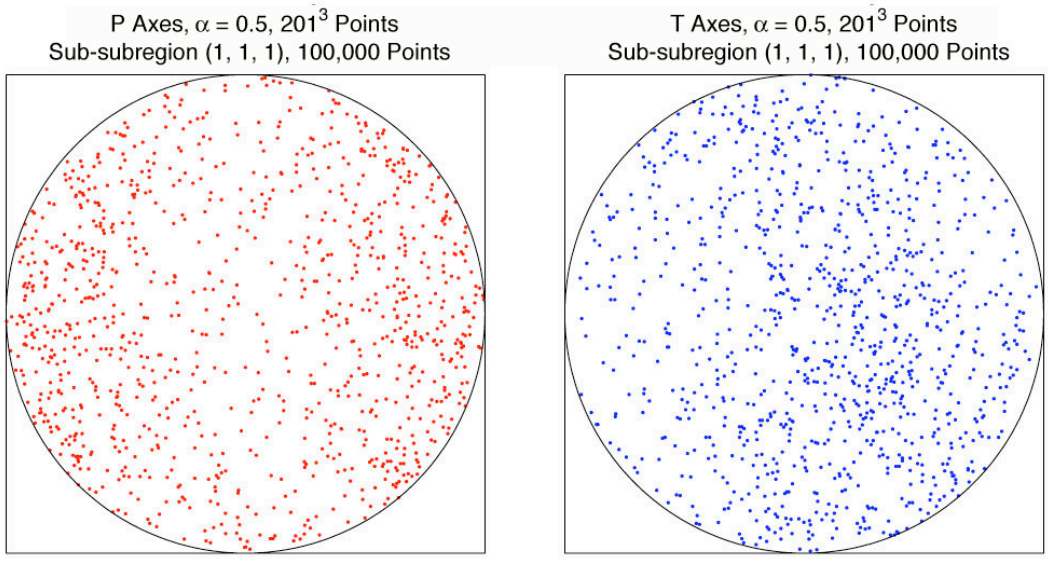

$$\boldsymbol{\sigma}'_{HeterogeneousMean} = \begin{pmatrix} 0.0398 & 0.0081 & 0.0167 \\ 0.0081 & -0.0094 & -0.0089 \\ 0.0167 & -0.0089 & -0.0304 \end{pmatrix} \text{ for 1,000 Points}$$

$$\sqrt{I'_{2\ HeterogeneousMean}} = 0.0592$$

Figure 3.21 b)

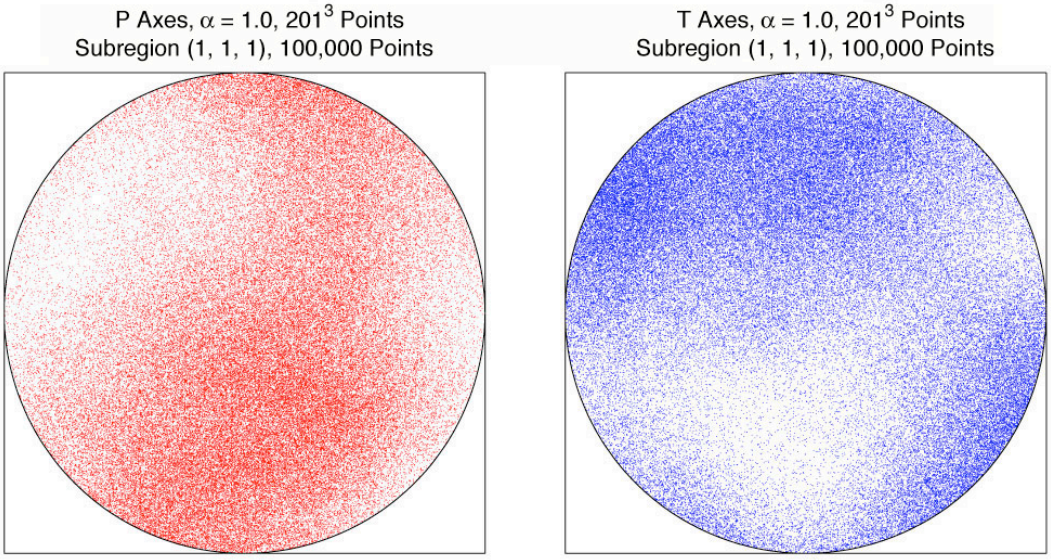

$$\boldsymbol{\sigma}'_{HeterogeneousMean} = \begin{pmatrix} 0.0696 & -0.0584 & 0.0259 \\ -0.0584 & -0.0212 & -0.0948 \\ 0.0259 & -0.0948 & -0.0483 \end{pmatrix} \text{ for 100,000 Points}$$

$$\sqrt{I'_{2\ HeterogeneousMean}} = 0.1836$$

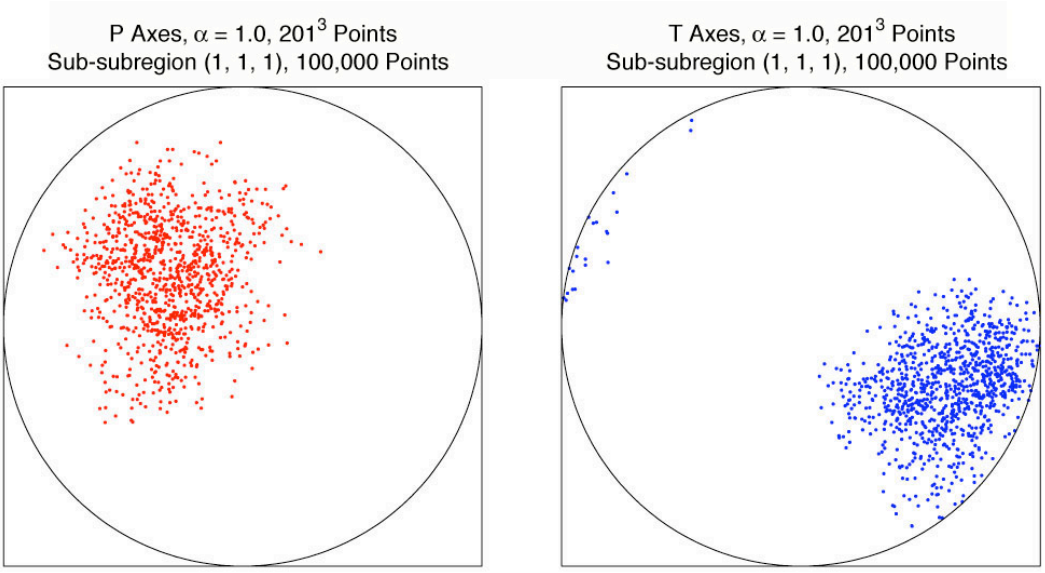

$$\boldsymbol{\sigma}'_{HeterogeneousMean} = \begin{pmatrix} 0.0887 & -0.1720 & -0.0753 \\ -0.1720 & -0.2653 & -0.0388 \\ -0.0753 & -0.0388 & 0.1766 \end{pmatrix} \text{ for 1,000 Points}$$

$$\sqrt{I'_{2\ HeterogeneousMean}} = 0.4277$$

Figure 3.21 c)

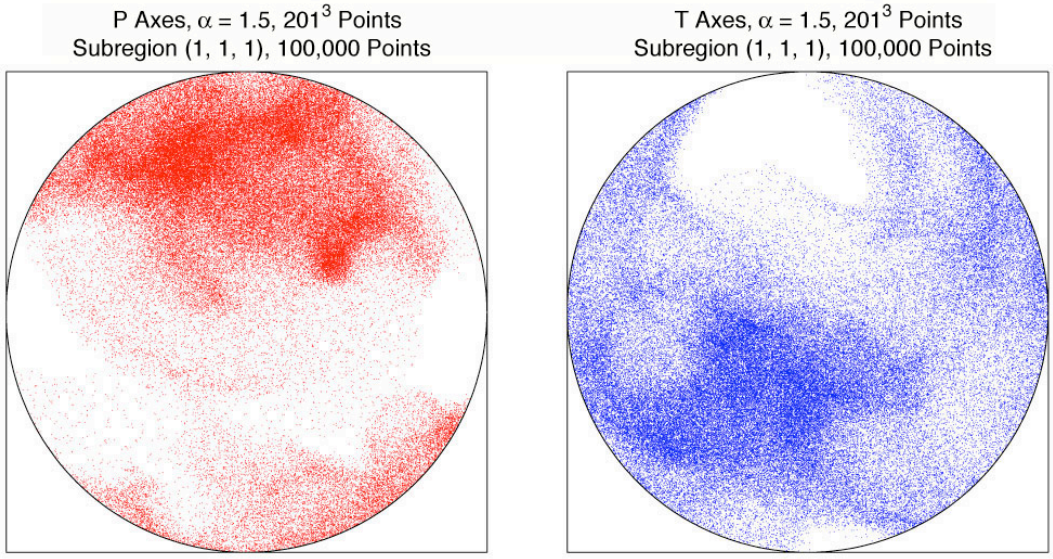

$$\boldsymbol{\sigma}'_{HeterogeneousMean} = \begin{pmatrix} -0.1565 & -0.0763 & -0.0053 \\ -0.0763 & 0.0753 & -0.1371 \\ -0.0053 & -0.1371 & 0.0811 \end{pmatrix} \text{ for 100,000 Points}$$

$$\sqrt{I'_{2\ HeterogeneousMean}} = 0.2933$$

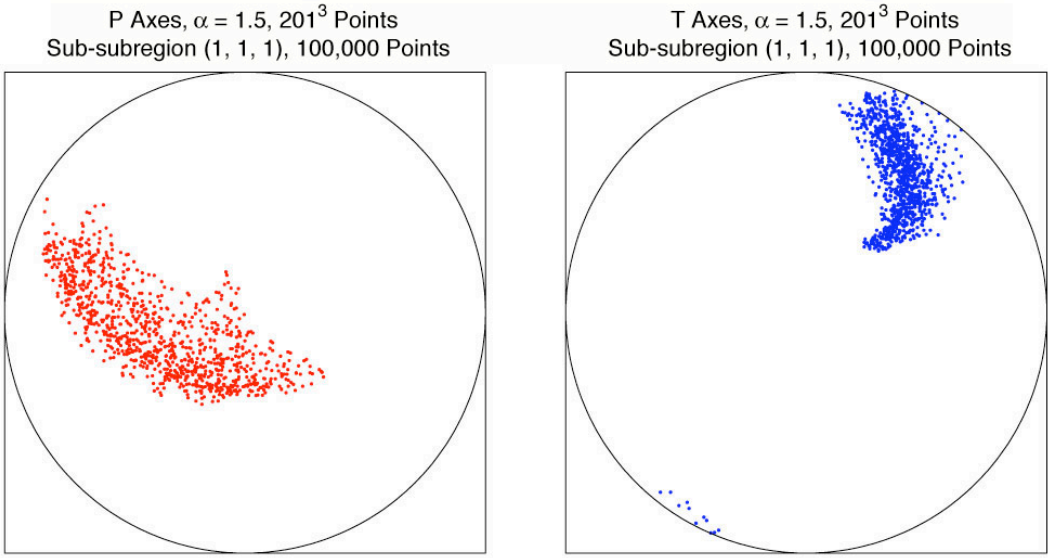

$$\boldsymbol{\sigma}'_{HeterogeneousMean} = \begin{pmatrix} 0.0746 & -0.4324 & 0.6902 \\ -0.4324 & -0.5582 & 0.5851 \\ 0.6902 & 0.5851 & 0.4836 \end{pmatrix} \text{ for 1,000 Points}$$

$$\sqrt{I'_{2\ HeterogeneousMean}} = 1.6007$$

Figure 3.21 d)

Figure 3.21. *This is similar to Figure 3.19, except that we plot the P and T axes for all the points within different subregions. The grid is first divided into 4x4x5 subregions of approximately 100,000 points each. Then the (1,1,1) subregion is subdivided into 5x5x4 sub-subregions, of approximately 1,000 points each. The purpose of this exercise is to show that as the spatial smoothing increases, subregions develop coherent orientation patterns. Therefore, even if the entire grid has little to no orientation bias, a subregion might have a significant orientation bias due to the long spatial wavelength coherence of orientations. We plot one sample subregion, (1,1,1), and one sample sub-subregion (1',1',1'), for each level of smoothing,* ***a)*** $\alpha = 0.0$, ***b)*** $\alpha = 0.5$, ***c)*** $\alpha = 1.0$, *and* ***d)*** $\alpha = 1.5$. *We find that for no smoothing,* ***a)*** $\alpha = 0.0$, *it does not matter whether we are looking at a subregion or the entire grid as in Figure 4.17. The subregions have random, uniform distributions of P and T axes on equal area plots. There is no appreciable clumping and* $\sqrt{I'_{2\ HeterogeneousMean}} \approx 0.0$ *for each subregion. Now as* α *increases so does the spatial clumping in P-T space and the value of* $\sqrt{I'_{2\ HeterogeneousMean}}$. *In fact, for* $\alpha = 1.5$, $\sqrt{I'_{2\ HeterogeneousMean}} \approx 1.6$, *for (1',1',1'), the same order magnitude as* $I'_2 = 1.0$, *the value of* I'_2 *for the input principal stresses. This indicates a very strong orientation bias in the sub-subregion. Therefore, as* α *increases the differential between subregion orientation bias and the entire grid orientation, grid bias increases. This is interesting, because as we will see in later chapters, this orientation clustering in space reproduces some of the clustering statistics seen in the real Earth.*

Summary of How to Create a Filtered 3D Heterogeneous Stress Tensor with Approximately Zero Mean

Now that we have explored some of the characteristics of our filtered principal stresses, orientation angles, and stress matrices in both 1D and 3D, let us summarize how to create our full heterogeneous stress matrices:

- Spatially filter three or two invariants of the stress tensor. We choose to filter the principal stresses for simplicity.
    - Generate 3D grids with Gaussian random noise for σ_1, σ_2, and σ_3 independently.
    - Filter each principal stress in 3D using the Chapter 2 methodology.
    - Use all three filtered, independent principal stresses, σ_1, σ_2, and σ_3, to create the full stress tensor with six independent quantities.
    - Or use the deviatoric principal stresses, σ_1', σ_2', and σ_3', where

      $\sigma_1' = \sigma_1 - p$
      $\sigma_2' = \sigma_2 - p$ and $p = (1/3)(\sigma_{11} + \sigma_{22} + \sigma_{33})$, so that the constraint
      $\sigma_3' = \sigma_3 - p$

      $\sigma_1' + \sigma_2' + \sigma_3' = 0$ is satisfied, to create the deviatoric stress tensor with five independent quantities.
- Create approximately random, spatially filtered orientations:
    - Generate a set of completely random orientations using a random unit quaternion generator.
    - Convert the quaternions into three angles, a rotation axis, $[\theta, \phi]$, and a rotation ω about the rotation axis.

- Spatially filter these three angles, $(\omega,[\theta,\phi])$.
- Resize the angles so that their spatial means have the following values, $\bar{\omega} = 180°$, $\bar{\theta} = 90°$, and $\bar{\phi} = 180°$, and their possible ranges fall within, $0° \le \omega \le 360°$, $0° \le \theta \le 180°$, and $0° \le \phi \le 360°$.
- Convert the spatially filtered $(\omega,[\theta,\phi])$, back into its associated filtered quaternion, $\vec{q}^{\,F} = \left[q_0^F, q_1^F, q_2^F, q_3^F\right]$.
- Add a random rotation to this filtered quaternion, using algebraic quaternion multiplication.
- Then convert this filtered, randomly rotated quaternion into strike, dip, and rake, (Θ,δ,λ).

- Combine the spatially filtered fault parameters, (Θ,δ,λ), with the spatially filtered principal stresses, to produce an approximately randomly oriented, spatially filtered, heterogeneous stress matrix.
- Use the heterogeneous stress matrix in simulations that produce synthetic focal mechanisms.
- Repeat the above steps at least ten times and stack the results to produce data that have no substantial orientation bias in the heterogeneity.

References

Heaton, T. H. (2006, in preparation), Scale dependence of the strength of the Earth's crust.

Marsaglia, G. (1972), Choosing a Point from the Surface of a Sphere, *Annual Mathematical Statistics*, *43*, 645–646.

Mathworks, I. (1994–2006), Aerospace Block Set - Quaternion Multiplication, *http://www.mathworks.com/access/helpdesk/help/toolbox/aeroblks/aeroblks.html*.

Weisstein, E. W. Hypersphere Point Picking, in *MathWorld -- A Wolfram Web Resource.* *http://mathworld.wolfram.com/HyperspherePointPicking.html*, edited.